Norwegian University
of Life Sciences

Master's Thesis 2021 60 ECTS
Faculty of Chemistry, Biotechnology and Food Science

Identification of Phospho- and Total-proteome in Glioma Cell Lines after Inhibition of Cyclin-Dependent Kinase 12 (CDK12) and Cyclin-Dependent Kinase 13 (CDK13)

Nora Elise Skyrud
Master of Science, Biotechnology

Acknowledgements

The work of this thesis was carried out at the Department of Microbiology at Oslo University Hospital (OUS), as part of a master's degree in Biotechnology, at the Faculty of Chemistry, Biotechnology and Food Science (KBM) at the Norwegian University of Life Sciences (NMBU).

First and foremost, I would like to thank my supervisor Deo Prakash Pandey for all supervision, support and enthusiasm throughout the year. His feedback has greatly contributed to my understanding of the field of molecular biology and helped me a lot with independent thinking in the lab. Thank you for always being available for guidance in the laboratory and in the process of writing this thesis. I would also like to express my gratitude to my internal supervisor, Professor Harald Carlsen, for his time proofreading the thesis. Additionally, I would like to express a note of gratitude to the whole department for their warm welcome.

Moreover, thanks to Sachin Singh, PhD, and the Proteomic Core Facility at Oslo University Hospital, Rikshospitalet, for conducting liquid chromatography tandem mass spectrometry (LC-MS/MS) and assisting me in performing bioinformatic analyses.

My sincerest thanks go to my fellow students in the student's office. Thanks to Silje Lier for helping me in the lab, and a special thanks to Martine Mesel Isom for her help in setting up procedures and for our theoretical discussions in my first few months.

Lastly, I am grateful for the everlasting support and encouragement of my family and friends.

Abstract

Numerous factors and mechanisms control proper gene expression. Transcription regulation by RNA polymerase II (RNAPII) carboxy-terminal domain (CTD) phosphorylation influences global transcription levels and manufacture the adjustment of final RNA products. Cyclin-dependent kinases (CDKs) have been reported to be involved in the phosphorylation of RNAPII CTD. Functional disturbance of CDKs is linked to reduced regulation of transcription and disease. CDK12 and CDK13 are two of the kinases phosphorylating RNAPII CTD. Research suggests for a role of CDK12 in phosphorylating CTD Serine 2 (Ser2) for productive elongation, while the evidence of CDK13 in its role as a CTD kinase is undefined.

A former student in the Pandey group, Sigrid Berg, revealed in her master thesis chromatin-bound interaction partners of CDK12. In this study we aimed to elucidate the discovered interaction partners of CDK12 in HeLa cells to acquire knowledge on its role in transcription and RNA processing events. This was performed using pulldown for CDK12 bound proteins using immuno-precipitation (IP) followed by mass spectrometry. In this part of the thesis, I set out to validate some of these interaction partners by immuno-blotting following IP under normal conditions. I was not able to detect interaction between CDK12 and interaction partners of interest, and for this cause, we chose to not proceed with this confirmation of interaction partners. Therefore, we aimed to identify the total- and phospho-proteome of glioma cell lines after inhibition of CDK12 and CDK13 using THZ531. THZ531 is a small molecule which inhibits the catalytic activity of both CDK12 and CDK13.

Mass spectrometry (MS) analysis revealed multiple proteins in various intracellular regulatory pathways affected by the inhibition of CDK12/13. Earlier work carried out by the Pandey group, found that inhibition of CDK12/CDK13 specifically compromises the proliferation of glioma cells. Furthermore, earlier work has also found that CDK12/CDK13 inhibition disrupts the cell cycle of glioma cells and leads to a rapid shutdown of DNA replication. Therefore, we chose to focus on a few pathways and protein groups, including cell cycle and DNA replication. Our data indicates that inhibition of CDK12/CDK13 in glioma cells influence proteins involved in the cell cycle and DNA replication.

Sammendrag

Flere faktorer og mekanismer kontrollerer riktig genekspresjon. Transkripsjonsregulering av RNAPII CTD fosforylering påvirker globale transkripsjonsnivåer og justerer endelig nivå av RNA-produkter. Såkalte kinaser, CDKer, er rapportert å være involvert i fosforylering av RNAPII CTD. En svekket funksjonalitet av disse CDKene er knyttet til feilregulering av transkripsjon og eventuell påfølgende sykdom. CDK12 og CDK13 er to av kinasene som fosforylerer RNAPII CTD. Forskning antyder en rolle for CDK12 i fosforylering av CTD Serine 2 (Ser2) for produktiv forlengelse, mens CDK13 sin rolle som CTD-kinase er fremdeles udefinert.

En tidligere student i Pandey-gruppen, Sigrid Berg, rapporterte i sin masteroppgave flere kromatinbundne interaksjonspartnere for CDK12. I denne studien hadde vi som mål å belyse de oppdagede interaksjonspartnerne til CDK12 i HeLa-celler for å bedre forstå dens rolle i transkripsjon og RNA-prosesseringshendelser. Vi benyttet IP for å trekke ut CDK12-GFP fra cellelysatet. Western blot-analyser avslørte ikke interaksjonspartnerne av interesse, og derfor valgte vi å ikke fortsette med denne bekreftelsen av interaksjonspartnere. Videre hadde vi derfor som mål å identifisere total- og phospho-proteomet til gliomceller etter inhibering av CDK12 og CDK13 ved bruk av THZ531. THZ531 hemmer CDK12/13 sin katalytiske aktivitet.

Massespektrometri (MS)-analyse avslørte flere proteiner i forskjellige intracellulære reguleringsveier som ble påvirket av inhiberingen av CDK12/13. Tidligere arbeid utført av Pandey-gruppen, fant at inhibering av CDK12/13 spesifikt kompromitterer prolifereringen av gliomaceller. Tidligere arbeid også funnet at CDK12/13-inhibering forstyrrer cellesyklusen til gliomaceller og fører til en rask shutdown av DNA-replikasjon. Derfor valgte vi å fokusere på noen få reguleringsveier og proteingrupper, inkludert cellesyklus, DNA-replikasjon og CDK2-substrater. Våre data indikerer at inhibering av CDK12/13 i gliomceller har en effekt på proteiner involvert i cellesyklusen og DNA-replikasjon.

List of Abbreviations

BAC	bacterial artificial chromosome
CAK	CDK-activity kinase
CDK	cyclin-dependent kinase
ChIP	chromatin immunoprecipitation
CTD	carboxy-terminal domain
Ctrl	control
CycK	Cyclin K
DDR	DNA damage repair
DNA	deoxyribonucleic acid
DSIF	DRB sensitivity factor
ES cell	embryonic stem cell
GBM	Glioblastoma multiforme
GFP	green fluorescent protein
HeLa	Henrietta Lacks
HRP	horseradish peroxidase
IP	immunoprecipitation
LC-MS/MS	liquid chromatography tandem mass spectrometry
mAb	monoclonal antibody
miRNA	micro RNA
mRNA	messenger RNA
MS	mass spectrometry
NMBU	Norwegian University of Life Sciences
OUS	Oslo University Hospital
pAb	polyclonal antibody
PAF	RNA polymerase-associated factor
PAS	polyadenylation signal
PIC	pre-initiation complex
P-TEFb	positive transcription factor b
RNA	ribonucleic acid
RNAi	RNA interference
RNAP	RNA polymerase
rRNA	Ribosomal RNA

RT	room temperature
SDS-PAGE	sodium dodecyl sulfate-polyacrylamide gel electrophoresis
Ser	serine
pSer2	phosphorylated serine 2
pSer5	phosphorylated serine 5
snoRNA	small nucleolar RNA
snRNA	small nuclear RNA
SRSF	serine/arginine-rich protein-specific kinase
tRNA	transfer RNA
Thr	threonine
Tyr	tyrosine
Xrn2	5´-3´exoribonuclease 2

Table of Contents

1. Introduction

1.1. Transcription and transcriptional regulation

Transcription is the process where RNA is being synthesized with DNA as template, and it is the first step in gene expression. Transcription occurs when there is a need for a particular gene product at a specific time or in a specific tissue (1). The transcript, or the RNA copy, carries the information that is needed to build a polypeptide. Only one DNA strand is normally copied during transcription. This strand is referred to as the template strand, and the molecules being produced are single-stranded mRNA. The template DNA strand that corresponds to the mRNA is called the coding or sense strand (1). Pre-mRNA is the initial product of transcription in eukaryotes and is edited through splicing before the mature mRNA is produced and is ready for translation by the ribosome. Different proteins and factors are involved in the transcription cycle, such as transcription factors (TFs), Mediator, general transcription factors (GTFs) and RNA polymerase (1).

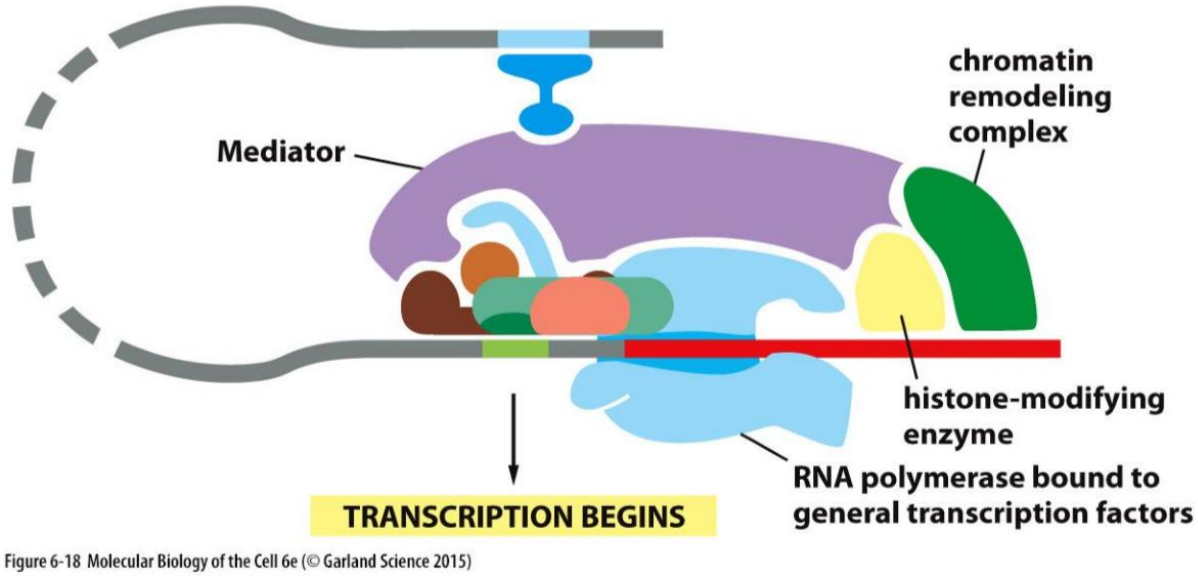

Figure 1.1: Transcriptional activators directs assembly of transcriptional machinery (2). Picture showing the different proteins and transcription factors involved in the transcription cycle, such as Mediator and RNA polymerase II. Picture obtained from Molecular Biology of the Cell (2).

1.1.1 RNA polymerase

The most important enzyme involved in transcription is RNA polymerase. It uses a single-stranded DNA template to synthesize a complementary strand of RNA. RNA polymerase builds the RNA strand in a 5’ to 3’ direction. There are three polymerases involved in transcription in eukaryotes: RNA polymerase I, II and III (3).

RNA polymerase I (RNAPI) is a 13-subunit enzyme that transcribes ribosomal RNA (rRNA) genes from the ribosomal DNA (rDNA) repeat loci. The rRNA genes are first transcribed into 47S pre-rRNA and processed into mature 28S, 18S and 5.8S rRNA (4). These rRNAs are involved in crucial structural and catalytic functions within the ribosomal core. RNAPI is important in the process of rRNA gene expression and a key factor in regulation of ribosomal biogenesis (5). Ribosome synthesis and rRNA transcription is linked to the rate of protein synthesis in a cell. Therefore, intracellular signals must coordinate the synthesis of rRNA with that of other components of protein translation (6).

RNA polymerase II (RNAPII) transcribes mRNA, miRNA, snRNA and snoRNA genes. The largest subunit of RNAPII, Rpb1, is in possession of a long, repetitive polypeptide extension called the carboxy-terminal domain (CTD), which is a unique feature of RNAPII and therefore distinguishes it from the other two polymerases. RNAPII CTD comprise a tandem array of seven evolutionary preserved amino acid repeats with the consensus sequence Tyr1-Ser2-Pro3-Thr4-Ser5-Pro6-Ser7 (also termed YSPTSPS) (7). The control of RNAPII activity is highly regulated at individual genes. This specific regulation is critical for both the homeostasis of the cells and the programmed development of multicellular organisms (8). Numerous factors have been found to contribute to the regulation of transcription, as will be described in greater detail below. These factors enable RNAPII to gain access to the gene's promoter, to initiate RNA synthesis at the transcription start site (TSS) of the gene and to generate a productively elongating transcription complex that produces a full-length RNA transcript (8).

RNA polymerase III (RNAPIII) transcribes short, abundant nonprotein-coding RNA transcripts, such as tRNA, 5S rRNA and other essential RNAs (9). The main mechanisms of RNAPIII transcription have been studied in great detail. Three transcription factors function together with RNAPIII: TFIIIA, TFIIIB and TFIIIC. The internal promoter elements and TATA box are the only known *cis*-acting elements for RNAPIII transcripts. This suggests that the regulatory mechanisms of RNAPIII are considerably simpler than for those of RNAPII. Mammalian RNAPIII is regulated by the RNAPIII repressor Maf1, Myc, p53 and retinoblastoma (10).

Majority of the cell-type specific transcription is carried by RNA polymerase II (RNAPII), which is a subject of this project and will be described in detail in the following sections.

1.1.2 RNA Polymerase II-based transcriptional regulation

Transcription by RNAPII are highly regulated processes within the cell, and during the transcription cycle it is subject to multiple regulatory events. RNAPII transcription is coordinated with distinct patterns of CTD phosphorylation (11).

1.1.2.1 Initiation

Transcription begins with initiation. The code that dictates when, where and at what level specific genes should be transcribed is found in the DNA sequences in and around specific gene promoters (8). During early transcription initiation, RNAPII is recruited to promoters creating a pre-initiation complex (PIC) with the Mediator complex and the General Transcription Factors (GTFs) TFIIA, TFIIB, TFIID, TFIIE, TFIIF and TFIIH (12). PICs are targeted by the elements of the core promoter sequence. Mediator is a highly conserved, transcriptional co-activator complex that physically connects activator proteins bound at enhancers and RNAPII bound at the promoter. It transmits signals from transcriptional regulators to the RNAPII initiation complex. When RNAPII gains access to the promoter, the transcription cycle begins. This requires, in some cases, that the promoter gets cleared of nucleosomes that block access to RNAPII and the GTFs. A PIC assembles on the core promoter, and the DNA is then unwound and RNAPII initiates transcription (8). RNAPII CTD is largely unphosphorylated during initiation but becomes phosphorylated by CDK7, which is part of TFIIH, upon initiation (13).

CDK7 phosphorylates the CTD at Ser5 and Ser7 upon initiation. The role of Ser7 phosphorylation is still being questioned, but it is suggested that that this modification helps prime the CTD for following phosphorylation events (14). The phosphorylation of Ser5 has clear roles in the early stages of transcription. This phosphorylation event interrupts interactions with Mediator and enables promoter escape. The Ser5 phosphorylation is additionally recognized by the 5’-end capping enzymes (14).

1.1.2.2 Elongation

Elongation by RNAPII is a highly regulated process, both during early elongation and in the phase of productive elongation. A key regulatory event during the elongation phase is promoter-proximal pausing, which is when RNAPII stays bound at the promoter before it either terminates transcription or enters productive elongation. RNAPII can pause and accumulate at very high levels during the early stages of elongation (15). This pause and accumulation happen in the promoter-proximal region,

30-60 nucleotides downstream of the transcription start site (TSS). It is a rate-limiting step for transcription, and the pausing can act as a quality checkpoint for transcript 5'capping and RNAPII modification before entering productive elongation (15).

The RNAPII promoter-proximal pausing depends on the core promoter features that recruit RNAPII to this region. Promoter-associated transcription factors (TFs) that function with negative elongation factor (NELF) and DRB-sensitivity-inducing-factor (DSIF) are involved to stabilize the paused RNAPII. The release of RNAPII into productive elongation is mediated by the positive transcription elongation factor-b (P-TEFb) complex. P-TEFb is comprised of cyclin T1 and cyclin-dependent kinase 9 (CDK9) and phosphorylates the CTD Ser2 of RNAPII, in addition to phosphorylating NELF and DSIF. Ser2-modifiaction by P-TEFb can only happen after successful transcription initiation has taken place and marks the shift of transcription initiation to elongation (14).

After RNAPII is released from the promoter-proximal pause site, it initiates productive elongation. Elongation rates can vary between and within genes, and the elongation rate seems to play a part in co-transcriptional processes such as splicing, transcriptional termination and genome stability (15). The features of promoter-proximal pausing and pause-escape will be described in greater detail in subsection 1.1.3.

1.1.2.3 Termination

The final step of transcription is termination where RNAPII and RNA are released from the DNA template. Transcription termination serves many important functions in the cell, such as preventing RNA polymerase interference with neighboring DNA elements, recycling RNA polymerase, promoting RNA 3′-end processing, and regulating gene expression via premature termination of transcription (11). Different pathways can cause termination depending on the phosphorylation status of the RNAPII CTD and the presence of various RNA signals and termination factors (11). RNAPII passes through the poly(A)-site (PAS) of the gene's 3'end and pauses before termination (15). Two CTD-dependent termination models have been described to date. The allosteric model proposes that RNAPII recognizes the PAS, and this induces a conformational change in the RNAPII active site, resulting in the release of RNAPII (16). The second model, the torpedo model, illustrates that the nascent transcript is still being synthesized by RNAPII after cleavage at the PAS. 5´-3´exoribonucelase 2 (Xrn2) is

recruited to PAS and degrades remaining downstream RNAPII transcripts. Xrn2 degrades nascent RNA faster than RNAPII synthetizes it. RNAPII is released from the DNA template when Xrn2 catches up with RNAPII (16).

Phosphorylation of RNAPII CTD plays a role in termination. Phosphorylation of Thr4 residues is required specifically for mRNA 3′ end processing and effective termination (17, 18). This pThr4 functions to facilitate recruitment of 3′ processing factors to genes. Like Ser2, Thr4 phosphorylation requires the CTD kinase CDK9 (17).

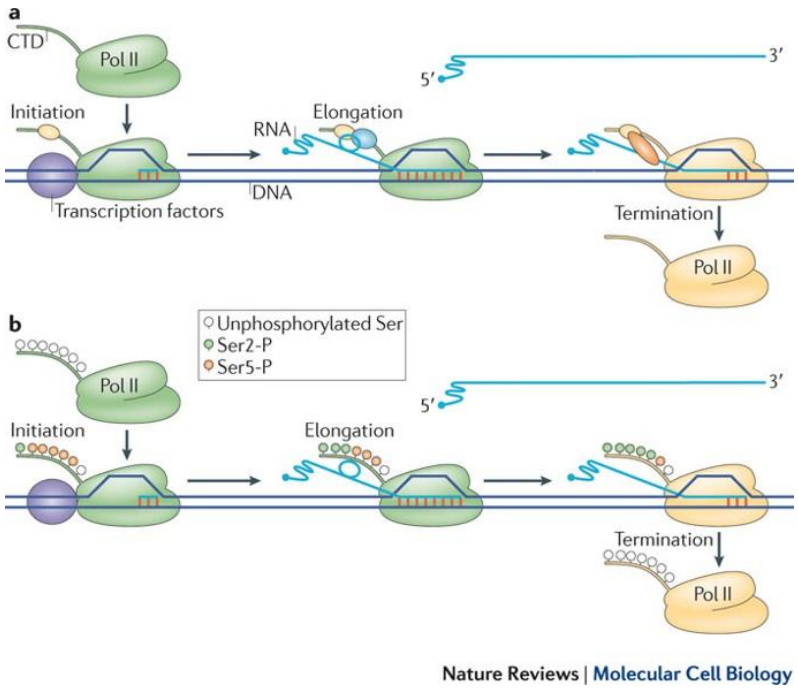

Figure 1.2: Transcriptional regulation by RNA polymerase II. Adapted from Kuehner et al.(11) **a)** Initiation: RNAPII is recruited to a gene promoter by transcription factors. Elongation: a full-length RNA–DNA hybrid is formed and RNAPII proceeds to extend the transcript. Termination: RNAPII terminates RNA synthesis and both RNAPII and the nascent RNA are released from the template. **b)** The phosphorylation status of the CTD heptad repeats changes as RNAPII progresses through the gene. Unphosphorylated RNAPII is recruited into the pre-initiation complexes and it is phosphorylated on Ser5 by CDK7 during initiation and on Ser2 by CDK9, CDK12 and CDK13 during elongation (further discussed below). The action of these kinases sets up a gradient of CTD modification, with Ser5-P and Ser2-P being more prevalent towards the 5′ end and the 3′ end of the gene, respectively. Each phosphorylation shown on the CTD represents a single heptad repeat (not all repeats are shown) with the general phosphorylation patterns indicated (11).

1.1.3 The role of the NELF-complex and PAF1 in transcriptional regulation

A major focus of this work is gene regulation by CDK12 and CDK13, which belongs to the family of cyclin-dependent kinases (CDK). There is a section on CDKs in which their function is described in detail. Briefly, like CDK9, CDK12/CDK13 are shown to phosphorylate RNAPII CTD at serine 2 (pSer2). As written above, pSer2 marks the shift of transcription initiation to elongation.

The NELF complex is composed of four subunits: NELF-A, NELF-B, NELF C/D and NELF-E. NELF binds the polymerase funnel, bridges two mobile polymerase modules, and contacts the trigger loop. This leads to a restraining of RNAPII mobility that is required for pause release (19). This complex binds to the RNAPII-Spt5 interface during early elongation. The NELF subunits have several RNA-binding motifs, which may suggest that RNA recognition could be involved in NELF association with the elongation complex (14). NELF is thought to increase pausing by interacting with RNA protruding from paused RNAPII (15). NELF homologs have not been identified in lower organisms, suggesting that NELF has a specialized role in metazoans (14).

Biochemical studies on NELF indicate that NELF is not required to initiate RNAPII pausing but plays a stabilizing role in the paused complex. The escape of RNAPII from its paused state into productive elongation involves the release of NELF from the RNAPII complex by phosphorylation by P-TEFb (14).

Yu et al. found that RNAPII-associated factor 1 (PAF1) is an important regulator of paused RNAPII release. The PAF complex (PAF) contains the subunits PAF1, LEO1, CTR9, CDC73 and WDR61 and is required for transcription elongation through chromatin (20). PAF1 depletion leads to a substantial release of paused RNAPII into productive elongation, suggesting that PAF1 functions in the maintenance of the paused state (21). P-TEFb directly regulates the initial recruitment of PAF to genes, and the ensuing recruitment of CDK12 is dependent on PAF. These findings show that there is an cooperativity between P-TEFb, PAF and CDK12 in pause release and RNAPII CTD phosphorylation, and they showed that CDK12 is important for RNAPII CTD pSer2 (22). Competition between NELF and elongation factor PAF leads to the discharge of NELF and binding of PAF, and therefore the shift to productive elongation (14).

1.2 Cell cycle and replication

The cell cycle is a complex process, and it involves numerous regulatory proteins that direct the cell through a sequence of events resulting in mitosis. Central to this process are the cyclin-dependent kinases (CDKs), which are dependent on the activation of cyclins to become catalytically active (23). The cell cycle is divided into a synthesis phase (S) and a mitotic segregation phase (M), with two intervenient gap phases (G1 and G2) preceding the S and M phases (24), schematically shown in Figure 1.3. The

progression of the G1 phase is tightly regulated by a “restriction point” in mammals. Cells enter the cell cycle by passing through the “restriction point”. This progression is possible due to a combination of intrinsic factors and extrinsic factors, such as the rate of protein synthesis and mitogenic signaling. However, absence of these factors results in cells exiting the cell cycle. Instead of progression through the cell cycle, the cells will enter a state known as the G0 phase (24).

There are three checkpoints for the cells entering the cell cycle: the G1/S, G2/M and mitotic spindle checkpoints (25). Figure 1.3 illustrates the different phases of the cell cycle. During the G1 phase, the cell synthesizes proteins that are needed for DNA replication and continuous growth. DNA replication takes place during the S phase and is followed by the G2 phase, where the duplicated DNA is checked for errors and repairs are performed. The cell divides into two daughter cells during the M phase. After the mitotic phase, the daughter cells re-enter the G1 phase or go into the cell cycle arrest state, the G0 phase (26).

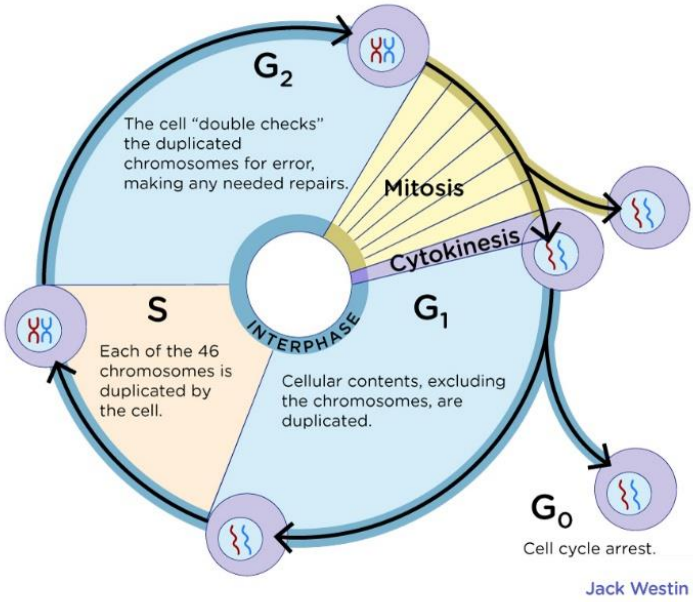

Figure 1.3: Cell cycle phases. Adapted from Jack Westin (25). Cells undergoing cell division proceed through a series of precisely timed and carefully regulated stages of growth, DNA replication, and division that produces two identical (clone) cells (25).

1.2.1 DNA replication

Timely and accurate duplication of DNA by semiconservative replication prior to cell division is required to ensure each daughter cell receives the full complement of chromosomes (27). DNA synthesis starts at distinct sites, called replication origins. It

proceeds in a bidirectional manner until all genomic DNA is replicated (27). Tens of thousands of start sites of DNA replication must be established for every cell cycle. The location and distribution of replication origins throughout the genome define replicons, which are large sequence domains copied by the bidirectional movement of the replication fork away from an origin (28).

DNA replication takes place during the S phase of the cell cycle. Efficient S phase entry is essential for development, tissue repair, and immune defenses. However, accelerated S phase entry causes replication stress, DNA damage and oncogenesis, highlighting the need for strict regulation (29). The cyclin-dependent kinases (CDKs), CDK4, CDK6 and CDK2 largely control the decision to enter S phase. The cell cycle CDKs will be discussed below.

The major stimulus for S phase entry are mitogens, including epidermal, fibroblast, and insulin growth factors (EGF, FGF and IGF). These growth factors activate intracellular signaling by binding cell surface receptors (29). The mitogen-activated protein kinase (MAPK) pathway is one pathway that gets activated. c-Myc is a key transcription factor acting downstream of this pathway, and the activation of c-Myc stimulates S phase entry through regulation of cell cycle genes, including *CCND2* (encoding cyclin D2) (30).

DNA damage is the major inhibitor of S phase entry. DNA is an unstable molecule and suffers numerous single and double strand breaks every day. Oxidative phosphorylation is a significant source of endogenous DNA damage. DNA is also subjected to exogenous damage, such as ultraviolet light and chemo/radio-therapies (29). Experiments have shown that by increasing the concentration of mitogens in the presence of exogenous DNA damage, DNA damage-resistant S phase entry proportionally increases (31). This leads to an interesting conclusion that mitogens and DNA damage are in direct competition with one another to regulate S phase entry (31, 32).

1.2.2 Cell cycle-dependent control and roles of DNA Topoisomerase II

Cell proliferation requires that the genetic information duplicates. The double-stranded DNA enables semiconservative replication. Superhelical tension is being produced when DNA unwinds, and this poses a topological challenge to the replicational process and leads to the entanglement of newly-replicated sister chromosomes (33). These

challenges can be evaded by the help of enzymes known as topoisomerases. Topoisomerases are divided into type I and type II, based on whether they form single- or double-stranded DNA breaks. Both types can alter DNA superhelicity, but type II cut both strands of the DNA helix simultaneously in order to manage DNA tangles and supercoils by the hydrolysis of ATP (33).

Mammalian cells have two topoisomerase II (TOP2) isoforms, TOP2A and TOP2B. TOP2A is essential for all cells and is primarily active during DNA replication and mitosis (34). TOP2B is required for normal development and has roles in transcriptional regulation of gene expression (33). Nielsen et al. (35) used an ultrafast protein depletion system in human cells to dissect the mitotic-specific function of TOP2A. They showed that TOP2A is necessary for keeping the structure of chromatids together once they have formed (maintenance), in addition to being involved in the establishment of the mitotic chromosome (35).

Topoisomerase inhibitors are frequently used in cancer therapy due to its ability to block the ligation step of the cell cycle, which generates DNA single- and double-strand breaks, leading to apoptotic cell death (36). Numerous anticancer agents for specific cancer types have been developed. However, traditional and non-specific anticancer drugs are still important for the treatment of many cancers that do not respond to or have developed resistance to cancer-specific anticancer agents (37). TOP2A are proven a therapeutic target of anticancer and antibacterial drugs. TOP2A-targeting anticancer drugs act through topoisomerase poisoning. This leads to replication fork arrest and double-strand break formation. However, this unique mechanism is associated with the development of secondary cancers and cardiotoxicity. Therefore, designing novel TOP2A poisons have been suggested as safer anticancer drugs (37).

1.3 Cyclin dependent kinases

The mammalian cell cycle is controlled by a subfamily of cyclin-dependent kinases (CDKs). CDKs are serine/threonine kinases and their catalytic activities are regulated by interactions with cyclins and CDK inhibitors (CKIs). CDKs were first discovered by genetic and biochemical studies in model organisms such as yeasts and frogs in the 1980s. This work established the importance of CDKs in promoting transitions through the cell cycle (38).

The CDK family consist of 20 kinases which are divided into two subclasses: cell cycle regulating kinases, including CDK1, CDK2, CDK4 and CDK6, and the transcription-associated CDKs, including CDK7, CDK8, CDK9, CDK12 and CDK13, which are critical regulators of gene expression (39). The CDKs range in size from approximately 250 amino acid residues to proteins of more than 1,500 residues. They consist of amino- and/or carboxy-terminal extensions of variable lengths. CDKs play important roles in the control of cell division, and they regulate transcription in response to several extra- and intracellular signals. The transcription-associated CDKs regulate gene transcription by phosphorylating the carboxy-terminal domain (CTD) of the RNAPII (40).

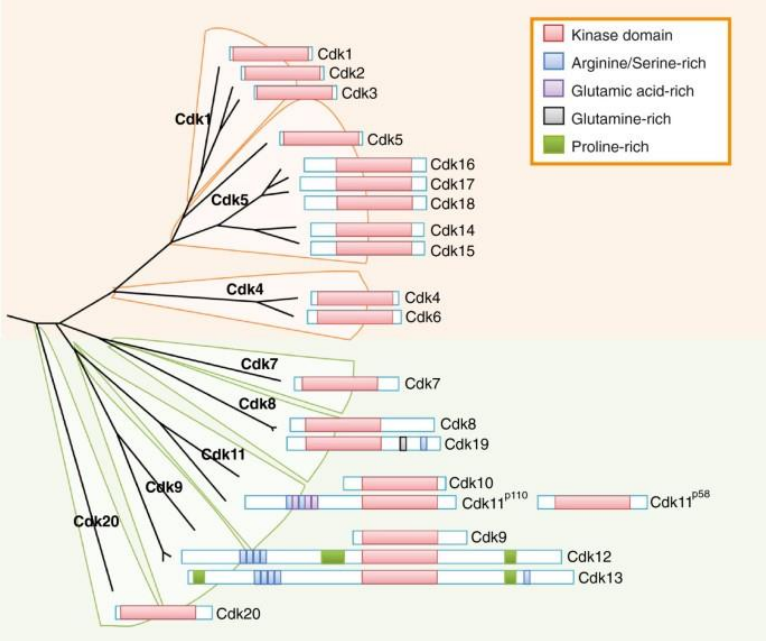

Figure 1.4: Evolutionary relationships among the mammalian CDK subfamilies. The name of the different CDK subfamilies functioning in the cell cycle (orange) or transcription (green) is shown in boldface, and the domain structure of the individual proteins is depicted. The conserved protein kinase domain (red) and some additional domains (see key) are indicated for each CDK. Human cells contain two separate genes, Cdk11A and Cdk11B, each of them encoding a long isoform, Cdk11p110, and a shorter protein, Cdk11p58, generated by an internal ribosome binding site. The phylogenetic tree is based on the comparison of the human kinase domains. Adapted from Malumbres et al. (38).

1.3.1. Regulation of cell cycle by cyclin-dependent kinases

The cell cycle is driven by a certain subset of CDK–cyclin complexes that are directly involved in the process. Cyclins are synthesized and destroyed at specific times during the cell cycle, and they are therefore regulating kinase activity in a timely manner. The CDKs include three interphase CDKs (CDK2, CDK4 and CDK6), a mitotic CDK (CDK1) and ten cyclins that belong to four different classes (A-, B-, D- and E-type cyclins) (41).

The D-type cyclins preferentially bind and activate CDK4 and CDK6 during G1, leading to the detection of mitogenic signals. CDK2/cyclin E complexes further phosphorylate

and inactivate the pocket proteins RB, RBL1 and RBL2. Later CDK2 is activated by cyclin A2 in the G2 phase to make the transition from S phase to mitosis. CDK1 is activated by A-type cyclins to enable the start of mitosis (41). The activity of the cell cycle CDKs is deregulated in cancer cells due to genetic or epigenetic changes in either the CDKs, their regulators or upstream mitogenic pathways (41).

1.3.1.1 Cyclin-dependent kinase 1

The cyclin-dependent kinase 1 (CDK1) drives cell division and cycle. CDK1 is a 297 amino acids protein and plays a key role in the control of eukaryotic cell cycle. CDK1 is the only essential CDK and is activated by binding to B-type cyclins, mainly cyclin B1, which then phosphorylates substrates critical for entry into mitosis (42). It modulates the centrosome cycle, promotes G2-M transition, regulates G1 progress and G1-S transition (43).

In Michowski et al., they uncovered that a large fraction of CDK1 substrates in embryonic stem (ES) cells is localized on chromatin. CDK1 phosphorylates many proteins involved in epigenetic regulation, including writers and erasers of all major histone marks. Consistent with these findings, they noticed that the inhibition of CDK1 altered histone-modification status of ES cells (44), lending support to the idea that CDK1 activity is also involved in regulating transcription.

1.3.1.2 Cyclin-dependent kinase 2

Cyclin-dependent kinase 2 (CDK2) is a 298 amino acids protein and plays an important role in cell cycle regulation and is involved in multiple biological processes (45). CDK2 is activated by Cyclin E and Cyclin A (46). CDK2/Cyclin E regulates cell cycle re-entry, G1 progression and S phase entry. CDK2/cyclin A operates later in the cell cycle and manages S phase progression and operates in G2 and M phase cells (46). CDK2 interacts with and phosphorylates proteins involved in DNA and RNA metabolism, intracellular transport, DNA damage, signal transduction, protein degradation and translation. In many human cancers, CDK2 is deregulated (45).

In Chi et al. they discovered 117 candidate CDK2 substrates, where approximately 40% were known CDK substrates, by in situ phosphorylation. Novel candidate substrates included proteins regulating histone modifications, chromatin, transcription, and RNA/DNA metabolism (46).

1.3.1.3 Cyclin-dependent kinase 4

Cyclin-dependent kinase 4 (CDK4) is a 303 amino acids protein which is activated by the D-type cyclins. It is important for the G1 phase progression, and its activity is restricted to the G1-S phase. CDK4 has been shown to phosphorylate retinoblastoma gene product (Rb) (47).

1.3.1.4 Cyclin-dependent kinase 6

Cyclin-dependent kinase 6 (CDK6) is a 326 amino acids protein and is, like CDK4, also activated by the D-type cyclins. Its functional activity is similar to CDK4. This kinase, as well as CDK4, has been shown to phosphorylate, and therefor regulate the activity of, tumor suppressor protein Rb (48). This phosphorylation of Rb relieves the inhibition on the E2 factor (E2F), allowing the activation of genes necessary for promoting S phase entry and DNA synthesis (49). CDK4 and CDK6 share a lot of similarities in their kinase activities. However, CDK6 has been discovered to have additional functions that differs from that of CDK4. CDK6 has been reported to be involved in the differentiation of T cells, which is unique to this kinase (50).

1.3.2 Regulation of transcription by transcriptional cyclin-dependent kinases

Members of the transcription-associated CDKs (tCDKs) phosphorylate the CTD of RNAPII in multiple steps during the transcription cycle to coordinate gene expression (51). tCDKs have important roles in cell proliferation and gene expression. They are deregulated in many cancers and have motivated efforts aimed at therapeutic targeting of CDKs. The tCDKs are central to orchestration of the transcription cycle and its coordination with cotranscriptional processes such as RNA capping, splicing, 3' end formation, export, and regulation of the chromatin landscape (52). CDK8 is a subunit of the Mediator complex and helps organize the pre-initiation complex (PIC) upon transcription initiation. Further transition into productive elongation, termination and 3´end processing involves CDK7, CDK9, CDK12 and CDK13 (51).

1.3.2.1. Cyclin-dependent kinase 7

Cyclin-dependent kinase 7 (CDK7) is a 346 amino acid protein that together with Cyclin H and MAT1 form a CDK-activating kinase (CAK) (40). CDK7 phosphorylates the CTD as well as functioning as a CDK-activating kinase, activating cell cycle and transcriptional CDKs (53). CDK7 is a component of TFIIH, which is important in releasing RNAPII from the PIC. RNAPII is largely unphosphorylated during initiation, which allows for stabilizing interactions of the unmodified CTD with the Mediator

complex. CDK7 phosphorylates the CTD at Ser5 and Ser7 upon initiation (14). TFIIH phosphorylates CDK9/P-TEFb, indirectly activating promoter-proximal pause release of RNAPII (54). CDK7/CAK-mediated CTD pSer5 additionally aids the recruitment of capping enzymes to nascent mRNA (55). The role of Ser7 phosphorylation is still being questioned, but it is suggested that that this modification helps prime the CTD for following phosphorylation events.

1.3.2.2. Cyclin-dependent kinase 8

Cyclin-dependent kinase 8 (CDK8) is a 464 amino acid protein that together with Cyclin C, MED12 and MED13 associate with the Mediator (56). The Mediator complex connects the processes between RNAPII and transcription factors, promoters and enhancers. It binds to enhancers and recruits RNAPII to core promoters, making it a required subset in most RNAPII-generated transcripts in mammals. The Mediator co-localizes with CDK8, and CDK8 is found at enhancers as well (57). Additionally, CDK8 phosphorylates transcription factors STAT1 and SREBP (58, 59).

CDK8 is also involved in negative regulation, as well as its role in positive transcriptional regulation. CDK8 is found to repress transcription initiation by disrupting the interaction between Mediator and RNAPII (60).

1.3.2.3. Cyclin-dependent kinase 9

Cyclin-dependent kinase 9 (CDK9) is a 372 amino acid protein that binds to Cyclin T or Cyclin K (CycK) to gain its catalytic activity of phosphorylating RNAPII CTD. CDK9 is critical for RNAPII transcription initiation, elongation, and termination (61). CDK9 and Cyclin K form the P-TEFb, which is necessary in global regulation of gene transcription. P-TEFb phosphorylates CTD Ser2, NELF and DSIF after promoter-proximal pausing. This phosphorylation leads RNAPII into productive elongation (62). CDK9 also phosphorylates transcription termination factor Xrn2, making it crucial in transcription termination (63).

1.3.2.4. Cyclin-dependent kinase 12

Cyclin-dependent kinase 12 (CDK12) is, compared to the other transcriptional CDKs, a large protein of 1,490 amino acids (64). It binds to Cyclin K and has catalytic activity to RNAPII Ser2 and possibly Ser5 (65). CDK12 associates with RNAPII as it elongates into the gene body and pSer2 levels increase significantly across gene bodies, with a peak at the 3′ ends (14).

CDK12 consist of proline-rich motifs that are involved in protein-protein interactions, arginine/serine-rich motifs involved in pre-mRNA processing, a kinase domain and a carboxy-terminal domain that assists in its interaction with Cyclin K (64).

Chirackal Manavalan et al. used a chemical genetic approach to inhibit analog-sensitive CDK12. They found that CDK12 kinase activity is required for transcription of core DNA replication genes and therefore for G1/S progression. Furthermore, they revealed that CDK12 inhibition triggers an RNAPII processivity defect characterized by a loss of mapped reads from 3′ends of predominantly long, poly(A)-signal-rich genes. Their experiments showed that CDK12 catalytic activity represents a novel link between regulation of transcription and cell cycle progression (66).

Other studies shed light on the importance of CDK12. Upon CDK12/CDK13 inhibition by a small molecule inhibitor THZ531, a decrease in CTD pSer2 strengthens the growing belief of CDK12 comprising an important role in the phosphorylation of RNAPII CTD Ser2 (67).

1.3.2.5 Cyclin-dependent kinase 13

Cyclin-dependent kinase 13 (CDK13) is closely related to CDK12, compared to the other transcriptional CDKs. It consists of 1,512 amino acids and share a 43% sequence identity with CDK12 (64). In similarity to CDK12, CDK13 also reacts with Cyclin K to gain catalytic activity (68). CDK12 is the best studied of the two, while less is known about the function of CDK13.

In addition to P-TEFb, CDK12 and CDK13 also phosphorylates the RNAPII CTD Ser2, and they contribute to the majority of the modification of Ser2, as well as possibly phosphorylating Ser5 (65). CDK12 and CDK13 are evolutionary related and structurally similar kinases. It has recently been demonstrated that CDK12 and CDK13 activity is necessary to prevent TSS-proximal early termination as RNAPII elongates through the gene body (69).

Table 1.1. Most extensively studied CDKs and their known physiological roles

CDKs	Cyclin partner(s)	Cellular functions
CDK1	Cyclin A, B1	DNA structure checkpoints during late G2 and the spindle assembly checkpoint during mitosis
CDK2	Cyclin A	Control of G1-S phase of cell cycle (DNA replication)
	Cyclin E1, E2	Rb/E2F transcription
CDK3	Cyclin C	Control of interphase NHEJ-mediated DNA damage repair
CDK4	Cyclin D	Control of G1 phase of cell cycle, Rb/E2F transcription
CDK5	p35, p39, Cyclin I	Senescence, post-mitotic neurons
CDK6	Cyclin D	Control of G1 phase of cell cycle, Rb/E2F transcription
CDK7	Cyclin H	CAK RNAP II transcription (initiation to elongation)
CDK8	Cyclin C	RNAP II transcription (transcriptional repressor)
CDK9	Cyclin T1, T2a, T2b	RNAP II transcription
	Cyclin K	DNA damage response
CDK10	Cyclin T	G2/M transition, suppression of Ets2 transactivation domain
CDK11	Cyclin L	G2/M transition, RNA processing
CDK12	Cyclin K	RNAP II transcription
CDK13	Cyclin K	RNAP II transcription

G1: growth phase; S: DNA synthesis; G2: second growth phase; M: mitosis; CDKs: cyclin-dependent kinases; Rb: retinoblastoma protein; NHEJ: non-homologous end joining; RNAP II: RNA polymerase II; CAK: cdk-activating kinase; E2F: E2 transcription factor; Ets2: E26 transformation-specific transcription factor 2. Table obtained from Juric et al. (70).

1.3.3 Inhibitors of cyclin-dependent kinases

Dysregulated cell division and gene dysregulation are key hallmarks of cancer (71). As mentioned above, cell division is mainly controlled by cyclins and CDKs. Therapeutic targets that block cell division would therefore be effective for cancer treatment (72). CDKs are found naturally in both non-tumor cells and tumor cells, which make them attractive therapeutic targets. CDK inhibitors have been studied since the 1990s. The first generation of CDK inhibitors are pan-CDK inhibitors, including Flavopiridol and Roscovitine (see table 1.2). The main function of these inhibitors is to block cell cycle and inhibit cell proliferation by inhibiting the CDK enzyme activity (71).

To date, CDK inhibitors (CKIs), like Palbociclib, have been approved for the treatment of metastatic hormone receptor positive breast cancer, specifically CKIs targeting

CDK4 and CDK6 (72). SY-1365, a CDK7 inhibitor, has shown initial encouraging data in phase I for solid tumors treatment (71).

Table 1.2. List of various CDK inhibitors and their target-CDKs

Name of CKI	Target-CDKs
Palbociclib (PD-0332991)	CDK4, CDK6
Roscovitine (CYC202)	CDK2, CDK5
SNS-032 (BMS-387032)	CDK2, CDK5, CDK7, CDK9
Dinaciclib (SCH727965)	CDK1, CDK2, CDK5, CDK9
Flavopiridol (L86-8275)	CDK1, CDK2, CDK4, CDK6, CDK7, CDK9
AT7519	CDK1, CDK2, CDK3, CDK4, CDK5, CDK6, CDK9
Flavopiridol (L86-8275) HCl	CDK1, CDK2, CDK4, CDK6, CDK7
JNJ-7706621	CDK1, CDK2, CDK3, CDK4, CDK6
SY-1365	CDK7
THZ531	CDK12, CDK13

Table obtained from Selleck Chemicals (73).

1.4 Gliomas

Glioma is a type of tumor that occurs in the brain and spinal cord (74). Gliomas are the most common primary tumors in the brain, accounting for 81% of central nervous system (CNS) malignancies (75). The number of new cases of gliomas per year can be estimated at around 14 per 100 000 person worldwide, and the risk of glioma increase with age, exposure to radiation and family history of gliomas (74).

The tumors can be produced by three types of glial cells. Gliomas are classified according to the type of glial cell involved in the tumor, as well as the tumor's genetic features (74). Symptoms are diverse and vary by location, manifesting as focal neurologic deficits, encephalopathy, or seizures (76).

The types of gliomas include astrocytomas, ependymomas and oligdendrogliomas. These three types include different subgroups of gliomas. Astrocytomas consist of astrocytoma, anaplastic astrocytoma and glioblastoma. Ependymomas include anaplastic ependymoma, myxopapillary ependymoma and subendymemoma. Oligodendrogliomas consist of oligodendroglioma, anaplastic oligodendroglioma and anaplastic oligoastrocytoma (74).

1.4.1. Glioblastoma

Glioblastoma multiforme (GBM) is the most lethal form of glioma, and <5% of patients survive longer than 5 years post diagnosis. The number of new cases of glioblastomas per year can be estimated at around 250,000 worldwide (74). Treatment options for patients with glioblastoma are limited, and there have been made many attempts to clarify the underlying mechanisms of gliomagenesis (77). The most advanced treatments involve combinations of surgery, radiotherapy and chemotherapy with drugs such as temozolomide (TMZ). According to genome-wide genomic and epigenomic analyses, mutations in epigenetic modifiers occur frequently in gliomas and dysregulation of epigenetic mechanisms is closely associated with glioma formation (77). GBM tumors harbour genomic alterations that lead to the constitutive activation of CDKs, resulting in tumor proliferation. Novel therapeutic approaches are urgently needed for both newly diagnosed and recurrent GBM patients (70).

1.4.2 Transcriptional dysregulation in gliomas

Essentially all cancers have genomic alterations that lead to the constitutive activation of CDKs, resulting in the proliferation of cancer cells (70). Combined with endocrine therapy, CDK inhibitors (CKIs) are currently in clinical use for treatment of breast cancer. The kinase activity of CDK-cyclin complexes is highly controlled by an abundance of CKIs, which serve as brakes to control cell-cycle progression according to the conditions in cells (70). It is now clear that CDKs, cyclins and CKIs play critical roles in cellular processes such as cell cycle, transcription, mRNA processing, epigenetic regulation, metabolism, stem cell self-renewal and differentiation of nerve cells (39). Different proteins and transcription factors serve as interesting targets for cancer treatment, and several experiments have been done to investigate this. Given that GBM is the most lethal form of glioma, it is urgent to discover novel treatments. In the following section, research on multiple CDKs and transcription factors and their effects on cancer treatment are explained.

The roles of CDKs in the intracellular control of the cell cycle and regulation of transcription and DNA repair make them highly suitable as targets of inhibitors for the treatment of cancer (70). In Meng et al., they discovered that the covalent CDK7 inhibitor THZ1 was one of the top hits in their anti-GBM screening. Additionally, CDK7 inhibition through CRISPR-Cas9 or RNA interference markedly disrupted GMB cell growth (78). Another paper, Greenall et.al., focused on high-grade glioma (HGG) (79).

They tested the activity of THZ1 on patient-derived primary HGG cell lines. THZ1 disturbed the transcriptome and disabled CDK activation, leading to cell cycle arrest at G2 and DNA damage. It also affected transcription of the nuclear-encoded mitochondrial ribosomal genes and inhibited the expression of receptor tyrosine kinases. Furthermore, THZ1 disrupted nuclear, Cajal body and nuclear speckle formation, resulting in reduced cytosolic translation and malfunction of the spliceosome and therefor leading to irregular mRNA processing. These findings indicate that CDK7 is crucial for gliomagenesis and provide new insight into the cellular processes that are affected by THZ1 and induce antitumor activity (79).

A similar study has been performed on a CDK9 inhibitor. In Rhun et al., they used a novel CDK9 inhibitor called TG02 (80). This inhibitor acts mainly via CDK9 inhibition-dependent depletion of short-lived oncoproteins such as MCL-1 and c-MYC. The study was conducted on long-term glioma cell lines and glioma-initiating cell lines. They discovered that TG02 exhibits strong anti-tumor cell activity, and that TG02 is a highly potent apoptosis-inducing agent in glioma cells in vitro, supporting the clinical evaluation of TG02 in glioblastoma (80).

A large number of tumorigenic events in brain cancer drive proliferation through the recruitment of CDKs in the G1 phase of the cell cycle. Furthermore, genomic instability in GBM is related to disturbances in the S phase and G2/M transition controlled by CDKs (81). Pre-clinical studies and clinical trials have generated mixed results over the past two decades. Testing of the effectiveness of CDK inhibitors (CKIs) has given a non-definite conclusion with regard to the efficiency of these inhibitors (81).

For instance, highly selective CDK4/CDK6 inhibitors, palbociclib and abemaciclib, induce cell cycle blockage through inhibition of Rb1 phosphorylation (82). In nearly 80% of human gliomas the cyclin D1-CDK4/CDK6-Rb pathway is altered (83). This suggests both inhibitors as promising agents in glioma treatment, and both palbociclib and abemaciclib have demonstrated an advantage in in vivo studies (82).

Bromodomain protein 4 (Brd4) plays critical roles in development, cancer progression, and virus-host pathogenesis (84). Brd4 regulates gene expression through its ability to bind to acetylated lysines (Kac) residues of histone tails, followed by recruiting the positive transcription elongation factor b (P-TEFb) to phosphorylate RNAPII (85). Brd4 dislocates negative regulators from P-TEFb, transforming it into an active form that can

phosphorylate RNAPII and thereby, this recruitment of P-TEFb stimulates transcription (84). In recent years, several BRD4 inhibitors have entered clinical trials and achieved exciting results in tumor treatment (86). One of these inhibitors is called JQ1. BRD4 expression in glioma tissues are significantly higher than in normal tissues and cells (87). Cheng et al. (88) discovered the antitumor effects of JQ1 by treating *ex vivo* cultures derived from xenografts of primary GBM cells. JQ1 induced G1 cell-cycle arrest and apoptosis. Liu et al. (89) demonstrated that JQ1 suppressed aggressive growth of GBM cells carrying oncogenic epidermal growth factor receptor (EGFR) mutations.

RNAPII-associated factor 1 (PAF1) modulates the release of paused RNAPII into productive elongation (21). Zhang et al. (90) demonstrated that endogenous circular RNAs (circRNAs) generated from a long noncoding RNA encodes regulatory peptides. They discovered several peptides potentially encoded by circRNAs, including a peptide encoded by the circular form of the long intergenic non-protein-coding RNA *p53*-induced transcript (*LINC-PINT*) that suppresses glioblastoma cell proliferation in vitro and in vivo. This peptide directly interacts with PAF and inhibits the transcriptional elongation of multiple oncogenes. The expression of this peptide and its corresponding circRNA are decreased in glioblastoma compared with the levels in normal tissues (90).

A central theme in Pandey group is to identify and characterize novel genes which can be used to target glioma cells with a focus on targeting factors which contribute to the transcriptional dysregulation in glioma cells. Ongoing work in the Pandey lab found that inhibition of CDK12/CDK13 compromises the proliferation of glioma cells and leads to a near total transcriptional shutdown. Furthermore, the CDK12/CDK13 inhibition disrupts the cell cycle of glioma cells and leads to a rapid shutdown on DNA replication, which was difficult to reconcile as a downstream effect of transcriptional shutdown. Through my project, we have aimed to identify and characterize the CDK12/CDK13 dependent total- and phospho-proteome changes in glioma cells to elucidate the effect of CDK12/CDK13 inhibition on DNA replication.

2. Aim of study

In the present study, we wanted to elucidate interaction partners of CDK12 in HeLa and mouse embryonic stem cells. Due to challenges in validation of interaction partners, we decided to investigate the phospho- and total-proteome of glioma cells after inhibition of CDK12/CDK13. We investigated the roles of CDK12/CDK13 in transcription and DNA replication, among other pathways, by examining the CDK12/CDK13-inhibition's effect on phospho- and total-proteome.

3. Materials and methods

3.1 Cell line and cultivation

3.1.1 Cell line

In this study, HeLa Kyoto cells (Riken, Japan, available in the Pandey lab) and mouse embryonic stem cells (E14, available in the Pandey lab) were used to investigate CDK9's, CDK12´s and CDK13's interaction partners. Glioma cells, G7 and G144 (available in the Pandey lab, originally derived by Pollard et al, 2009 (91)), were used to investigate total- and phospho-proteome after inhibition of CDK12/CDK13. The HeLa cell line was the first human cell line, originally derived from Henrietta Lacks, a female patient who in 1951 died from an aggressive adenocarcinoma of the cervix (92).

3.1.2 Thawing

Cells were collected from a N_2- container and immediately thawed at 37°C for 5-10 minutes. The cell suspensions were subsequently resuspended in appropriate cell media (see section 3.1.5) and transferred to an appropriate plate (Table 1). Cells were incubated at 37°C in a humidified chamber containing 5% CO2.

3.1.3 Coating for embryonic stem cell culturing

Dishes used for mouse embryonic stem cell culturing were coated with 0.1% gelatin (Sigma) in MQ-H_2O for at least 1 hour at 37°C, according to table 1.

Table 1. Volumes and cell density for culturing ES cells in different plates sizes. K, $\times 10^3$, M, $\times 10^6$.

Size	To culture cells	To coat	TrypLE	PBS+TI	Cells seeded
Tray	70 (50-100) mL	50 mL	8 mL	30 mL	10-20 M
15 cm	20 (16-25) mL	10 (8-12) mL	1,5 mL	8-12 mL	3 (2-10) M
10 cm	10 (7-12) mL	5 (4-6) mL	1 mL	4-9 mL	2,5 (1-5) M
6 cm	4 (3-5) mL	2 (1,5-3) mL	350 µL	1-4 mL	0,5 (0,2-1) M
6-well	2 (1,5-3) mL	1 (0,8-1,5) mL	200 µL	1 mL	200 (50-500) K
12-well	1 (0,5-2) mL	0,5 (1) mL	100 µL	1 mL	100 (20-200) K
24-well	1 (0,5-1,2) mL	0,5 (0,3-1) mL	50 µL	1 mL	50 (10-100) K

3.1.4 Coating for glioma cell culturing

Dishes used for the glioma cell culturing were coated with 500 ng/mL poly-D-lysine ([PDL], Merckmillipore A-003-E) in 1x PBS (Oslo University Hospital) for 1 hour at 37°C. PDL was aspirated before the dishes were coated with 200 ng/mL laminin (RD systems) in 1x PBS for at least 3 hours, according to the volumes listed in table 1.

3.1.5 Cell cultivation

Cell culture is a process where cells are removed from the organism and introduced into an artificial environment with favorable conditions for growth.

The three different cell lines were cultured in Falcon® Cell Culture Dishes (Corning) of required size. The HeLa cell line's cultural needs were acquired in Dulbecco´s Modified Eagle Medium (DMEM) - high glucose, with a 10% concentration of fetal bovine serum ([FBS], SigmaAldrich®) and 1% Penicillin-Streptomycin (Thermo Fisher Scientific).

The mouse embryonic stem cells were cultured in embryonic stem cell media and the glioma cells were cultured in neural stem cell media. Media compositions for ES cell media and neural stem cell media are listed in supplementary "7.1 Media compositions".

Cells were cultivated at 37°C in a humidified chamber containing 5% CO_2. When reached a confluency of approximately 80%, the cells were counted and seeded according to table 1.

3.1.6 Cell splitting

Adherent cell cultures have to be split in order to preserve cell viability, and to maintain exponential log-phase growth.

Cells were split by gently aspirating media and adding appropriate amount of TrypLE™ (Gibco) to the dish (Table 1). To detach the cells, the dish was tapped, and if necessary, incubated at 37°C for ~1 minute. Appropriate volume (table 1) of PBS+TI (500 mL 1x PBS and 100 mg Trypsin inhibitor (Glycine max soybean, Sigma)) was added and pipetted to obtain detached and dispersed cells. The cell suspension was centrifuged at 1200g for 5 minutes in Megafuge 1.0 tabletop refrigerated centrifuge (Heraeus Instruments) to create a cell pellet, and the supernatant was aspirated. The pellet was resuspended in 1 mL media by pipetting up and down to create a single cell suspension. The cell suspension was counted with Countless II FL (Invitrogen) and the

appropriate number of cells were transferred directly a dish containing the media (HeLa cells) or to a laminin- or gelatin-coated dish (glioma cells and mES cells, respectively) containing the media (table 1).

3.2 Treatments

3.2.1 THZ531 treatment

THZ531 inhibits CDK12/13 catalytic activity (93). The mechanism behind will be described in detail in chapter 4, subsection 4.2. Glioma cells, G7 and G144, were treated with 0.5 µM THZ531 (MedChemExpress) diluted in culture medium and incubated at 37ºC for 1 hour and 6 hours. 0.0003% dimethyl sulfoxide ([DMSO], Sigma-Aldrich®) in culture medium was used as control.

3.3 Cell lysis, protein isolation- and quantification

3.3.1 Cell lysis

Cell lysis was performed to extract the proteins from the cells.

Adherent cell cultures were either washed in cold PBS, scraped off the plate and collected in cold 1.5 mL Eppendorf tubes, or leftover cells from cell splitting were centrifuged, supernatant was discarded, and cell pellet was collected in 1.5 mL Eppendorf tubes. Cell suspensions were centrifuged in Microcentrifuge 5424 R (Eppendorf®) at 1000g for 5 minutes at RT, and excessive PBS/media was removed. Cells were resuspended with 3-4 times pellet size High Salt (HS) buffer (subsection 7.2.1) supplemented with protease inhibitors (1 µg/ml aprotinin ([AP] Sigma-Aldrich®), 1 µg/ml leupeptin ([LP], Sigma-Aldrich®) and 1 mM dithiothreitol (DTT) (Saween & Werner) and incubated on ice for 5-10 minutes to allow for complete lysis of cells. Cell lysate was transferred to new cold sonication tubes and sonicated in Bioruptor® Pico sonication device (Diagenode) 30s ON/OFF for 10 cycles at 4°C. Protein extracts were then incubated on ice for 10 minutes. Lysate was subsequently centrifuged at 15.000rpm for 10 minutes at 4°C in a microcentrifuge, and supernatant was transferred to a new cold 1.5 mL tube.

3.3.2 Measurement of protein concentration

Protein concentration was measured with Bradford Protein Assay. 800 µL MQ-H2O supplemented with 200 µL Protein Assay Dye Reagent Concentrate (Bio-Rad) and 2 µL protein sample were mixed in disposable cuvettes (Bio-Rad). As blank control, protein sample was replaced with HS buffer used in protein samples. Solutions were

mixed thoroughly. Absorbance was measured at 595 nm using a Smartspec Plus Spectrophotometer (Bio-Rad). Protein concentration was further calculated from absorbance values based on the standard curve “y=15,266*x-1,1232”. This standard curve was generated earlier and used by the group.

3.3.3 Co-immunoprecipitation

Co-immunoprecipitation is a biochemical method used to isolate proteins of interest from cell lysate. The concept is to investigate the proteins binding the immunoprecipitated protein. The method takes advantage of antibody-recognition of target molecule (94). In this study, GFP Trap Magnetic Agarose affinity beads (Chromotek) were applied to purify GFP-CDK12 from whole cell HeLa and mES lysate. Whole cell lysate was first thawed on ice. 50 µL GFP Trap Magnetic Agarose beads was transferred to a 1.5 mL Eppendorf tube and resuspended in 1 mL HS buffer supplemented with protease inhibitors (AP and LP) and DTT, before magnetic separation was performed using a magnetic rack. This washing step was repeated once, before HS buffer was discarded. 1 mL HS buffer (subsection 7.2.1) supplemented with protease inhibitors and DTT and 1 mg lysate (calculated by Bradford Protein Assay, subsection 3.3.2) was subsequently added to the beads, and tumbled at 4°C ON.

The following day, beads were washed in 1 mL ice cold HS buffer supplemented with protease inhibitors and DTT, followed by a magnetic separation to discard the buffer. Beads were subsequently washed x2 in 1 mL cold Washing buffer (subsection 7.2.1) supplemented protease inhibitors, before magnetic separation. Washing buffer was discarded. Beads were subsequently washed x1 in cold PBS and again separated in the magnetic rack where PBS was discarded. Bead-bound protein was eluted by incubation at 95°C, in 100 µL NuPAGE™ LDS Sample Buffer (4X) ([LSB], Thermo Fisher Scientific) supplemented with 100 mM Dithiotreitol ([DTT], Saveen Werner AB), for 5 minutes. The Eppendorf tube was subsequently centrifuged at 1200g for 1 minute at RT, and eluate was transferred to a new Eppendorf tube.

3.4 Western blot

Western blotting is a technique in cell and molecular biology that is used to detect specific proteins in complex cell homogenates. Proteins are separated by electrophoresis based on molecular weight, transferred to a membrane and incubated with antibodies specific to the target protein (95).

All buffer compositions are listed in supplementary “7.2.2 Western blotting”.

Five rounds of blotting procedures were executed in this study. The first round of western blot experiments was performed to detect CDK9-, CDK12- and CDK13-GFP in mES cells. The second round was conducted to determine successful IP of CDK9-, CDK12- and CDK13- GFP in mES cells. The third round was executed to detect CDK12-GFP in HeLa cells. The fourth round was performed in order to determine successful IP of CDK12-GFP in HeLa cells, while the last round was performed on glioma cells in order to validate results from MS analysis.

3.4.1 Sample preparation

The cell lysates were thawed on ice, before diluted in MQ-H2O and LSB to obtain equal protein concentration in all samples (usually 2 µg/µL). Prepared samples contained 50 µg protein. 10% DTT was added to each sample to reduce disulfide bonds of proteins, and samples were heated at 95°C for 5 minutes for truly denaturation of protein tertiary structure, before they were loaded on the gel.

3.4.2 Protein separation by sodium dodecyl sulfate-polyacrylamide gel electrophoresis

Protein extracts were separated by sodium dodecyl sulphate-polyacrylamide gel electrophoresis (SDS-PAGE). Protein samples were loaded on 6- or 8% NuPAGE® Novex Tris-Glycine gels (Thermo Fisher Scientific) or 10% BoltTM Bis-Tris Plus gels (Thermo Fisher Scientific), respectively with 1X Tris-Glycine SDS Running Buffer (Thermo Fisher Scientific) or 1X NuPage® MOPS SDS Running Buffer (Thermo Fisher Scientific), both diluted in dH2O. All gels were run in XCell SureLock Mini-Cell chamber (Thermo Fisher Scientific). Precision Plus Protein™ Dual Color Standards (Bio-Rad) was used as a ladder and loaded in the first well, and protein samples were loaded in the following wells. Proteins were separated at 120 Volt for ~1,5 hours.

3.4.3 Blotting

The protein gel was then transferred to Trans-Blot® Turbo™ 0.2 µm nitrocellulose Single Application membrane (Bio-Rad), before proteins were transmitted from gel to membrane in a Trans-Blot® Turbo™ Transfer System (Bio-Rad) at 25V for 2x 10 minutes.

The protein-containing membrane was covered with Ponceau S solution (SigmaAldrich®) for 5 minutes at RT to stain the proteins on the membrane, before

briefly de-stained in TBS-T (subsection 7.2.2) and then incubated in blocking solution (5% skim milk powder (Sigma-Aldrich®) in TBS-T), for 1 hour at RT or overnight (ON) at 4°C. Thereafter, primary antibodies (table 2) were diluted in blocking solution, and the membrane was subsequently incubated in primary antibody-solution on a shaking platform for 2 hours at RT or at 4°C ON. Excess primary antibody was washed off with 1% blocking milk for 3x10 minutes. Secondary antibodies (table 3) were diluted in blocking solution. The membrane was incubated in secondary antibody solution on shaking platform for 45 minutes at RT, before washed 3x10 minutes in TBS-T.

Table 2. Primary antibodies used in western blotting.

Antibody	Host species	Dilution	Producer	Catalog nr.
mAb Anti-Vinculin	Mouse	1:10.000	Sigma-Aldrich®, Germany	V9131
pAb Anti-GFP	Rabbit	1:50.000	Abcam, UK	ab6556
pAb LEO1	Rabbit	1:100.000	Bethyl Laboratories, USA	A300-175A
pAb CDC73	Rabbit	1:20.000	Bethyl Laboratories, USA	A300-170A
mAb CDK12	Rabbit	1:1000	Cell Signaling Technology, USA	11973S
mAb CDK9	Rabbit	1:5000	Cell Signaling Technology, USA	C127F
pAb CDK13	Rabbit	1:2000	Bethyl Laboratories, USA	A301-458A
mAb TOP2A	Rabbit	1:500	Abcam, UK	ab52934
mAb p-TOP2A	Rabbit	1:10.000	Abcam, UK	ab75765
pAb NELF-A	Rabbit	1:10.000	Bethyl Laboratories, USA	A301-910A
pAb NELF-B	Rabbit	1:5000	Bethyl Laboratories, USA	A301-911A

Abbreviations: mAb = monoclonal antibody, pAb = polyclonal antibody.

Table 3. HRP (horseradish peroxidase)-conjugated secondary antibodies.

Target protein	Dilution	Producer	Catalog nr.
Anti-Rabbit IgG, HRP conjugate	1:5000	Sigma-Aldrich®, Darmstadt, Germany	12-348
Anti-Mouse IgG, HRP conjugate	1:5000	Sigma-Aldrich®, Darmstadt, Germany	A9917

Abbreviations: IgG = immunoglobulin G, HRP = horseradish peroxidase.

Detection of proteins on the membrane was conducted by SuperSignal™ West Pico PLUS Chemiluminiscent Substrate (Thermo Fisher Scientific). Membrane was incubated in these reagents for 5 minutes, before the mix was wiped off. Pictures were conducted with the ChemiDoc™ MP system (Bio-Rad).

3.5 Total- and phospho-proteome by mass spectrometry

Mass spectrometry is a technique that identifies chemical substances by sorting of gaseous ions in electric and magnetic fields according to their mass-to-charge ratios (96). Mass spectroscopes consist of five basic parts. 1) a high vacuum system, 2) a sample handling system, where the sample is introduced, 3) an ion source, where a beam of charged particles characteristic of the sample can be produces, 4) an analyzer, where the beam is separated into its components, and 5) a detector which collects the separated ion beams (96). The method was in this study performed to identify total- and phospho-proteome in glioma cells after inhibition of CDK12/CDK13, to gain insight into the role of CDK12/CDK13 in transcription and cell cycle.

3.5.1 Cell preparation

6 million glioma cells were seeded in 2x10-cm plates per condition (1 hour THZ531 treatment, 6 hours THZ531 treatment and 6 hours DMSO treatment) on day 1. The following day, the cells were treated for the indicated time. The THZ531 treated cells were treated with 0.5 µM THZ531 in culture media, while the control cells were treated with 0.0003% DMSO in culture media. PBS+ was made by adding 250 µL AP/LP and a tablet of cOmplete Protease Inhibitor Tablet (Roche). Right before use, a PhosSTOP™ tablet (Roche) was added to the PBS+. After THZ531 treatment, the media was decanted, and the plates were put on ice. 1 mL of cold PBS+ was subsequently added to the plates. The cells were harvested by scraping the plates and transferred to a 1.5 mL Eppendorf tube. The cell suspensions were centrifuged in Microcentrifuge 5424 R (Eppendorf®) at 2000 rpm for 5 minutes, and the supernatant

was carefully removed. The cell pellets were snap-frozen in liquid N_2 and delivered to the Proteomic Core Facility at Oslo University Hospital, Rikshospitalet, for conducting liquid chromatography tandem mass spectrometry (LC-MS/MS).

3.6 Analysis of mass spectrometry data

3.6.1 Venn diagram analysis

Venn diagrams were provided by the use of Venny 2.1.0 software (97).

3.6.2 Gene list annotation and analysis

The Metascape software (98) was used to interpret gene lists provided from MS analysis. For functional annotation, enrichment analysis was performed. This is a tool containing gene annotation portals to sort and visualize significantly enriched clusters in the input gene list. Terms with a p-value < 0.05, a minimal overlap of 3, and an enrichment factor > 1.5 were clustered based on their similarities.

3.6.3 Network analyses

Proteomic analyses were first conducted in Metascape software for sorting of proteins into functional groups, before visualized in Cytoscape software (99). To gain a better understanding of the functional groups, Enrichr (100) and MSigDB (101) were used. Moreover, the STRING protein network tool (102) in Cytoscape was used to determine interactions between proteins.

3.6.4 Statistical analysis

All statistical analyses were performed in Microsoft® Excel software. Data was analyzed, and significant differences investigated using Student´s t-test, 2-tailed, equal variance.

4. Results

4.1. Experimental setup

4.1.1. Generation of CDK9-, CDK12- and CDK13-GFP in mouse embryonic cells

We first wanted to identify interaction partners of CDK9, CDK12 and CDK13 in mouse embryonic stem cells (mES cells), E14. We chose to focus on CDK12 and CDK13, while keeping CDK9 as a control, since all of these CDKs phosphorylate serine-2 of RNAPII CTD. Our approach was to establish CDK9-/12-/13-GFP BAC-tagged mES cells with the idea that we can differentiate them into mouse neural progenitor cells (mNPC), since the mNPCs have similar proteome to glioma cells, which is a central theme of the research of our team. The E14 cells were transfected with recombinant bacterial artificial chromosome (BAC) CDK9-GFP, CDK12-GFP and CDK13-GFP. G418 selection was done followed by single cell sorting to make stable cell lines, leaving four cell lines to study: E14 negative control, E14 CDK9-GFP, E14 CDK12-GFP and E14 CDK13-GFP. This establishment of BAC-tagged mES cells were conducted before my arrival in the lab. To be able to validate interaction partners of these proteins, the proteins needed to be successfully immunoprecipitated.

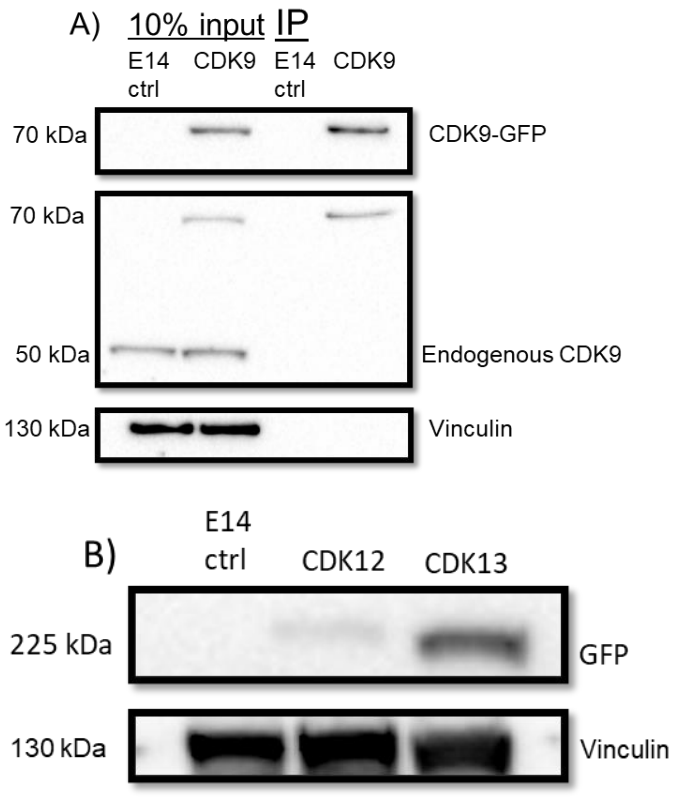

Figure 4.1. Western blot analyses of CDK9-GFP, CDK12-GFP and CDK13-GFP in E14 cells. Western blot analysis on untransfected (CTRL) and CDK9-GFP (CDK9) transfected E14 cell lysates. The panel represents protein analysis of 10% input lysate and immunoprecipitated (IP) proteins (A). Upper panel represents anti-GFP stained lysate, the middle panel represents anti-CDK9 stained lysate, while the bottom panel represents anti-vinculin stained lysate. (B) visualizes a western blot using primary antibodies against GFP done on untransfected (CTRL), CDK12-GFP and CDK13-GFP transfected cell lysates. Lower panel represents anti-vinculin stained lysate as positive control.

CDK9-GFP was successfully pulled down using GFP magnetic beads (figure 4.2, (A)). This immunoprecipitation turned out to be harder to perform on CDK12-GFP and CDK13-GFP and no IP was valid. Figure 4.1 (B) shows a western blot using primary antibodies against GFP. The CDK12 band is very weak, but both CDK12-GFP and CDK13-GFP were present in the input cell lysate. When we were not able to immunoprecipitate CDK12-GFP and CDK13-GFP, we chose to focus on HeLa cells, which had been used in a previous study in the Pandey lab (67).

4.1.2. Validation of CDK12-GFP immunoprecipitation

Sigrid Berg's data revealed that chromatin-bound CDK12 using ChIP (Chromating immunoprecipitation) interacts with transcription regulation factors NELF-E, NELF-C/D, CDC73 and FIP1L1 in HeLa cells (67). The HeLa cells were in this study transfected with recombinant bacterial artificial chromosome (BAC) CDK9-, CDK12- and CDK13-GFP. She performed a chromatin immunoprecipitation (ChIP) and ChIP-MS. ChIP is a technique used to investigate the interaction between proteins and chromatin in the cell.

CDC73 is part of the PAF1-complex together with LEO1, among other proteins. PAF1 is a transcriptional elongation factor, and an earlier study had reported that PAF1 interacts with CDK12 and regulated transcription (103). Therefore, we decided to validate the interaction of CDK12 and PAF1 complex after immunoprecipitation (IP) of lysates from the same HeLa cells that was earlier generated by Sigrid Berg. CDK12-GFP was pulled down using GFP magnetic beads to look at proteins directly interacting with CDK12. The negative control is non-transfected HeLa cells.

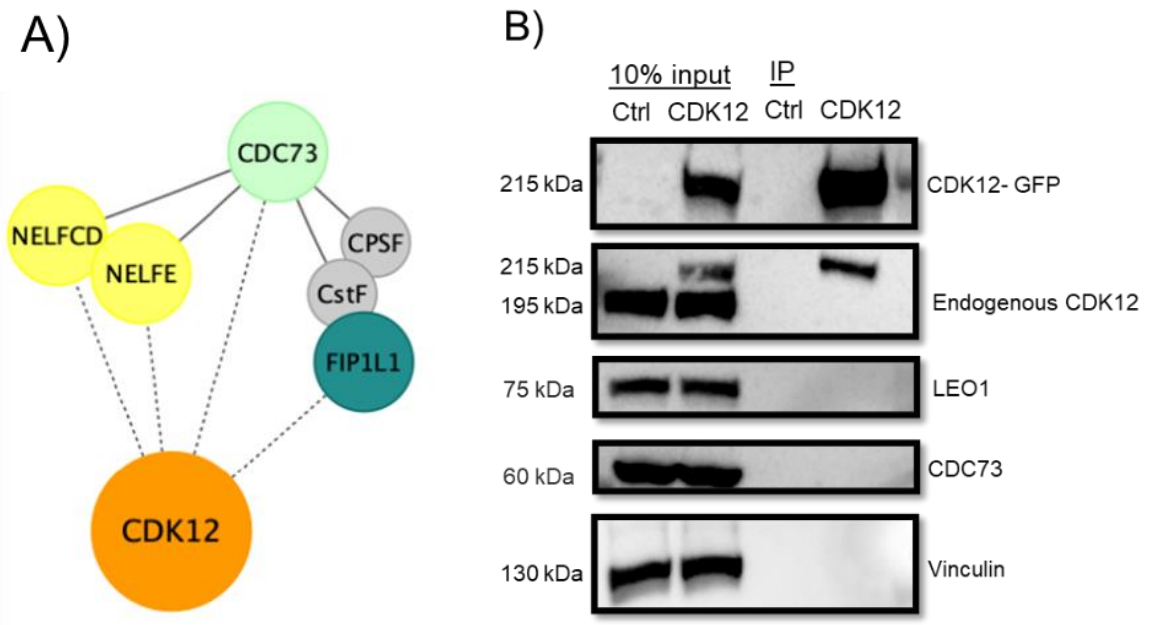

Figure 4.2. Validation of the interaction between CDK12 and PAF1-complex in HeLa cells. The interaction network in (A) represents interaction of CDK12 to transcription regulating factors. MS data revealed chromatin-bound CDK12 to interact with transcription regulation factors NELFE, NELFCD, CDC73 and FIP1L1. This interaction was found in a previous thesis written for Pandey lab (67). To try to validate this interaction we did a western blot (B) with CDK12-immunoprecipitated HeLa cells. Primary antibodies against GFP, CDK12, LEO1, CDC73 and vinculin (in descending order) were used on the untransfected (CTRL) and CDK12-GFP transfected HeLa cell lysates. We could not see any interaction between CDK12 and LEO1 and CDC73, which are part of the PAF1-complex.

The immunoprecipitation was successful as viewed in figure 4.2 (B). CDK12-GFP was pulled down as shown in the IP lanes of the western blot and the negative control is correctly blank. LEO1 and CDC73 were detected together with CDK12 when assessing the cell lysate, but we could not confirm an interaction of CDK12 with LEO1 and CDC73 in the IP samples (Fig 4.2; IP lane). We similarly attempted to validate the interaction between CDK12 and the NELF-complex, but these western blot analyses were also unsuccessful. We failed to detect the interaction of CDK12 with either PAF1 or NELF complex members. We therefore decided to work on the second project described in the following section.

4.2. Identification and characterization of total and phospho-proteome dependent on CDK12/CDK13 in glioma cells

Through other projects carried out in the group, we have found that inhibition of CDK12/CDK13, either pharmacologically or by knock-out of CDK12/13, compromises proliferation of glioma cells, but not the proliferation of control cells. Furthermore, earlier work has also found that CDK12/CDK13 inhibition disrupts the cell cycle of glioma cells and leads to a rapid shutdown on DNA replication, shown in Figure 4.3 (ongoing work, Pandey lab).

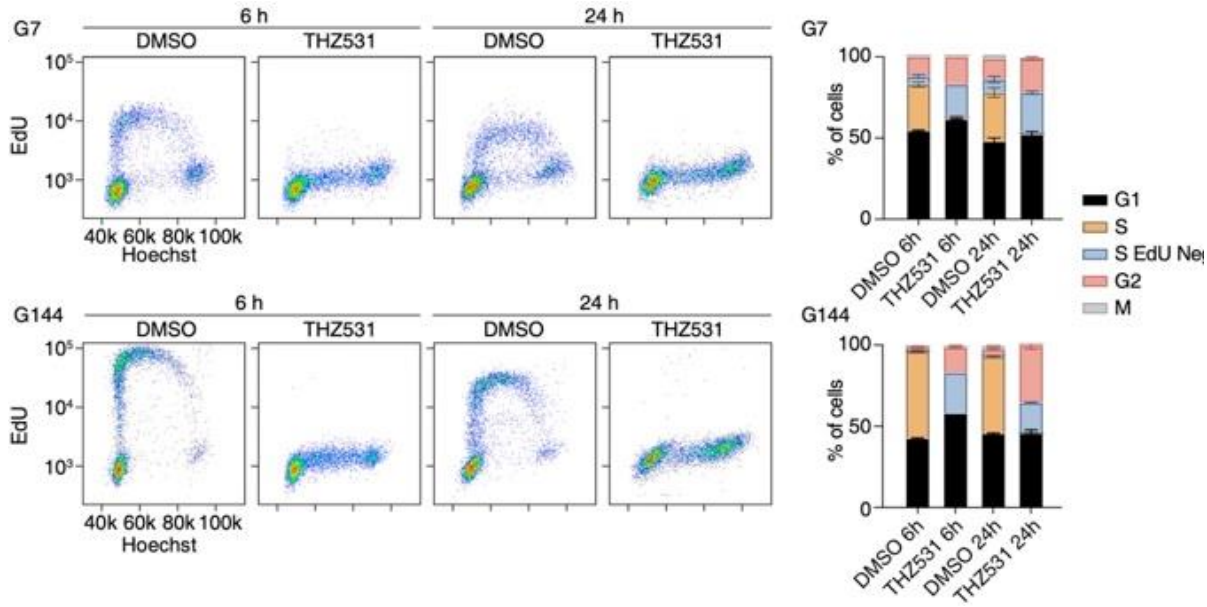

Figure 4.3. (A). Cell cycle analysis in G7 and G144 cells after 6- and 24-hours treatment with either vehicle alone (DMSO) or 500 nM THZ531. Replication was measured by addition of 1 µM EdU 3 hours prior to harvest. The flow cytometry data analyses included only viable, non-apoptotic, single cells. The dot plots show intensity of EdU (Alexa Flour 647) relative to DNA content (Hoechst 33258) in 6283 interphase cells (one representative replicate shown). (B) Cell cycle distributions in the samples were defined by combined flow cytometry analysis of DNA content, EdU incorporation and pS10HistoneH3-staining (mitosis). Stacked bar graph show mean cell cycle fractions with SD error bars from two biological replicates.

The effect on DNA replication after inhibition of CDK12/13 was rapid and strong which led us to hypothesize that this is independent of the effect CDK12/13-inhibition has on transcription (67). Since CDK12 and CDK13 are kinases with kinase activity ascribed towards serine-2 of RNA polymerase, we decided to investigate the effect of CDK12/CDK13 inhibition with THZ531 on total- and phospho-proteome in glioma cells, G7 and G144.

THZ531 is a specific inhibitor of CDK12/13 (93). THZ531 is found to covalently inhibit both CDK12 and CDK13 by modification of the Cys-1039 residue, which is situated nearby the active site. THZ531 additionally interacts with the ATP binding site to prevent ATP binding (93). Together, these two features of THZ531 blocks the catalytic activity of CDK12/13. THZ531 is further found to downregulate expression of DDR genes in Jurkat cells, consistent with the role of CDK12 in DDR gene transcription, and to significant downregulate key Jurkat transcription factors (93). In addition, THZ531 dramatically induced apoptotic cell death, and may therefore help identify cancer subtypes that are particularly dependent on their kinase activities (93). Since then, THZ531 has been used regularly as selective inhibitor of CDK12/13 (104, 105).

The glioma cells were in this experiment treated with 500 nM THZ531 or DMSO as control for 1 hour and 6 hours. 500 nM THZ531 was applied for two reasons, a) to capture the primary effects of CDK12/CDK13 inhibition and b) the transcriptional studies were done using the same conditions (ongoing work, Pandey lab).

4.2.1 Alterations in G7 and G144 cells' proteome during THZ531 conditions

To organize total- and phospho-proteome in glioma cells after THZ531 inhibition for 1 hour and 6 hours, Venny 2.1.0 software was applied to visualize which proteins are downregulated and upregulated for the two different cell lines. The intensity values log2 transformed were used for all the following methods described in chapter 4. The Venn diagram in figure 4.4 represents proteins of the total- and phospho-proteome that are upregulated and downregulated, comparing 1 hour treatment and 6 hours treatment of THZ531.

A)

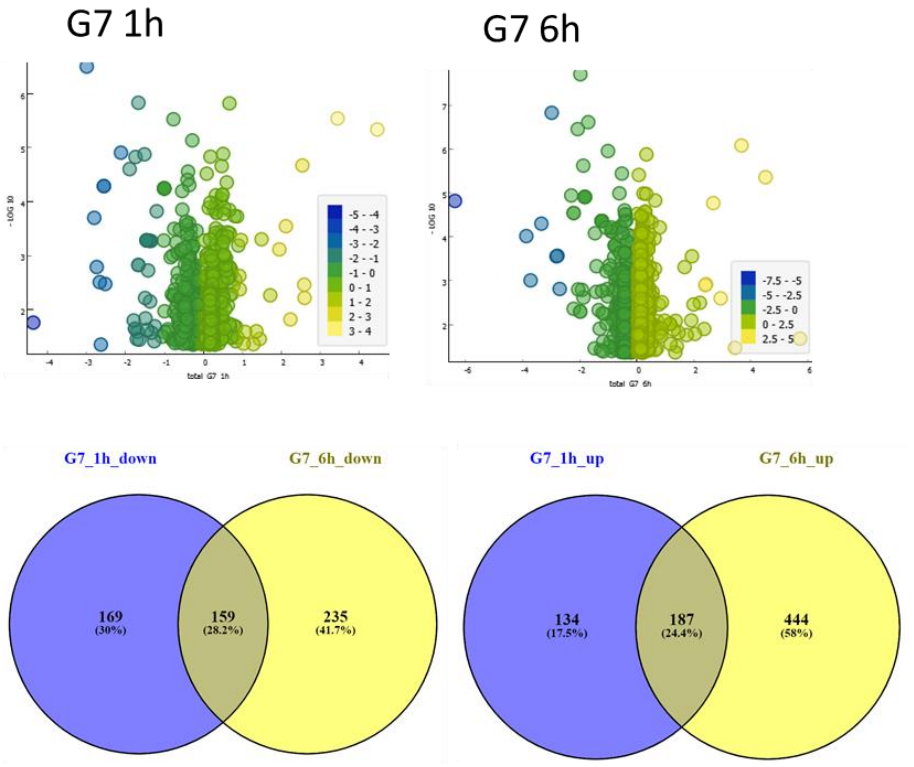
G7 1h
G7 6h
G7_1h_down
G7_6h_down
169
(30%)
159
(28.2%)
235
(41.7%)
G7_1h_up
G7_6h_up
134
(17.5%)
187
(24.4%)
444
(58%)

B)

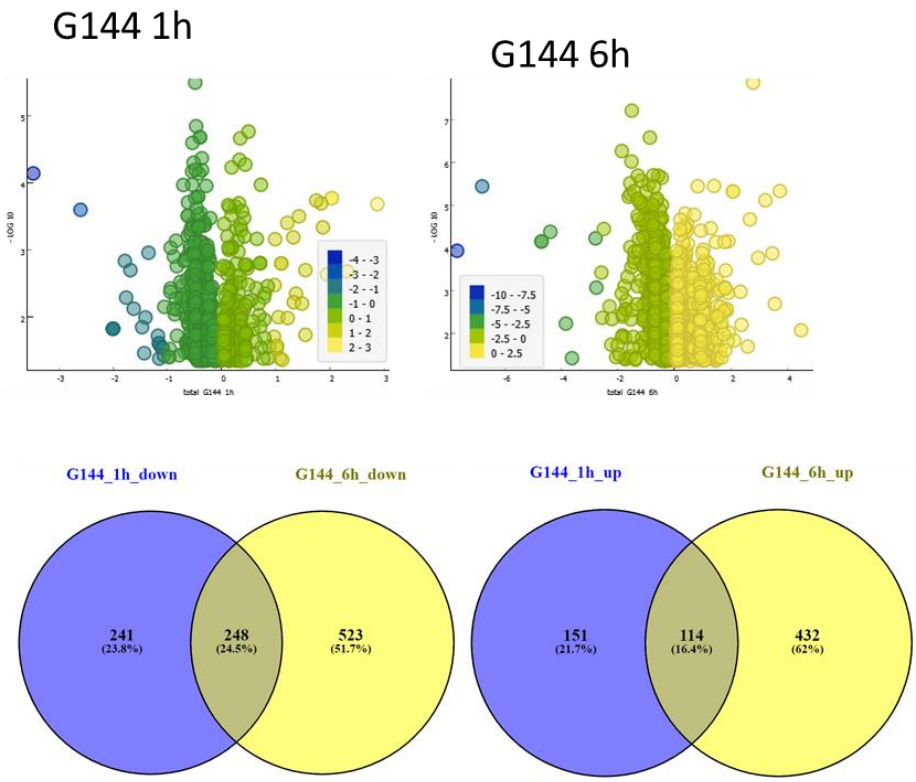
G144 1h
G144 6h
G144_1h_down
G144_6h_down
241
(23.8%)
248
(24.5%)
523
(51.7%)
G144_1h_up
G144_6h_up
151
(21.7%)
114
(16.4%)
432
(62%)

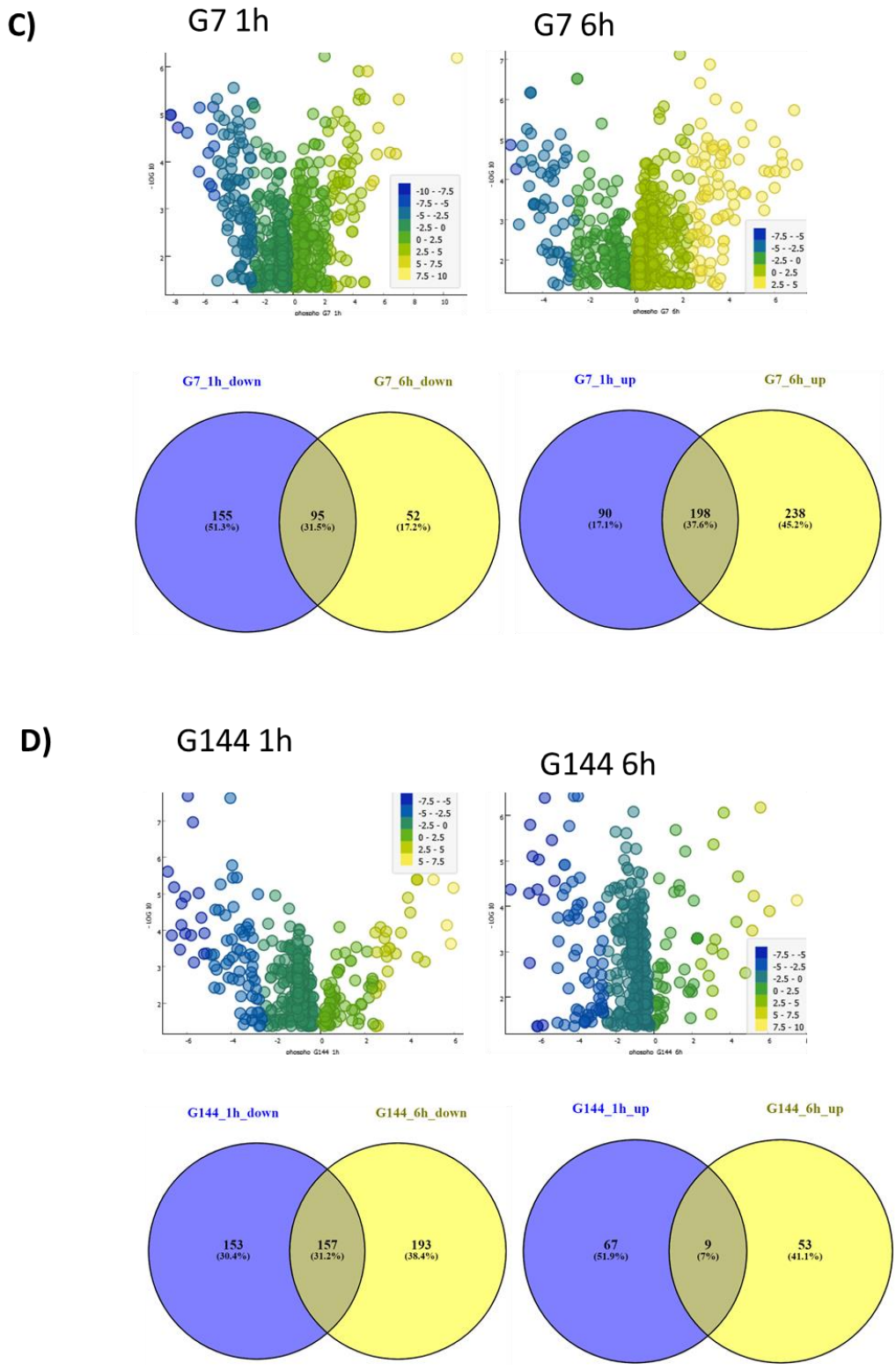

Figure 4.4. Volcano plots and Venn diagrams displaying shared and distinct proteins after CDK12/13 inhibition. MS results from CDK12/13-inhibition MS, compiling total- and phospho-proteome after 1 hour and 6 hours treatment of THZ531. The volcano plots visualize the distribution of proteins from downregulated to upregulated in the different conditions. (A) and (B) represent total-proteome, while (C) and (D) represent phospho-proteome. The Venn diagrams show proteins being upregulated or downregulated after inhibition of CDK12/13 and which proteins are down-/upregulated after both 1h and 6h treatment. The figures were obtained using Venny 2.1.0 software and Orange 3.28. software.

(A) represents cell line G7 for the total-proteome. There are 159 proteins in common between the 1h and 6h THZ531 inhibition in the G7 downregulated Venn diagram. In the G7 upregulated Venn diagram, 1h and 6h inhibition have 187 proteins in common. There is a smaller percentage of upregulated proteins in common compared to proteins that are downregulated (24,4% compared to 28,2% in G7 downregulated). (B) represents cell line G144 for total-proteome. There are 248 proteins in common between 1h and 6h THZ531 inhibition in the G144 downregulated Venn diagram. In the G144 upregulated Venn diagram, there are 114 proteins in common (16,4% compared to 24,5% in the downregulated Venn diagram). (C) represents cell line G7 for the phospho-proteome. There are 95 proteins in common between 1h and 6h inhibition in the G7 downregulated Venn diagram. 1h and 6h inhibition have 198 proteins in common in the G7 upregulated Venn diagram (37,6% compared to 31,5% in G7 downregulated). (D) represents cell line G144 for the phospho-proteome. There are 157 proteins in common between 1h and 6h inhibition in the G144 downregulated Venn diagram. In the G144 upregulated Venn diagram there are 9 proteins in common (7% compared to 31,2% in the downregulated Venn diagram). The volcano plots were made with Orange 3.28 software (106). The y-axis represents -log10 transformed p-value and the x-axis represents intensity values log2 transformed. The total-proteome volcano plots (A and B) have less spread than the phospho-proteome volcano plots (C and D).

After inhibition of CDK12/13, multiple proteins were affected and were either downregulated or upregulated. Figure 4.4 shows the distribution of affected proteins.

4.2.2 Heatmap analysis of CDK12/13 inhibited total- and phospho-proteome

Heatmaps were constructed to visualize which proteins were downregulated and which ones were upregulated. The protein lists generated from the MS were split into four different lists: Phospho-proteome downregulated, phospho-proteome upregulated, total-proteome downregulated and total-proteome upregulated. The two different cell lines with their different conditions were combined in the four lists. In the heatmaps (A) and (C) the downregulated proteins were sorted out of our data, meaning that the proteins were downregulated in at least one out of four conditions. In heatmaps (B) and (D) the upregulated proteins were sorted out, where the specific protein is upregulated in at least one out of four conditions. The phospho-proteome

downregulated list consists of 674 proteins, while the phospho-proteome upregulated list consists of 590 proteins. The total-proteome downregulated list consists of 1366 proteins, and the total-proteome upregulated list consists of 1278 proteins. All these proteins were declared as significant hits after the MS analysis compared to the DMSO negative control. The heatmaps were constructed in the Orange 3.28. software without clustering. The protein lists were put into the software, and the heatmaps were constructed automatically.

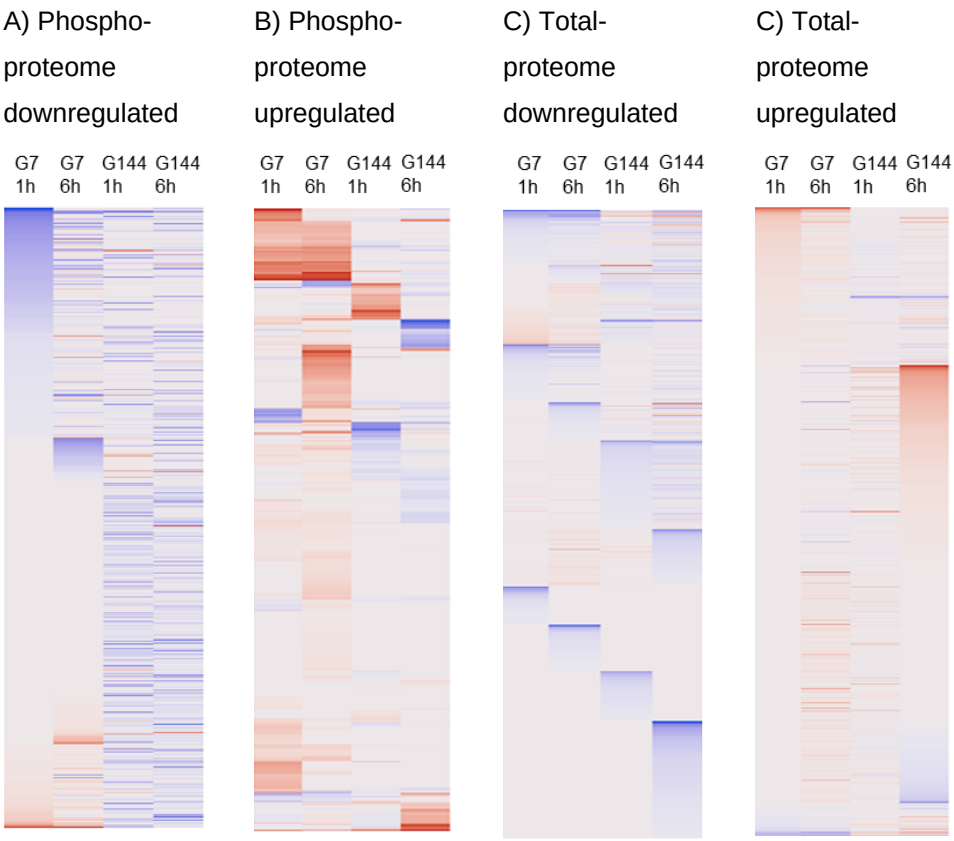

Figure 4.5. Heatmaps showing the distribution of downregulated and upregulated proteins. Results from CDK12/13-inhibition MS shows which genes are downregulated and which genes are upregulated compared to the control cells treated with DMSO. Blue color represents the downregulated genes and red color represents the upregulated genes. When the color approaches white, the closer the value is to 0.

The stronger the blue or red color is, the stronger the protein is down-/upregulated. The nearly white color in the heatmaps represents proteins that have a log2 transformed p-value close to zero, meaning that they are not heavily upregulated or downregulated even though they are significantly changed compared to the DMSO negative control. There are a lot of these proteins in our lists, as visualized in the heatmaps.

The heatmaps in figure 4.5 show the distribution of proteins that are downregulated and the ones that are upregulated in the four different protein lists. Given the large size of the lists, we decided to reduce the number of proteins as described in 4.2.3.

4.2.3 Enrichment analysis of CDK12/13 inhibited total- and phospho-proteome

The MS run identified 500-800 significant proteins in the four different phospho-proteome runs, while the total-proteome run identified between 600-1300 proteins for the four different conditions. Some proteins were present multiple times in the lists and were therefor filtered out.

Enrichment analysis was performed in the Metascape software to identify enriched functional groups of total-proteome and phospho-proteome (figure 4.6). Terms with a p-value < 0.05, a minimal overlap of 3, and an enrichment factor > 1.5 were clustered based on their similarities. Darker color and longer bars indicate a lower p-value, and a lower p-value indicate lower chance of that the observed enrichment is obtained by randomness. The input protein list was compared to Gene Ontology (GO) Biological Processes, Reactome Gene Sets and the TRRUST database (human and mouse transcriptional regulatory networks).

A) Phospho-proteome downregulated

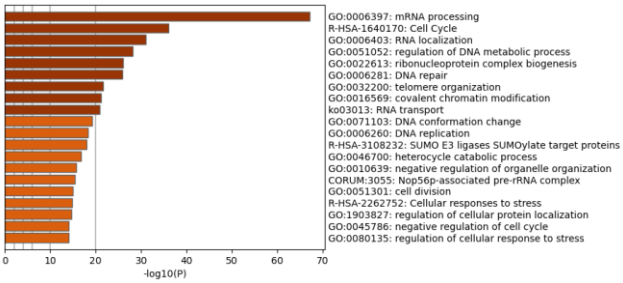

B) Phospho-proteome upregulated

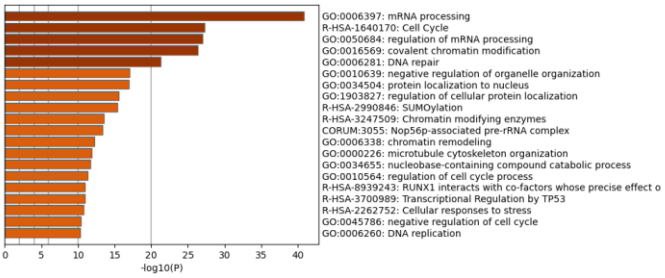

C) Total-proteome downregulated

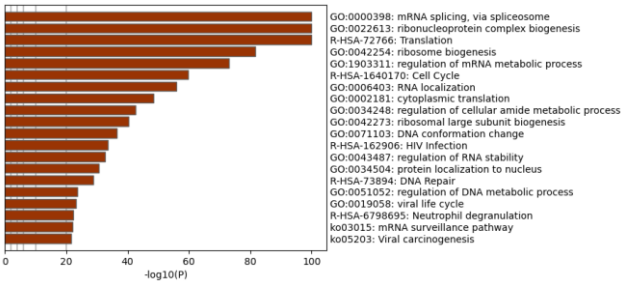

D) Total-proteome upregulated

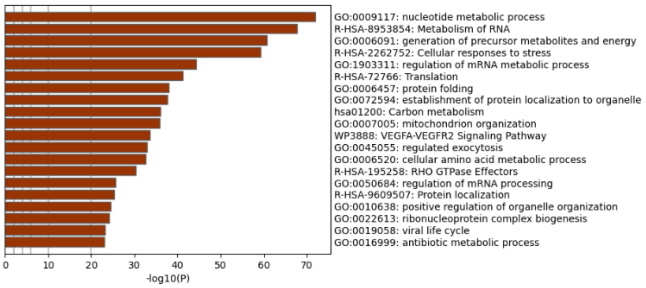

Figure 4.6. Enriched terms of CDK12-inhibited proteome identified by Metascape. Bar graph of Gene Ontology (GO), Reactome Gene Sets and TRRUST enriched terms analyzed in Metascape. Statistical significance is indicated by p-value, in which darker color and longer bars implies a lower p-value.

The total-proteome bar graphs have an overall lower p-value than the phospho-proteome bar graphs. The statistical significance of the total-proteome's enriched terms are therefore higher than that of phospho-proteome, where mRNA processing is prominent for the phospho-proteome.

After the first enrichment analysis, we decided to pull out the proteins that were present in at least three out of the four conditions. This sorting was performed to minimize the number of proteins and to rule out proteins that were only significant in one or two of the conditions, leaving a "gap" in the remaining two or three conditions. We focused on these new protein lists for the rest of the analyses. The new protein lists were reduced to less than 300 genes after this extraction. A new enrichment analysis was performed on these lists under the same conditions as mentioned above (figure 4.7).

A) Phospho-proteome downregulated

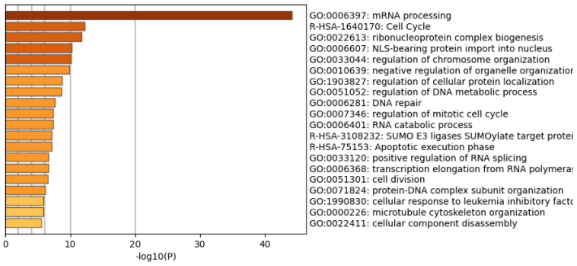

B) Phospho-proteome upregulated

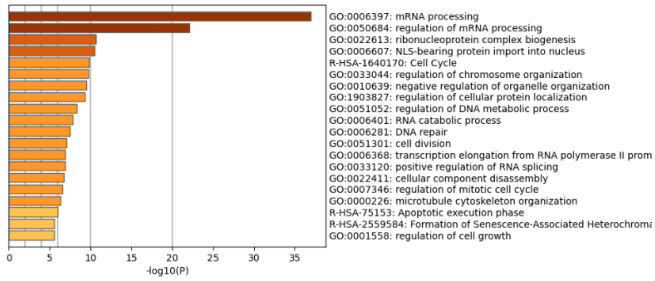

C) Total-proteome downregulated

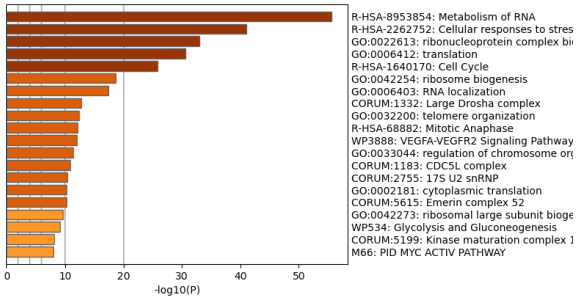

D) Total-proteome upregulated

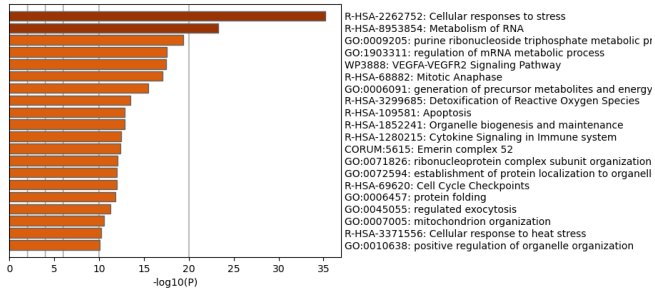

Figure 4.7. Enriched terms of CDK12-inhibited proteome identified by Metascape. Bar graph of Gene Ontology (GO), Reactome Gene Sets and TRRUST enriched terms. Proteins present in at least three out of our four conditions were analyzed in Metascape. Statistical significance is indicated by p-value, in which darker color and longer bars implies a lower p-value.

The order of the enriched terms changed with these new conditions. mRNA processing clearly stands out for the phospho-proteome, both upregulated and downregulated. The total-proteome enriched terms are no longer as significant statistically as in figure 4.6.

4.2.4 Heatmaps of top five enriched functional groups after CDK12/CDK13 inhibition

Heatmaps were constructed from the top 5 enriched functional groups from the newly developed protein lists. Figure 4.8, A to E, visualizes the top 5 enriched groups for the phospho-proteome downregulated proteins, and F to J visualize the top 5 enriched groups for the phospho-proteome upregulated proteins.

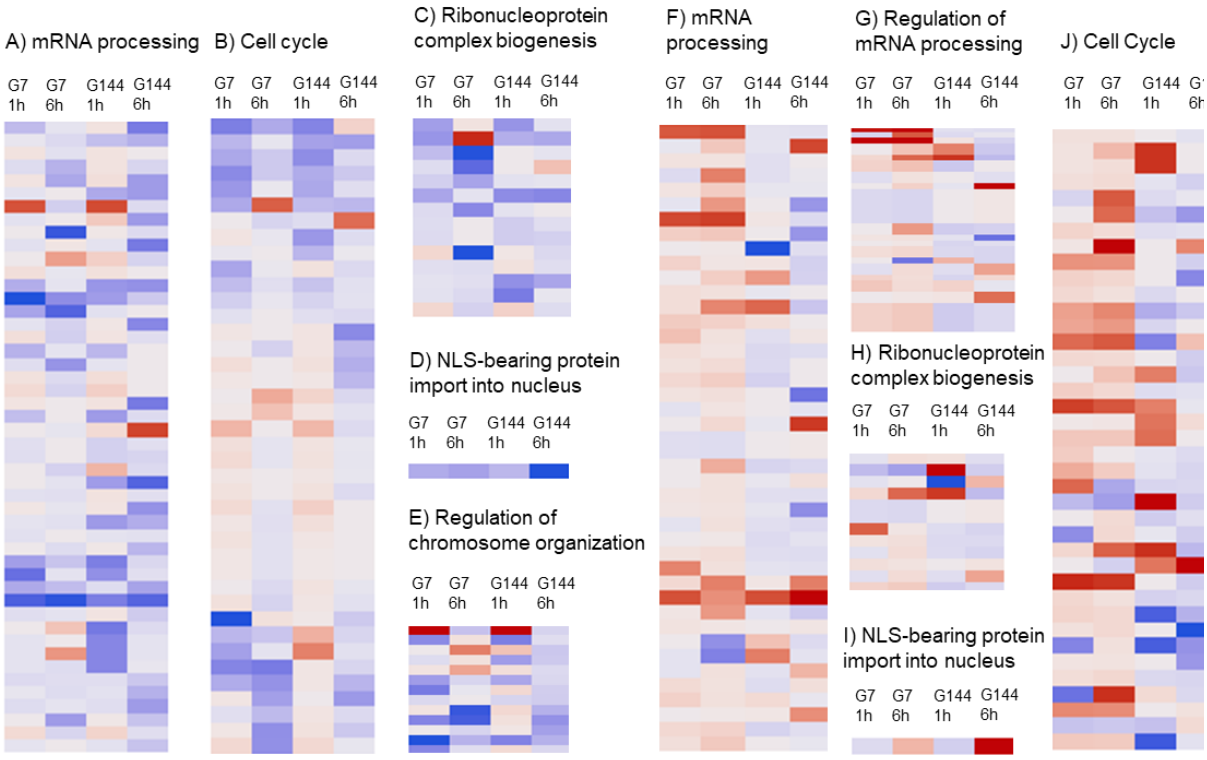

Figure 4.8. Heatmaps showing the distribution of downregulated and upregulated proteins in the top 5 enriched groups for phospho-proteome (three out of four). Results from our CDK12-inhibition MS shows which genes are downregulated and which genes are upregulated compared to the control cells treated with DMSO. A to E represents the top 5 downregulated enriched groups, and F to J represents the top 5 upregulated enriched groups. Blue color signifies the downregulated genes and red color signifies the upregulated genes.

Identical heatmaps were made for the total-proteome (figure 4.9). It became clear that many of the same GO groups were enriched for both the downregulated and the upregulated proteins, especially for the phospho-proteome. mRNA processing is the most heavily affected for both downregulated and upregulated phospho-proteome, whereas cell cycle is the second most downregulated for the phospho-proteome. However, the top 5 enriched groups differed between phospho-proteome and total-proteome. This is also seen in figure 4.8 and 4.9. This implements that the CDK12/13 inhibition affects the same functional groups within the same proteome-analysis, but it does not affect the same functional groups between phospho- and total-proteome.

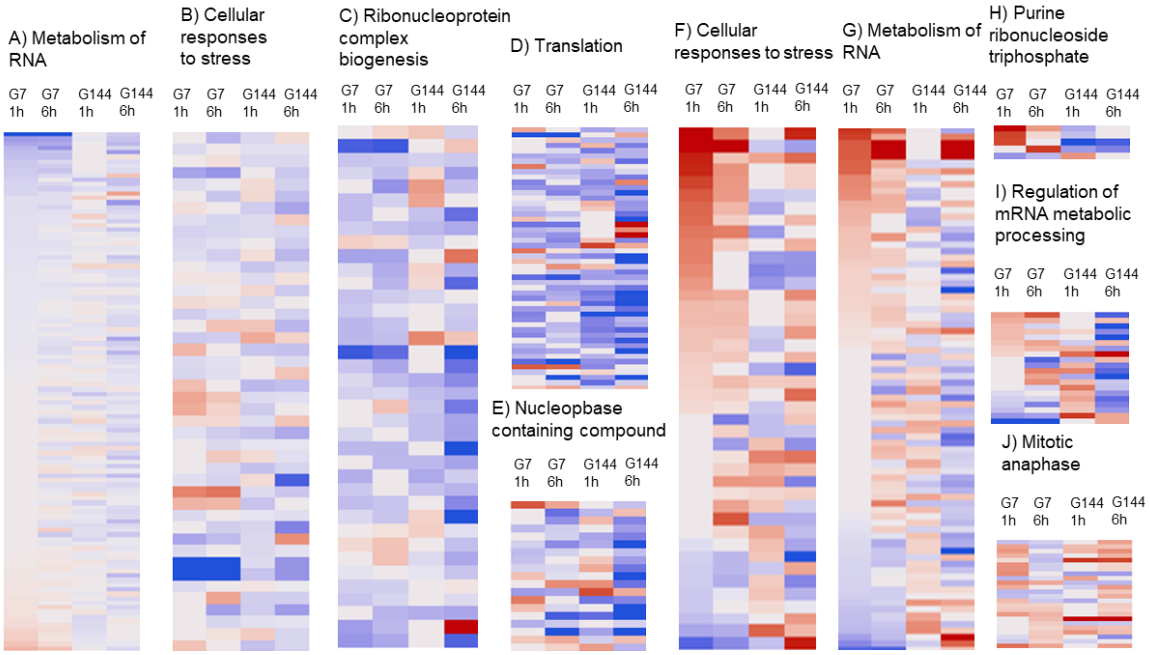

Figure 4.9. Heatmaps showing the distribution of downregulated and upregulated proteins in the top 5 enriched groups for total-proteome (three out of four). Results from our CDK12-inhibition MS shows which genes are downregulated and which genes are upregulated compared to the control cells treated with DMSO. A to E represents the top 5 downregulated enriched groups, and F to J represents the top 5 upregulated enriched groups. Blue color signifies the downregulated genes and red color signifies the upregulated genes.

Although the downregulated heatmaps consist of mostly blue (downregulated proteins) and the upregulated heatmaps consist of mostly red (upregulated proteins), there are still several inconsistencies in all of the heatmaps. This comes from the fact that just one out of the four different conditions has to be downregulated/upregulated in order to obtain all of the relevant proteins.

4.2.5 Heatmaps of proteins involved in cell cycle, CDK2 substrates and DNA replication

We have seen that the 6 hours treatment of THZ531 leads to a loss of DNA replication as measured by EdU update (figure 4.3). We would like to see if proteins involved in DNA replication, cell cycle and known CDK2 substrates are affected in our dataset. In Chi et.al. (46) they discovered 117 proteins to be CDK2 substrates, some known and some novel. CDK2 is an important part of cell division and is central to oncogenic signaling. Based on the experiments showing that CDK12/13 inhibition affects cell division (Pandey lab), we wanted to look more into how CDK12/13 inhibition affected these CDK2 substrates, as well as investigate CDK12/13 inhibition's effect on proteins involved in cell cycle. Additionally, proteins involved in DNA replication were

investigated in closer detail. Heatmaps were made in the Orange 3.28. software, comparing DNA replication and cell cycle gene lists found on MSigDB (101) to our dataset, and by comparing Chi et.al.'s CDK2 substrate dataset to our own gene lists.

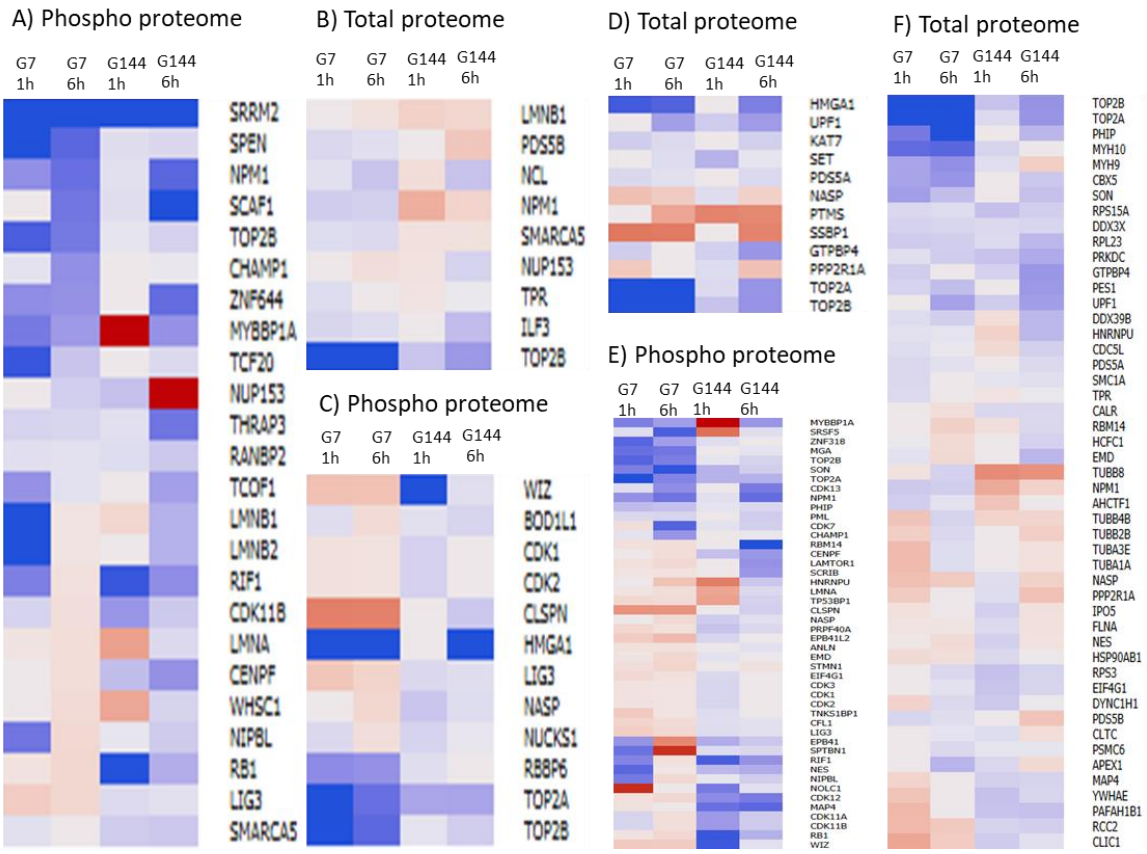

Figure 4.10. Heatmaps showing the distribution of downregulated proteins found to be CDK2 substrates (46), proteins involved in DNA replication and proteins involved in cell cycle. The proteins in heatmap A and B were found to be CDK2 substrates in Chi et.al. (46). Genes like SRRM2 and TOP2B, which are some of the most downregulated proteins found in our phospho-proteome MS dataset, are present in the CDK2 list. Heatmap C and D are proteins involved in DNA replication (list found on MSigDB). The proteins in heatmap E and F are involved in cell cycle. Blue color signifies the downregulated genes and red color signifies the upregulated genes.

In these heatmaps we chose to continue with the criteria that the proteins are present in minimum three out of four conditions. We focused on the downregulated proteins for both phospho- and total-proteome. The proteins in heatmap A and B were found to be CDK2 substrates in Chi et.al. (2). Heatmap C and D are proteins involved in DNA replication. The proteins in heatmap E and F are involved in cell cycle. Blue color signifies the downregulated proteins and red color signifies the upregulated proteins. Genes like SRRM2 and TOP2B, which are some of the most downregulated proteins found for phospho-proteome in our MS dataset (subsection 7.3), are present in the CDK2 list.

The heatmaps in figure 4.10 show downregulated proteins involved in different pathways. We chose to focus on some of the most downregulated proteins in our phospho-proteome protein list.

4.2.6. Visual representation of TOP2A after inhibition of CDK12/CDK13

To gain a deeper understanding in the functional assets of CDK12/13 depletion on the phospho-proteome, the phospho-proteome was investigated further in Cytoscape and by western blotting. TOP2A promptly became a protein of interest given its strong downregulation in our dataset (figure 4.11).

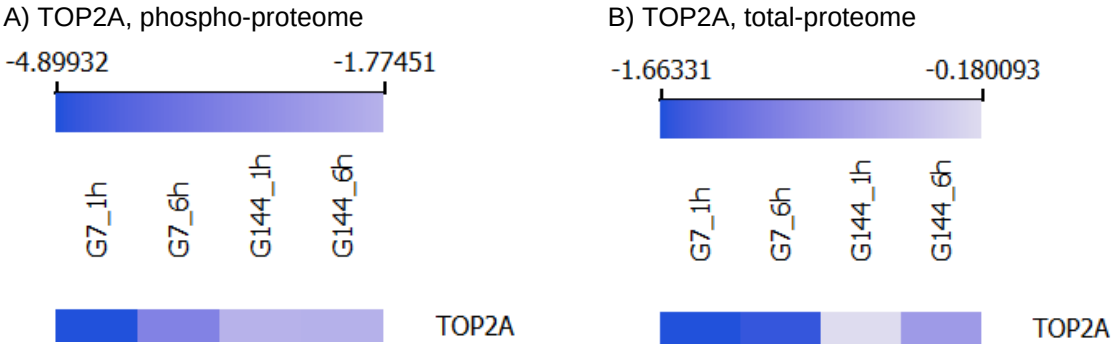

Figure 4.11. Heatmaps of TOP2A in phospho- and total-proteome. Downregulation of TOP2A in (A) phospho-proteome and (B) total-proteome. The legends show the difference in downregulation between the two proteome-analyses, where G7 1 hour treatment is the most strongly downregulated in both datasets. The phospho-proteome is overall more downregulated than the total-proteome.

Figure 4.11 show the difference in downregulation of TOP2A for (A) phospho-proteome and (B) total-proteome. G7 1 hour treatment in the phospho-proteome is the most heavily downregulated with a log2 transformed p-value of -4.9. In the total-proteome, G7 1 hour treatment is the most heavily downregulated with a log2 transformed p-value of -1.7. We wanted to investigate if we could visualize the downregulation in the phospho-proteome doing a western blot with antibodies against both TOP2A and p-TOP2A. Serine 1106 was chosen as the phosphorylation site to investigate, since this site was down-phosphorylated in both cell lines (data not shown).

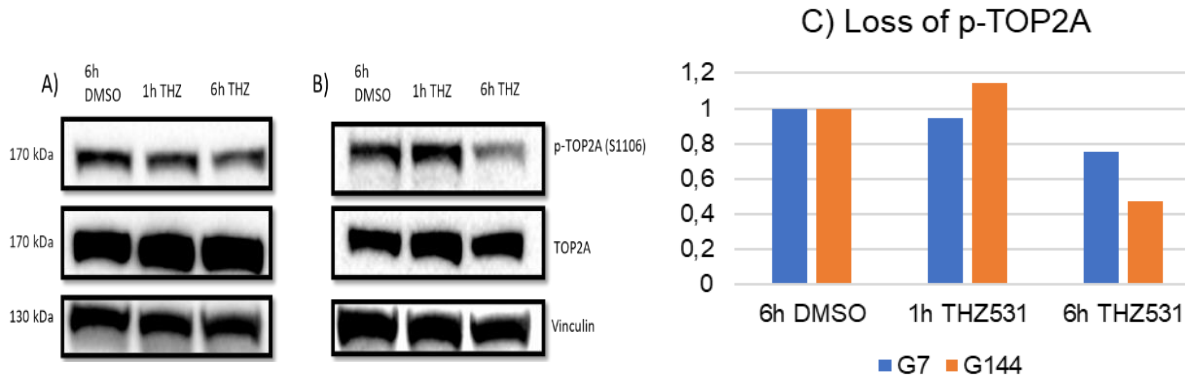

Figure 4.12. Western blot of TOP2A and p-TOP2A in G7 and G144 cells. Protein analysis of THZ531-treated G7 and G144 cells. The G7 cells are represented in (A), while the G144 cells are represented in (B). Cell lysates from 6 hours DMSO treated cells (negative control) were compared to cells treated for 1 hour and 6 hours with THZ531. The cell lysates were stained in anti-p-TOP2A (S1106) and anti-TOP2A primary antibodies (the four upper panels). The two lower panels represent anti-vinculin stained cell lysates as positive control. (C) visualizes the loss of p-TOP2A in the G7 cell line, as quantified by Image Lab 6.1. Blue bars visualize the change in p-TOP2A in the G7 cell line. Orange bars visualize the change in p-TOP2A in the G144 cell line. The loss after 6 hours treatment of THZ531 is stronger for the G144 cell line compared to the G7 cell line. The 6 hours treatment of DMSO was used as reference band.

In figure 4.12, (A) represents the G7 cell line while (B) represents the G144 cell line. TOP2A does not seem to be affected by THZ531's inhibition of CDK12 and CDK13 in both the G7 cells (A) and the G144 cells (B). On the other hand, the phosphorylation of S1106 of TOP2A is weakened after 6h treatment for both cell lines. This is also indicated by our MS data, where the phosphorylation of TOP2A is more strongly downregulated than TOP2A in the total-proteome (figure 4.11). The loss of p-TOP2A is visualized in (C). The 6 hours DMSO-treated cells were used as reference band for the calculations of relative quantity by Image Lab 6.1. After 1 hour treatment of THZ531 on the G7 cells, the relative quantity is down to 0.9 of that of the reference band's (relative quantity of 1). For 6 hours treatment the relative quantity is down to 0.75, suggesting a loss of p-TOP2A of 1/4 (figure 4.12, (C)). For the G144 cells, the relative quantity went up to 1.1 after 1 hour treatment. After 6 hours treatment it is 0.4, suggesting a loss of 3/5 (figure 4.12, (D)).

4.2.7. Visual representation of chosen proteins and protein groups of CDK12/CDK13 inhibited phospho-proteome

To gain a better understanding of the interaction partners and functional groups of some of the most downregulated proteins, the downregulated phospho-proteome was further processed in Cytoscape and interaction networks were made from the Metascape data. The proteins of interest were pulled out of the phospho-proteome networks and visualized next to each other as shown in figure 4.13.

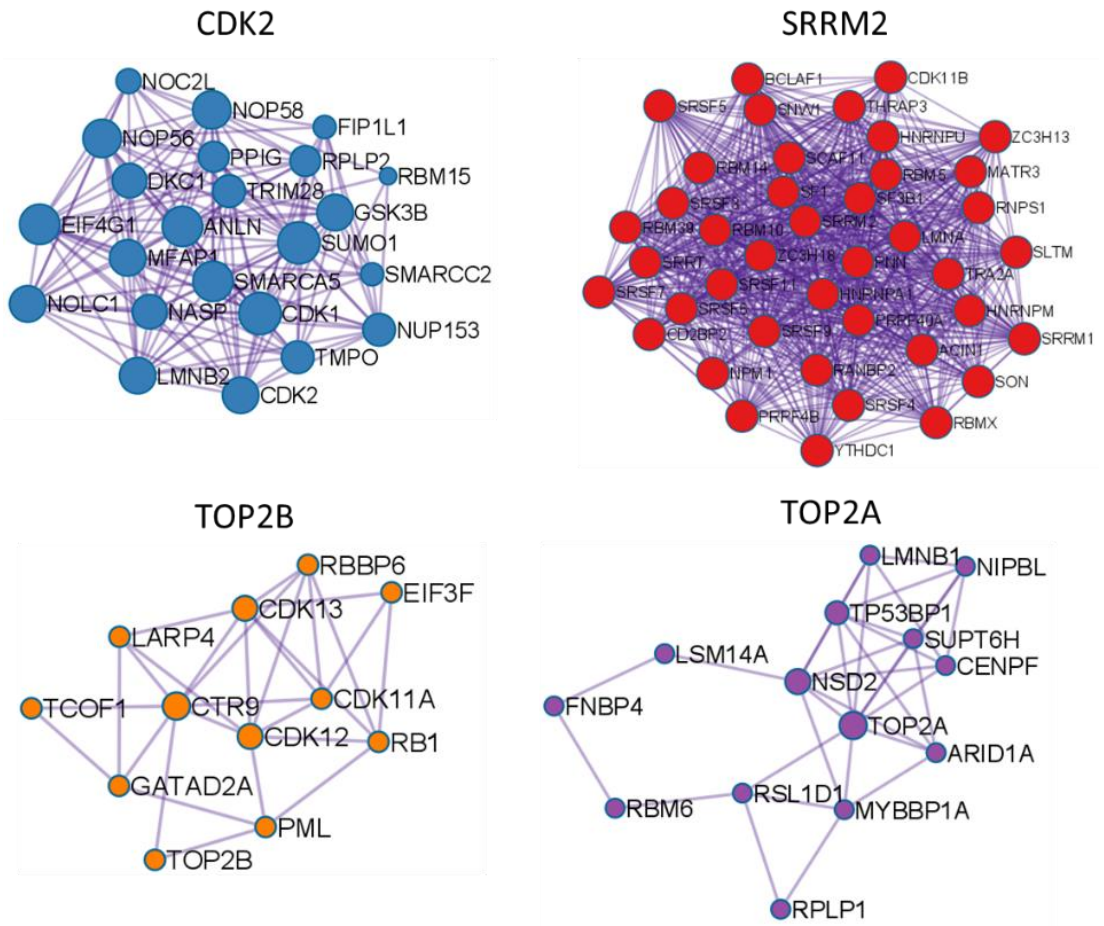

Figure 4.13. Protein interaction network representing proteins of interest and their close neighbors. Network representing four chosen downregulated proteins (CDK2, SRRM2, TOP2B and TOP2A) after CDK12/13 inhibition. SRRM2, TOP2B and TOP2A are strongly downregulated in our phospho-proteome MS dataset, while CDK2 is a protein of interest given its role in cell division. The minimum three out of four values MS dataset was processed in Metascape before network was visualized in Cytoscape. Edges connects nodes of functionally correlated proteins (GO Biological Processes and TRRUST databases). Blue color represents proteins involved in cell cycle, regulation of protein localization to nucleus and protein localization to nucleus. Red color represents proteins involved in mRNA Splicing and the processing of capped intron-containing pre-mRNA. Orange color represents proteins involved in mRNA processing, regulation of mitotic cell cycle and transcription elongation from RNA polymerase II promoter. Purple color represents proteins involved in DNA recombination, cell cycle and regulation of isotype switching.

TOP2B was found to be involved with proteins in mRNA processing, regulation of mitotic cell cycle and transcription elongation from RNA polymerase II promoter. Other proteins involved in this network are CDK12 and CDK13. TOP2A was found to be involved with proteins involved in DNA recombination, cell cycle and regulation of isotype switching. We chose to investigate CDK2 and SRRM2 as well. CDK2 was a protein of interest given its role in cell division, while SRRM2 was another highly downregulated protein in our phospho-proteome data set (figure 4.10, (A)). SRRM2 was found to be involved with proteins in mRNA splicing and the processing of capped intron-containing pre-mRNA. CDK2 was found to be involved with proteins in cell cycle, regulation of protein localization to nucleus and protein localization to nucleus.

The phospho-proteome data was further processed in Cytoscape, and our three out of four-list was used as input to the software (figure 4.14). CDK12's close neighbors, based on the STRING database (102), were put in a new interaction network. Proteins in this network includes CDK13, CDK2, CDK1, CDK3 and CDK7. CDK7 is an essential component of the transcription factor TFIIH, that is involved in transcription initiation and DNA repair. This network captures CDKs involved in both transcription (CDK12, CDK13, CDK7) and cell division (CDK1, CDK2 and CDK3).

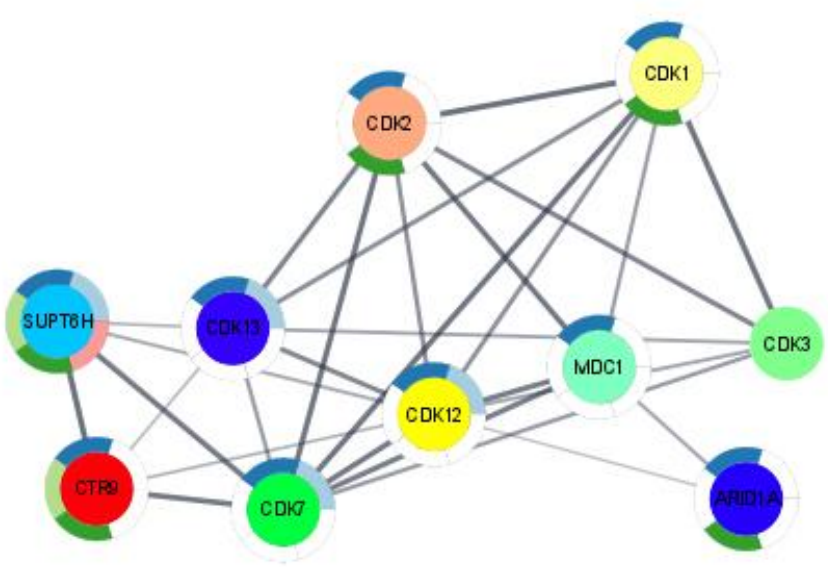

Figure 4.14. Protein interaction network representing CDK12's close neighbors. Network representing CDK12 and its close neighbors in our MS dataset after CDK12/13 inhibition. The STRING database in the Cytoscape software was used to find the close neighbors of CDK12 in the three out of four downregulated dataset for phospho-proteome.

The interaction network in figure 4.14 locates CDK12 and CDK13 in close proximity to e.g. CDK2, which caught our interest given its role in cell division. In addition to this, a handful of the proteins found to be CDK2 substrates were seen to be downregulated in our dataset after the CDK12/13 inhibition (figure 4.10, (A)).

4.2.8 Visual representation of chosen protein groups of CDK12/CDK13 inhibited total-proteome

To gain a deeper understanding in the functional assets of CDK12/13 depletion on the total-proteome, the downregulated total-proteome was investigated in Cytoscape (figure 4.15). TOP2B and TOP2A were also downregulated in the total-proteome dataset, all though less downregulated than in the phospho-proteome dataset (figure 4.11). We chose to look at close neighbors of TOP2A and TOP2B using the STRING database in Cytoscape.

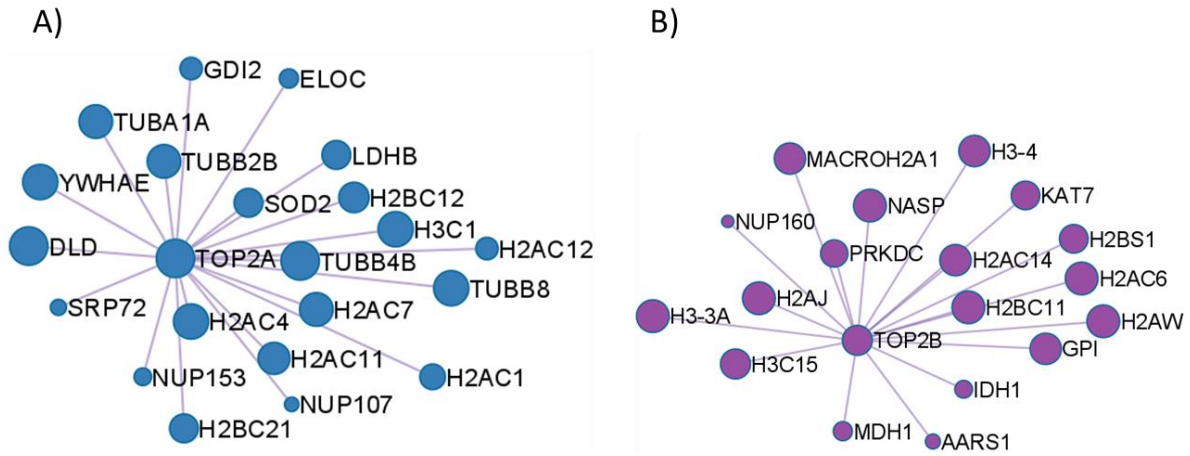

Figure 4.15. Protein interaction network of TOP2A and TOP2B and their close neighbors in the total-proteome. Networks representing close neighbors of TOP2A and TOP2B after CDK12/13 inhibition for the total-proteome. The three out of four MS dataset was processed in Metascape before network was visualized in Cytoscape. Network A) is interaction partners of TOP2A, while network B) is interaction partners of TOP2B. Edges connects nodes of functionally correlated proteins (GO Biological Processes and TRRUST databases). Blue color represents proteins involved in HCMV Early Events, HCMV Infection and HCMV Late Events. Purple color represents proteins involved in nucleosome organization, nucleosome assembly and chromatin assembly or disassembly.

TOP2A was found to be involved with proteins involved in HCMV early events, HCMV infection and HCMV late events. TOP2B was found to be involved with proteins in nucleosome organization, nucleosome assembly and chromatin assembly or disassembly. In both networks there are multiple histone proteins present. Multiple histone proteins are also downregulated in the total-proteome dataset (subsection 7.3).

This downregulation may further visualize CDK12 inhibition’s observed phenotype (figure 4.10, C and D) on DNA replication.

5. Discussion

5.1 Generation of CDK9, CDK12 and CDK13 BAC-GFP tagged mouse embryonic stem cells

Our idea was to validate CDK12's interaction partners already identified earlier in the CDK12-GFP tagged Hela cells using GFP beads under ChIP conditions (67). Furthermore, we wanted to generate stably expressing CDK9-, CDK12- and CDK13-BAC GFP tagged mouse embryonic stem cells, E14, with the goal that we will in vitro differentiate these mES cells to mNPC cells. After this differentiation, we could perform the GFP pull-down in these mNPC cells to identify the interaction partners of these proteins in neural stem cell proteome. We successfully generated mES cells BAC GFP-tagged for CDK9, CDK12 and CDK13. As a proof-of-principle, we were able to pull-down CDK9-GFP using GFP beads, but due to lack of time, we were not able to perform successful pull-down for the CDK12- and CDK13-GFP from the respectively tagged mES cells. As for CDK9, clear bands were present in whole cell- and immunoprecipitated protein analysis of endogenous CDK9, as well as for CDK9-GFP (figure 4.1). No bands were to be detected in the immunoprecipitated protein analysis of CDK12 or CDK13 (data not shown). However, bands were detected in the western blot analysis using primary antibodies against GFP (figure 4.1) on input cell lysate, indicating that the CDK12- and CDK13-GFP are, in fact, present in the cell lysate.

A possible scenario of the unsuccessful IP western blot analyses is improper pull-down of the GFP-tagged CDK12 and CDK13 in mES cells using GFP magnetic beads. Another explanation may be the usage of improper percentage on the gel used for western blots. Too high percentage may cause the big proteins, like CDK12 and CDK13, to not be able to travel through the gel. After multiple attempts to pull-down CDK9-, CDK12- and CDK13-GFP in mES cells, we concluded that we would perform the validation of CDK12 interaction partners identified earlier in the lab using CDK12-BAC-GFP HeLa cells.

5.2 Identification of interaction partners of CDK12 in HeLa cells

Sigrid Berg's data revealed chromatin-bound CDK12 to interact with transcription regulation factors NELF-E, NELF-C/D, CDC73 and FIP1L1 in HeLa cells (67). She performed a chromatin immunoprecipitation (ChIP) and a ChIP-MS. ChIP is a technique used to investigate the interaction between proteins and chromatin in the

cell. We performed an immunoprecipitation (IP) on the same HeLa cells that was earlier generated by Sigrid Berg. CDK12-GFP was pulled down using GFP magnetic beads to look at proteins directly interacting with CDK12. This immunoprecipitation on HeLa cells was successful, in comparison to the mES cells. The ChIP-MS was initially performed by Sigrid since CDK12 operate on DNA, and they wanted to investigate if it would be possible to elucidate the roles of chromatin-bound CDK12 expressed at endogenous levels.

CDC73 is part of the PAF complex. The PAF complex is crucial in the pause release of RNAPII, and P-TEFb regulates the initial recruitment of PAF to genes. The subsequent recruitment of CDK12 is dependent on PAF (103). Therefore, the interaction between CDK12 and PAF found by Sigrid was an interesting finding.

Our regular IP did not show an interaction between CDK12 and proteins in the NELF-complex (data not shown) or with subunits of PAF (figure 4.2). This lack of interaction at the IP-western blot on a physical level does not necessarily indicate that the proteins do not interact on chromatin. The ChIP performed by Sigrid confirmed that CDK12, CDC73 and members of the NELF-complex were pulled down on the same piece of chromatin, but they might not be in direct contact with each other, as the IP could have confirmed.

Our next move was to do ChIP-qPCR or ChIP-seq to investigate this observed interaction on chromatin. We requested a model cell line to perform these experiments, but we did not receive them and could therefore not make further progress. At this point we decided to perform MS on two glioma cell lines, G7 and G144, after 1 hour and 6 hours treatment of THZ531. This was done to investigate the total-proteome and phospho-proteome after inhibition of CDK12/CDK13.

5.3 Identification of total- and phospho-proteome after CDK12/CDK13-inhibiton by mass spectrometry analysis

Through other projects carried out in the group, we have found that inhibition of CDK12/CDK13 specifically compromises the proliferation of glioma cells. Additionally, earlier work has also found that CDK12/CDK13 inhibition disrupts the cell cycle of glioma cells and leads to a rapid shutdown of DNA replication (figure 4.3). The effect on DNA replication was rapid and strong, and it was hypothesized that this effect might be independent of the effect CDK12/13-inhibition has on transcription (67). Since

CDK12 and CDK13 are kinases with kinase activity ascribed towards serine-2 of RNAPII, we decided to investigate the effect of CDK12/CDK13 inhibition with THZ531 on total- and phospho-proteome in glioma cells, G7 and G144.

5.3.1 Identifying the effect on cell cycle and DNA replication after CDK12/CDK13-inhibiton after mass spectrometry analysis

We have observed that the 6 hours treatment of THZ531 leads to a loss of DNA replication as measured by EdU update (figure 4.3). Proteins involved in DNA replication, such as HMGA1, TOP2A and TOP2B, are downregulated in both the phospho-proteome and the total-proteome datasets in our project (figure 4.10).

In Pilarova et al., they discovered that inhibition of CDK12 resulted in downregulation of a common subset of genes involved in DNA replication and DNA repair. They hypothesized that the inhibition of CDK12 causes subtle changes in the CTD phosphorylation that are critical for the ideal transcription of this subset of genes (104).

The cell cycle gene list found on MsigDB was the largest list of all our target lists. Chirackal Manavalan et al. (66) reported that CDK12 catalytic activity represents a novel link between regulation of transcription and cell cycle progression, and that CDK12 kinase activity is required for transcription of core DNA replication genes and for G1/S progression (66). As mentioned, earlier work in the Pandey lab found that inhibition of CDK12/CDK13 compromises the proliferation of glioma cells, and that CDK12/CDK13 inhibition disrupts the cell cycle of glioma cells and leads to a rapid shutdown on DNA replication, shown in figure 4.3 (earlier work, Pandey lab). In our dataset, we discovered proteins involved in cell cycle and DNA replication to be heavily downregulated upon CDK12/CDK13 inhibition.

In our project, we discovered that the phosphorylation of a handful of DNA replication proteins was down as well, and their total protein levels were also down following CDK12/CDK13 inhibition (figure 4.10). Given the well-established role of TOP2A in regulating of DNA replication, we decided to validate the effect of CDK12/CDK13 inhibition on both total and phosphorylated TOP2A levels. The 17q12-q21 locus, a frequently amplified and overexpressed locus in breast cancer, contains several genes, including TOP2A. Genes involved in the 17q12-q21 amplicon might therefore be oncogene candidates, meaning that TOP2A might serve an oncogene feature (107). Other studies have found that TOP2A is highly expressed in glioma tissues

compared with corresponding normal controls (108). TOP2A is downregulated in our total-proteome dataset upon treatment with THZ531, possibly indicating that TOP2A function is compromised upon CDK12/CDK13 inhibition leading to a shutdown of replication effect.

Huang et al. demonstrated that FAK autophosphorylation inhibitor, Y15, significantly decreased tumor growth of DBTRG and U87 cells, especially in combination with temozolomide (109). They found TOP2A to be down-phosphorylated upon treatment with Y15, which coincides with our results after treatment with THZ531. Phosphorylation of TOP2A is heavily compromised in both of the glioma cell lines (figure 4.11), a finding that we have validated successfully (figure 4.12).

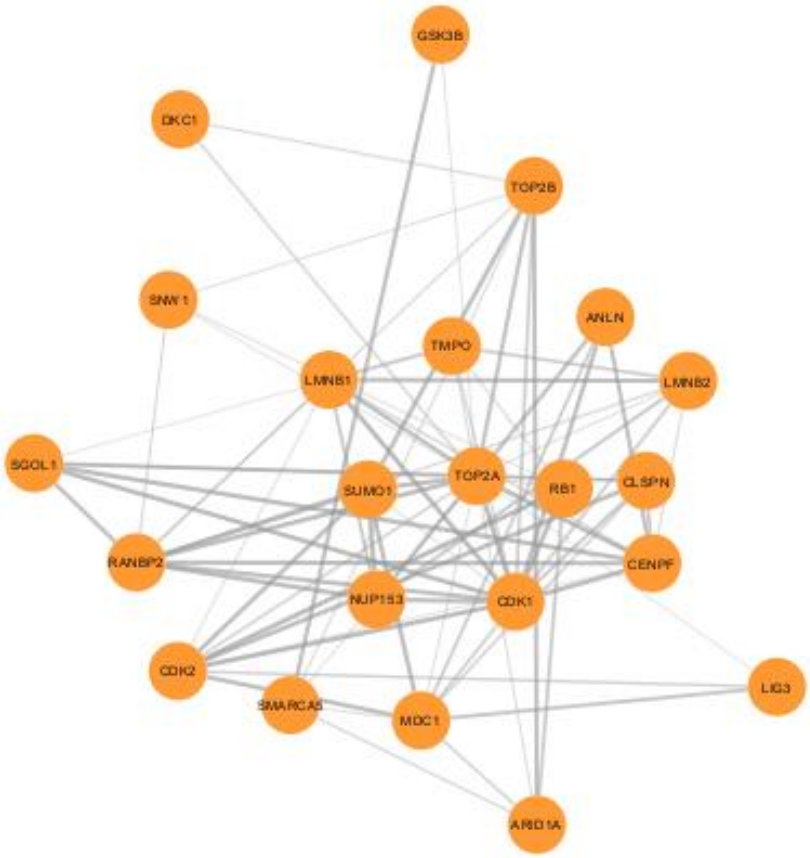

Figure 5.1. TOP2A close neighbors in phospho-proteome. Network representing TOP2A and its close neighbors in our MS dataset after CDK12/13 inhibition. The STRING database in the Cytoscape software was used to find the close neighbors of TOP2A in the three out of four downregulated dataset for phospho-proteome. Other proteins in this network are, among others, TOP2B and CDK2.

The STRING database in Cytoscape was applied to investigate close neighbors of TOP2A (figure 5.1), given its strong downregulation in our phospho-proteome dataset. In this network we found TOP2A to interact with TOP2B and CDK2, among other

proteins. CDK2, being a regulator of cell division, caught an interest given the novel substrates discovered in Chi et. al (46).

5.3.2 Identifying the effect on CDK2 substrates after CDK12/CDK13-inhibiton after mass spectrometry analysis

CDK2 is a critical regulator of the cell cycle and cell division, and it is central to oncogenic signaling. Active DNA replication, which is often regulated by CDK2 activity, is firmly affected by CDK12/CDK13-inhibition measured by EdU incorporation (figure 4.3). The CDK2/cyclin E complex phosphorylates substrates at the proper time during the cell cycle, which releases and activates transcription factors, driving cells to the S phase and synthesis of DNA (figure 1.2) (110). Krasinska et al. describe how CDK activity controls the efficiency of DNA replication. Both CDK1 and CDK2 are necessary for efficient DNA replication in *Xenopus* egg extracts. CDK2/cyclin E is rate-limiting for DNA replication as depletion of either subunit reduced replication efficiency to around 30% of the control. However, the remaining 30% replication was no longer dependent on CDK2, but, rather, on CDK1 (111).

Based on the experiments showing that CDK12/13 inhibition affects cell division (figure 4.3), we wanted to look into how CDK12/13 inhibition affected the CDK2 substrates found in Chi et. al. (46). They identified 117 candidate substrates, whereas ~40% of which are known CDK substrates, including CDK11B, LIG3 and FOXK2. Previously unknown candidates were validated to be CDK2 substrates, including TOP2B and SRRM2. Candidate substrates include proteins that regulate histone modifications, chromatin, transcription, and RNA/DNA metabolism. 9 of the 117 CDK2 substrates identified in their experiment, including TOP2B, LMNB1, NMP1 and SMARCA5, were downregulated in our total-proteome dataset. Of these 9 substrates, TOP2B, which is involved in DNA replication, protrudes as a heavily downregulated protein.

25 of these 117 CDK2 substrates were down-phosphorylated in our phospho-proteome dataset. Several of these proteins were strongly downregulated in at least one of the four conditions (figure 4.10), including TOP2B, which is more downregulated in the phospho-proteome dataset than in the total-proteome dataset (16-fold compared to 4-fold in at least one of the conditions).

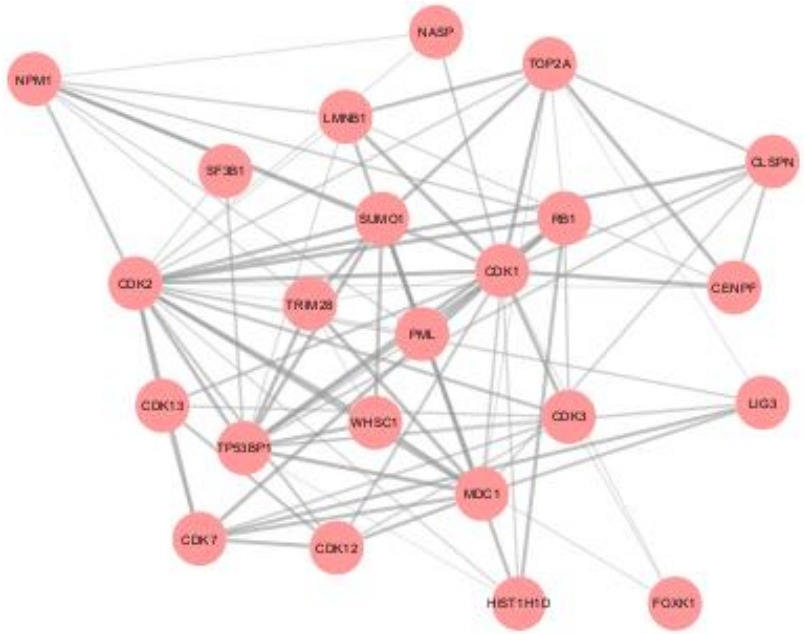

Figure 5.2. CDK2 close neighbors in phospho-proteome. Network representing CDK2 and its close neighbors in our MS dataset after CDK12/13 inhibition. The STRING database in the Cytoscape software was used to find the close neighbors of CDK2 in the three out of four downregulated dataset for phospho-proteome. Other proteins in this network are, among others, TOP2A and CDK12.

Figure 5.2 illustrates the close neighbors of CDK2 found by the STRING database in Cytoscape. This network shows different proteins to interact with CDK2 than the substrates found by Chi et al. (46), all though some, like TOP2A, LIG3, NPM1, are present in this network as well. This network shows CDK2 to interact with CDK12, CDK13 and TOP2A, and places both CDK12 and CDK13 in proximity to proteins involved in cell cycle and DNA replication.

The effect observed on the CDK2 substrates in our dataset may substantiate the loss of DNA replication caused by CDK12/CDK13 inhibition. CDK2 itself is not heavily downregulated in our phospho-proteome dataset and was not a significant hit in our total-proteome dataset (section 7.3), indicating that CDK2 itself is not heavily affected by the inhibition of CDK12/13. On the other hand, multiple of its substrates are down-phosphorylated upon treatment with THZ531, as shown in figure 4.10. Given these findings, CDK12/CDK13 inhibition may compromise active replication by affecting replication genes and affecting phosphorylation of CDK2 substrates.

5.3.3 Heavily downregulated proteins in the phospho-proteome dataset

Among the top down-phosphorylated proteins is SRRM2, which is required for pre-mRNA splicing as a component of the spliceosome. SRRM2 was revealed as a CDK2

substrate in Chi. et. al (46). Fan (112) revealed the redundant and individual roles of CDK12 and CDK13 in maintaining global transcription elongation by inhibiting CDK12 and CDK13. They wanted to identify substrates of CDK12 and CDK13 responsible for the phenotypes caused by CDK12 and CDK13 inhibition. Depletion of SRRM2 led to similar differential gene expression and alternative polyadenylation profiles as CDK12 and CDK13 inhibition. This is in agreement with previously published studies which have reported that CDK12/CDK13 inhibition leads to down-phosphorylation of many proteins involved in RNA processing including splicing and alternative polyadenylation (69, 105). Considering these findings, SRRM2 could be a potential substrate of CDK12 and CDK13, and it might be partially responsible for the transcriptional phenotype caused by the dual inhibition of CDK12 and CDK13 (112). Our data shows that SRRM2 is heavily downregulated in both cell lines and all four conditions (subsection 7.3), suggesting that SRRM2 is affected by the inhibition of CDK12 and CDK13.

HMGA1, which is involved in the regulation of inducible gene transcription and metastatic progression of cancer cells, is another protein found to be heavily downregulated in our phospho-proteome dataset, as well as in the total-proteome dataset (figure 4.10). Higher protein levels of HMGA1 in human breast cancer tissues are significantly associated with breast cancer progression and poor prognosis (113). HMGA1 was identified by Chi et al. as a cyclin A-CDK2 substrate (114). This finding further connects CDK12/CDK13 inhibition to the down-phosphorylation of CDK2 substrates mentioned above. In our total-proteome dataset, HMGA1 is found to be downregulated (subsection 7.3), which might indicate that THZ531 affects HMGA1's effect on cancer tissues.

5.4 Future perspectives

Future studies would benefit from further investigation of CDK12 interaction partners, as demonstrated by Sigrid Berg (67). NELF-E and NELF-C/D, as well as CDC73 could have been interesting alternatives to study further. ChIP-MS in triplicate samples could be performed to gain insight into intra-sample variations.

In our study of identifying the changes in total- and phospho-proteome of glioma cells upon CDK12/CDK13 inhibition, we used three replicates per condition. The difference in log2 transformed values between the G7 and G144 cell lines was large for many

proteins. A replication of the experiment should be considered to validate the decrease in value seen in the most interesting pathways mentioned in this project.

CDK12/CDK13 inhibition compromises active replication, as demonstrated by earlier work in the Pandey lab. CDK12/CDK13 inhibition may compromise active replication by affecting replication genes and affecting phosphorylation of CDK2 substrates. Further experiments should be conducted on the role of CDK12/CDK13 in DNA replication and CDK2 activity, for example, whether CDK12/CDK13 inhibition compromises CDK2 activity. This can be done by pulling down CDK12 following THZ531 treatment and performing kinase assay with a known substrate. Additionally, CDK2 reporters can be used to investigate CDK2 activity (115, 116).

Furthermore, the replication phenotype should also be expanded upon using EdU/BrdU treatment of the cells with earlier time-points to understand how quickly DNA replication is affected following CDK12/CDK13 inhibition. Another interesting approach would be DNA fiber assay for the study of replication fork dynamics.

6. Concluding remarks

The aim of the study was originally to elucidate interaction partners of CDK12 in HeLa and mouse embryonic stem cells. Because of challenges in the experiments investigating these interaction partners, the new aim of study became to investigate phospho- and total-proteome of glioma cells after inhibition of CDK12/CDK13. We investigated the roles of CDK12/CDK13 in transcription and DNA replication, among other pathways, by examining the CDK12/CDK13-inhibition's effect on phospho- and total-proteome.

The MS data identified approximately 1200 proteins as significant hits for the different glioma cells, G7 and G144. Keeping in line with earlier published work, Sigrid Berg's study pointed at CDK12 as a factor involved in transcription and RNA processing events. Because of previous studies done in the Pandey lab and newly published papers, we decided to focus on CDK12/13 as a novel regulator in several yet to be reported pathways, including cell cycle, DNA replication and CDK2 substrates.

The inhibition of CDK12/13 lead to a down-phosphorylation of multiple proteins involved in cell cycle and DNA replication, and numerous CDK2 substrates were down-phosphorylated. Multiple of these proteins were also downregulated in the total-proteome dataset, but in general, less downregulated than they were down-phosphorylated. Our observations point to a role of CDK12/13 in the cell cycle and DNA replication. However, further research is required to validate these observations.

6. References

1. Britannica Encyclopedia. Transcription, 2019. [July 16, 2020]. Available from: https://www.britannica.com/science/transcription-genetics.
2. Alberts B. Molecular Biology of the Cell. USA: Garland Publishing Inc; 2014.
3. Sjøberg NO. Molekylær genetikk. Oslo: Vett og viten; 2013.
4. Khatter H, Vorländer MK, Müller CW. RNA polymerase I and III: similar yet unique. Current Opinion in Structural Biology. 2017;47:88-94.
5. Sharifi S, Bierhoff H. Regulation of RNA Polymerase I Transcription in Development, Disease, and Aging. Annu Rev Biochem. 2018;87:51-73.
6. RNA polymerase I Absoluteastronomy [Available from: http://www.absoluteastronomy.com/topics/RNA_polymerase_I].
7. Corden JL, Cadena DL, Ahearn JM, Jr., Dahmus ME. A unique structure at the carboxyl terminus of the largest subunit of eukaryotic RNA polymerase II. Proc Natl Acad Sci U S A. 1985;82(23):7934-8.
8. Fuda NJ, Ardehali MB, Lis JT. Defining mechanisms that regulate RNA polymerase II transcription in vivo. Nature. 2009;461(7261):186-92.
9. Carter R, Drouin G. Structural differentiation of the three eukaryotic RNA polymerases. Genomics. 2009;94(6):388-96.
10. Turowski TW, Tollervey D. Transcription by RNA polymerase III: insights into mechanism and regulation. Biochem Soc Trans. 2016;44(5):1367-75.
11. Kuehner JN, Pearson EL, Moore C. Unravelling the means to an end: RNA polymerase II transcription termination. Nature Reviews Molecular Cell Biology. 2011;12(5):283-94.
12. Hahn S. Structure and mechanism of the RNA polymerase II transcription machinery. Nat Struct Mol Biol. 2004;11(5):394-403.
13. Adelman K, Lis JT. Promoter-proximal pausing of RNA polymerase II: emerging roles in metazoans. Nat Rev Genet. 2012;13(10):720-31.
14. Core L, Adelman K. Promoter-proximal pausing of RNA polymerase II: a nexus of gene regulation. Genes Dev. 2019;33(15-16):960-82.
15. Jonkers I, Lis JT. Getting up to speed with transcription elongation by RNA polymerase II. Nat Rev Mol Cell Biol. 2015;16(3):167-77.
16. Proudfoot NJ. Transcriptional termination in mammals: Stopping the RNA polymerase II juggernaut. Science. 2016;352(6291):aad9926.
17. Hsin J-P, Sheth A, Manley JL. RNAP II CTD Phosphorylated on Threonine-4 Is Required for Histone mRNA 3′ End Processing. Science. 2011;334(6056):683-6.
18. Nemec CM, Yang F, Gilmore JM, Hintermair C, Ho Y-H, Tseng SC, et al. Different phosphoisoforms of RNA polymerase II engage the Rtt103 termination factor in a structurally analogous manner. Proceedings of the National Academy of Sciences. 2017;114(20):E3944-E53.
19. Vos SM, Farnung L, Urlaub H, Cramer P. Structure of paused transcription complex Pol II-DSIF-NELF. Nature. 2018;560(7720):601-6.
20. Vos SM, Farnung L, Boehning M, Wigge C, Linden A, Urlaub H, et al. Structure of activated transcription complex Pol II–DSIF–PAF–SPT6. Nature. 2018;560(7720):607-12.
21. Chen FX, Xie P, Collings CK, Cao K, Aoi Y, Marshall SA, et al. PAF1 regulation of promoter-proximal pause release via enhancer activation. Science. 2017;357(6357):1294-8.
22. Yu M, Yang W, Ni T, Tang Z, Nakadai T, Zhu J, et al. RNA polymerase II–associated factor 1 regulates the release and phosphorylation of paused RNA polymerase II. Science. 2015;350(6266):1383-6.
23. Schafer KA. The Cell Cycle: A Review. Veterinary Pathology. 1998;35(6):461-78.
24. Gao SW, Liu F. Novel insights into cell cycle regulation of cell fate determination. J Zhejiang Univ Sci B. 2019;20(6):467-75.
25. Westin J. Phases of cell cycle: G0, G1, S, G2, M [Available from: https://jackwestin.com/resources/mcat-content/mitosis/phases-of-cell-cycle-g0-g1-s-g2-m].

26. Mens MMJ, Ghanbari M. Cell Cycle Regulation of Stem Cells by MicroRNAs. Stem Cell Rev Rep. 2018;14(3):309-22.
27. Ekundayo B, Bleichert F. Origins of DNA replication. PLoS Genet. 2019;15(9):e1008320.
28. Prioleau MN, MacAlpine DM. DNA replication origins-where do we begin? Genes Dev. 2016;30(15):1683-97.
29. Hume S, Dianov GL, Ramadan K. A unified model for the G1/S cell cycle transition. Nucleic Acids Res. 2020;48(22):12483-501.
30. Pelengaris S, Khan M, Evan G. c-MYC: more than just a matter of life and death. Nature Reviews Cancer. 2002;2(10):764-76.
31. Yang HW, Chung M, Kudo T, Meyer T. Competing memories of mitogen and p53 signalling control cell-cycle entry. Nature. 2017;549(7672):404-8.
32. Heldt FS, Barr AR, Cooper S, Bakal C, Novák B. A comprehensive model for the proliferation-quiescence decision in response to endogenous DNA damage in human cells. Proc Natl Acad Sci U S A. 2018;115(10):2532-7.
33. Lee JH, Berger JM. Cell Cycle-Dependent Control and Roles of DNA Topoisomerase II. Genes (Basel). 2019;10(11).
34. Nitiss JL. DNA topoisomerase II and its growing repertoire of biological functions. Nature Reviews Cancer. 2009;9(5):327-37.
35. Nielsen CF, Zhang T, Barisic M, Kalitsis P, Hudson DF. Topoisomerase IIα is essential for maintenance of mitotic chromosome structure. Proc Natl Acad Sci U S A. 2020;117(22):12131-42.
36. Kuroda S, Kagawa S, Fujiwara T. Chapter 12 - Selectively Replicating Oncolytic Adenoviruses Combined with Chemotherapy, Radiotherapy, or Molecular Targeted Therapy for Treatment of Human Cancers. In: Lattime EC, Gerson SL, editors. Gene Therapy of Cancer (Third Edition). San Diego: Academic Press; 2014. p. 171-83.
37. Delgado JL, Hsieh CM, Chan NL, Hiasa H. Topoisomerases as anticancer targets. Biochem J. 2018;475(2):373-98.
38. Malumbres M. Cyclin-dependent kinases. Genome Biology. 2014;15(6):122.
39. Lim S, Kaldis P. Cdks, cyclins and CKIs: roles beyond cell cycle regulation. Development. 2013;140(15):3079-93.
40. Chou J, Quigley DA, Robinson TM, Feng FY, Ashworth A. Transcription-Associated Cyclin-Dependent Kinases as Targets and Biomarkers for Cancer Therapy. Cancer Discovery. 2020;10(3):351-70.
41. Malumbres M, Barbacid M. Cell cycle, CDKs and cancer: a changing paradigm. Nature Reviews Cancer. 2009;9(3):153-66.
42. Poon RYC. Mitotic Catastrophe. In: Bradshaw RA, Stahl PD, editors. Encyclopedia of Cell Biology. Waltham: Academic Press; 2016. p. 399-403.
43. UniProt. UniProtKB - P06493 (CDK1_HUMAN) [Available from: https://www.uniprot.org/uniprot/P06493.
44. Michowski W, Chick JM, Chu C, Kolodziejczyk A, Wang Y, Suski JM, et al. Cdk1 Controls Global Epigenetic Landscape in Embryonic Stem Cells. Mol Cell. 2020;78(3):459-76.e13.
45. Tadesse S, Anshabo AT, Portman N, Lim E, Tilley W, Caldon CE, et al. Targeting CDK2 in cancer: challenges and opportunities for therapy. Drug Discov Today. 2020;25(2):406-13.
46. Chi Y, Carter JH, Swanger J, Mazin AV, Moritz RL, Clurman BE. A novel landscape of nuclear human CDK2 substrates revealed by in situ phosphorylation. Science Advances. 2020;6(16):eaaz9899.
47. NCBI. Entrez gene: CDK4 cyclin dependent kinase 4 [Available from: https://www.ncbi.nlm.nih.gov/gene?Db=gene&Cmd=ShowDetailView&TermToSearch=1019.
48. NCBI. Entrez gene: CDK6 cyclin dependent kinase 6 [Available from: https://www.ncbi.nlm.nih.gov/gene?Db=gene&Cmd=DetailsSearch&Term=1021.
49. Lim S, Kaldis P. Cdks, cyclins and CKIs: roles beyond cell cycle regulation. Development. 2013;140(15):3079-93.
50. Grossel MJ, Hinds PW. From cell cycle to differentiation: an expanding role for cdk6. Cell Cycle. 2006;5(3):266-70.

51. Chou J, Quigley DA, Robinson TM, Feng FY, Ashworth A. Transcription-Associated Cyclin-Dependent Kinases as Targets and Biomarkers for Cancer Therapy. Cancer Discov. 2020;10(3):351-70.
52. Galbraith MD, Bender H, Espinosa JM. Therapeutic targeting of transcriptional cyclin-dependent kinases. Transcription. 2019;10(2):118-36.
53. Ma H, Dean DC, Wei R, Hornicek FJ, Duan Z. Cyclin-dependent kinase 7 (CDK7) is an emerging prognostic biomarker and therapeutic target in osteosarcoma. Ther Adv Musculoskelet Dis. 2021;13:1759720x21995069.
54. Larochelle S, Amat R, Glover-Cutter K, Sansó M, Zhang C, Allen JJ, et al. Cyclin-dependent kinase control of the initiation-to-elongation switch of RNA polymerase II. Nat Struct Mol Biol. 2012;19(11):1108-15.
55. Ebmeier CC, Erickson B, Allen BL, Allen MA, Kim H, Fong N, et al. Human TFIIH Kinase CDK7 Regulates Transcription-Associated Chromatin Modifications. Cell Rep. 2017;20(5):1173-86.
56. Allen BL, Taatjes DJ. The Mediator complex: a central integrator of transcription. Nat Rev Mol Cell Biol. 2015;16(3):155-66.
57. Kagey MH, Newman JJ, Bilodeau S, Zhan Y, Orlando DA, van Berkum NL, et al. Mediator and cohesin connect gene expression and chromatin architecture. Nature. 2010;467(7314):430-5.
58. Bancerek J, Poss ZC, Steinparzer I, Sedlyarov V, Pfaffenwimmer T, Mikulic I, et al. CDK8 kinase phosphorylates transcription factor STAT1 to selectively regulate the interferon response. Immunity. 2013;38(2):250-62.
59. Zhao X, Feng D, Wang Q, Abdulla A, Xie XJ, Zhou J, et al. Regulation of lipogenesis by cyclin-dependent kinase 8-mediated control of SREBP-1. J Clin Invest. 2012;122(7):2417-27.
60. Elmlund H, Baraznenok V, Lindahl M, Samuelsen CO, Koeck PJ, Holmberg S, et al. The cyclin-dependent kinase 8 module sterically blocks Mediator interactions with RNA polymerase II. Proc Natl Acad Sci U S A. 2006;103(43):15788-93.
61. Bacon CW, D'Orso I. CDK9: a signaling hub for transcriptional control. Transcription. 2019;10(2):57-75.
62. Yamada T, Yamaguchi Y, Inukai N, Okamoto S, Mura T, Handa H. P-TEFb-mediated phosphorylation of hSpt5 C-terminal repeats is critical for processive transcription elongation. Mol Cell. 2006;21(2):227-37.
63. Sansó M, Levin RS, Lipp JJ, Wang VY, Greifenberg AK, Quezada EM, et al. P-TEFb regulation of transcription termination factor Xrn2 revealed by a chemical genetic screen for Cdk9 substrates. Genes Dev. 2016;30(1):117-31.
64. Bösken CA, Farnung L, Hintermair C, Merzel Schachter M, Vogel-Bachmayr K, Blazek D, et al. The structure and substrate specificity of human Cdk12/Cyclin K. Nat Commun. 2014;5:3505.
65. Cheng SWG, Kuzyk MA, Moradian A, Ichu T-A, Chang VCD, Tien JF, et al. Interaction of cyclin-dependent kinase 12/CrkRS with cyclin K1 is required for the phosphorylation of the C-terminal domain of RNA polymerase II. Mol Cell Biol. 2012;32(22):4691-704.
66. Chirackal Manavalan AP, Pilarova K, Kluge M, Bartholomeeusen K, Rajecky M, Oppelt J, et al. CDK12 controls G1/S progression by regulating RNAPII processivity at core DNA replication genes. EMBO reports. 2019;20(9):e47592.
67. Berg S. Characterization of Kinase Activity and Chromatin-Bound Interactome of Cyclin-Dependent Kinase 12 (CDK12) Oslo University Hospital, Rikshospitalet, Department of Microbiology: The Norwegian University of Life Sciences; 2020.
68. Greifenberg AK, Hönig D, Pilarova K, Düster R, Bartholomeeusen K, Bösken CA, et al. Structural and Functional Analysis of the Cdk13/Cyclin K Complex. Cell Rep. 2016;14(2):320-31.
69. Fan Z, Devlin JR, Hogg SJ, Doyle MA, Harrison PF, Todorovski I, et al. CDK13 cooperates with CDK12 to control global RNA polymerase II processivity. Sci Adv. 2020;6(18):eaaz5041.
70. Juric V, Murphy B. Cyclin-dependent kinase inhibitors in brain cancer: current state and future directions. Cancer Drug Resistance. 2020;3(1):48-62.
71. Sánchez-Martínez C, Lallena MJ, Sanfeliciano SG, de Dios A. Cyclin dependent kinase (CDK) inhibitors as anticancer drugs: Recent advances (2015–2019). Bioorganic & Medicinal Chemistry Letters. 2019;29(20):126637.

72. Zhang M, Zhang L, Hei R, Li X, Cai H, Wu X, et al. CDK inhibitors in cancer therapy, an overview of recent development. Am J Cancer Res. 2021;11(5):1913-35.
73. Inhibitors: CDK: Selleck Chemicals; [Available from: https://www.selleckchem.com/CDK.html.
74. Clinic M. Glioma. Mayo Foundation for Medical Education and Research 2020.
75. Xu S, Tang L, Li X, Fan F, Liu Z. Immunotherapy for glioma: Current management and future application. Cancer Letters. 2020;476:1-12.
76. Goldman SA. Gliomas NJ, USA: Merck Sharp & Dohme Corp.; 2021 [Available from: https://www.merckmanuals.com/professional/neurologic-disorders/intracranial-and-spinal-tumors/gliomas#v51042823.
77. Kondo Y, Katsushima K, Ohka F, Natsume A, Shinjo K. Epigenetic dysregulation in glioma. Cancer Science. 2014;105(4):363-9.
78. Meng W, Wang J, Wang B, Liu F, Li M, Zhao Y, et al. CDK7 inhibition is a novel therapeutic strategy against GBM both in vitro and in vivo. Cancer Manag Res. 2018;10:5747-58.
79. Greenall SA, Lim YC, Mitchell CB, Ensbey KS, Stringer BW, Wilding AL, et al. Cyclin-dependent kinase 7 is a therapeutic target in high-grade glioma. Oncogenesis. 2017;6(5):e336.
80. Le Rhun E, von Achenbach C, Lohmann B, Silginer M, Schneider H, Meetze K, et al. Profound, durable and MGMT-independent sensitivity of glioblastoma cells to cyclin-dependent kinase inhibition. International Journal of Cancer. 2019;145(1):242-53.
81. Lubanska D, Porter L. Revisiting CDK Inhibitors for Treatment of Glioblastoma Multiforme. Drugs R D. 2017;17(2):255-63.
82. Raub TJ, Wishart GN, Kulanthaivel P, Staton BA, Ajamie RT, Sawada GA, et al. Brain Exposure of Two Selective Dual CDK4 and CDK6 Inhibitors and the Antitumor Activity of CDK4 and CDK6 Inhibition in Combination with Temozolomide in an Intracranial Glioblastoma Xenograft. Drug Metab Dispos. 2015;43(9):1360-71.
83. Comprehensive genomic characterization defines human glioblastoma genes and core pathways. Nature. 2008;455(7216):1061-8.
84. Rahman S, Sowa ME, Ottinger M, Smith JA, Shi Y, Harper JW, et al. The Brd4 extraterminal domain confers transcription activation independent of pTEFb by recruiting multiple proteins, including NSD3. Mol Cell Biol. 2011;31(13):2641-52.
85. Duan Y, Guan Y, Qin W, Zhai X, Yu B, Liu H. Targeting Brd4 for cancer therapy: inhibitors and degraders. Medchemcomm. 2018;9(11):1779-802.
86. Yang H, Wei L, Xun Y, Yang A, You H. BRD4: An emerging prospective therapeutic target in glioma. Mol Ther Oncolytics. 2021;21:1-14.
87. Donati B, Lorenzini E, Ciarrocchi A. BRD4 and Cancer: going beyond transcriptional regulation. Mol Cancer. 2018;17(1):164.
88. Cheng Z, Gong Y, Ma Y, Lu K, Lu X, Pierce LA, et al. Inhibition of BET bromodomain targets genetically diverse glioblastoma. Clin Cancer Res. 2013;19(7):1748-59.
89. Liu F, Hon GC, Villa GR, Turner KM, Ikegami S, Yang H, et al. EGFR Mutation Promotes Glioblastoma through Epigenome and Transcription Factor Network Remodeling. Mol Cell. 2015;60(2):307-18.
90. Zhang M, Zhao K, Xu X, Yang Y, Yan S, Wei P, et al. A peptide encoded by circular form of LINC-PINT suppresses oncogenic transcriptional elongation in glioblastoma. Nat Commun. 2018;9(1):4475.
91. Pollard SM, Yoshikawa K, Clarke ID, Danovi D, Stricker S, Russell R, et al. Glioma stem cell lines expanded in adherent culture have tumor-specific phenotypes and are suitable for chemical and genetic screens. Cell Stem Cell. 2009;4(6):568-80.
92. Lucey BP, Nelson-Rees WA, Hutchins GM. Henrietta Lacks, HeLa cells, and cell culture contamination. Arch Pathol Lab Med. 2009;133(9):1463-7.
93. Zhang T, Kwiatkowski N, Olson CM, Dixon-Clarke SE, Abraham BJ, Greifenberg AK, et al. Covalent targeting of remote cysteine residues to develop CDK12 and CDK13 inhibitors. Nat Chem Biol. 2016;12(10):876-84.
94. Nelson JD, Denisenko O, Bomsztyk K. Protocol for the fast chromatin immunoprecipitation (ChIP) method. Nat Protoc. 2006;1(1):179-85.

95. Taylor SC, Posch A. The design of a quantitative western blot experiment. Biomed Res Int. 2014;2014:361590.
96. Brown L, Beynon, L.H. Mass spectrometry: Additional Information Encyclopedia Britannica, Inc.2020 [Available from: https://www.britannica.com/science/mass-spectrometry.
97. Oliveros JC. VENNY. An interactive tool for comparing lists with Venn Diagrams. 2007 [Available from: https://bioinfogp.cnb.csic.es/tools/venny/.
98. Zhou Y, Zhou B, Pache L, Chang M, Khodabakhshi AH, Tanaseichuk O, et al. Metascape provides a biologist-oriented resource for the analysis of systems-level datasets. Nature Communications. 2019;10(1):1523.
99. Shannon P, Markiel A, Ozier O, Baliga NS, Wang JT, Ramage D, et al. Cytoscape: a software environment for integrated models of biomolecular interaction networks. Genome Res. 2003;13(11):2498-504.
100. Kuleshov MV, Jones MR, Rouillard AD, Fernandez NF, Duan Q, Wang Z, et al. Enrichr: a comprehensive gene set enrichment analysis web server 2016 update. Nucleic Acids Res. 2016;44(W1):W90-7.
101. Liberzon A, Subramanian A, Pinchback R, Thorvaldsdóttir H, Tamayo P, Mesirov JP. Molecular signatures database (MSigDB) 3.0. Bioinformatics. 2011;27(12):1739-40.
102. Szklarczyk D, Franceschini A, Wyder S, Forslund K, Heller D, Huerta-Cepas J, et al. STRING v10: protein-protein interaction networks, integrated over the tree of life. Nucleic Acids Res. 2015;43(Database issue):D447-52.
103. Yu M, Yang W, Ni T, Tang Z, Nakadai T, Zhu J, et al. RNA polymerase II-associated factor 1 regulates the release and phosphorylation of paused RNA polymerase II. Science. 2015;350(6266):1383-6.
104. Pilarova K, Herudek J, Blazek D. CDK12: cellular functions and therapeutic potential of versatile player in cancer. NAR Cancer. 2020;2(1).
105. Krajewska M, Dries R, Grassetti AV, Dust S, Gao Y, Huang H, et al. CDK12 loss in cancer cells affects DNA damage response genes through premature cleavage and polyadenylation. Nature Communications. 2019;10(1):1757.
106. Demsar J CT, Erjavec A, Gorup C, Hocevar T, Milutinovic M, Mozina M, Polajnar M, Toplak M, Staric A, Stajdohar M, Umek L, Zagar L, Zbontar J, Zitnik M, Zupan B. Orange: Data Mining Toolbox in Python. 2013.
107. Paculová H, Kohoutek J. The emerging roles of CDK12 in tumorigenesis. Cell Div. 2017;12:7.
108. Zhou T, Wang Y, Qian D, Liang Q, Wang B. Over-expression of TOP2A as a prognostic biomarker in patients with glioma. Int J Clin Exp Pathol. 2018;11(3):1228-37.
109. Huang G, Ho B, Conroy J, Liu S, Qiang H, Golubovskaya V. The microarray gene profiling analysis of glioblastoma cancer cells reveals genes affected by FAK inhibitor Y15 and combination of Y15 and temozolomide. Anticancer Agents Med Chem. 2014;14(1):9-17.
110. Peng C, Zeng W, Su J, Kuang Y, He Y, Zhao S, et al. Cyclin-dependent kinase 2 (CDK2) is a key mediator for EGF-induced cell transformation mediated through the ELK4/c-Fos signaling pathway. Oncogene. 2016;35(9):1170-9.
111. Krasinska L, Besnard E, Cot E, Dohet C, Méchali M, Lemaitre JM, et al. Cdk1 and Cdk2 activity levels determine the efficiency of replication origin firing in Xenopus. Embo j. 2008;27(5):758-69.
112. Fan Z. CDK12 and CDK13 cooperatively regulate RNA polymerase II elongation and alternative polyadenylation of mRNA 2020.
113. Qi C, Cao J, Li M, Liang C, He Y, Li Y, et al. HMGA1 Overexpression is Associated With the Malignant Status and Progression of Breast Cancer. The Anatomical Record. 2018;301(6):1061-7.
114. Chi Y, Welcker M, Hizli AA, Posakony JJ, Aebersold R, Clurman BE. Identification of CDK2 substrates in human cell lysates. Genome Biol. 2008;9(10):R149.
115. Spencer SL, Cappell SD, Tsai FC, Overton KW, Wang CL, Meyer T. The proliferation-quiescence decision is controlled by a bifurcation in CDK2 activity at mitotic exit. Cell. 2013;155(2):369-83.

116. Yang HW, Cappell SD, Jaimovich A, Liu C, Chung M, Daigh LH, et al. Stress-mediated exit to quiescence restricted by increasing persistence in CDK4/6 activation. Elife. 2020;9.

7. Appendix

7.1 Media compositions

N2B27 media

250 mL Dulbecco's Modified Eagle Medium/Nutrient Mixture F-12 (DMEM/F-12)(1X), 250 mL Neurobasal Medium 1X (Gibco), N2 supplement (16 µg putricine dihydrochloride, 6,25 µg insulin, 50 µg apotransferrin, 21.6 ng progesterone in EtOH, 15 nM sodium selenite), 1 vial B27 supplement, 5 mL Penicillin Streptomycin Glutamine (100X) (Gibco), 5 mL glutaMAX (100X) (Gibco), 5 mL Minimum Essential Medium – Non-essential Amino Acids Solution (MEM-NEAA) (100X) (Gibco), 5 mL 100 mM Sodium Pyruvat (100X) (Gibco), 50 µM b-mercaptoethanol (Gibco), 10 mM Hepes (Fisher BioReagents), 50 µg BSA (Saween & Werner), and 4 µg Heparin (Merck Life Science). N2 and B27 were internally laboratory made, using the protocol from Weizmann Institute of Science (Science, 2016).

ES cell media

N2B27 media supplemented with 10 µM MEKi and 1 mM GSKi (Sigma, Life Science, CHIR99021) (2i), and LIF (internally laboratory made, expressed from the COS cells and harvested as supernatant). Used on ES cells.

NSC media

N2B27 media supplemented with EGF and FGFb. EGF (Perprotech (315-09)) used at the final concentration of 10 ng/mL and FGFb (Perprtech (100-18B)) used at the final concentration of 10 ng/mL. Used on glioma cells.

7.2 Buffer compositions

7.2.1 Cell lysis and immunoprecipitation

Lysis buffer

50 mM Tris-HCl pH 7.5 (Gibco), 300 mM NaCl (Oslo University Hospital), 0.5% ICEPA® CA-630 (Sigma-Aldrich), 1 mM EDTA pH8 (Oslo University Hospital). 1 mM DTT (Saween & Werner), 1 µg AP (Sigma-Aldrich) and 0.5 µg LP (Sigma-Aldrich) per mL buffer was added to the cold media before use.

Washing buffer

50 mM Tris-HCl (Oslo University Hospital), 150 mM NaCl (Oslo University Hospital), 1 mM EDTA (Oslo University Hospital), 0.5% IGEPAL CA-630 (Sigma-Aldrich)

7.2.2 Western blotting

20x TBS

0.4 M TRIS pH 7.5 and 3 M NaCl (Oslo University Hospital)

TBS-T

25 mL 20x TBS, 475 mL milli-Q water, and 500 µl TweenÒ 20 (Sigma)

Blocking milk (5% milk)

30 mL TBS-T, 1.5 g skim milk powder, and 6 µl sodium azide (Sigma-Aldrich)

7.3 MS results

7.3.1 Phospho-proteome dataset

The phospho-proteome dataset was sorted so that at least 3 out of the 4 conditions were significant hits. The hits that were not significant have the value “0,001”.

Name	G7_1h	G7_6h	G144_1h	G144_6h
LMNB2	-8,02585	0,242521	0,001	-1,73631
LMNB1	-8,02585	0,242521	0,599974	-1,73631
PHRF1	-6,91762	-3,39285	-4,08125	-1,52431
SRRM2	-6,12494	-4,76055	-6,74019	-5,91024
FOXK1	-5,49224	-5,25224	-3,27428	1,206647
SPEN	-5,43524	-3,93368	-0,46396	-0,66036
MDC1	-5,17968	0,389178	-5,69201	-1,19233
SMARCC2	-5,12372	0,372611	-1,45432	-0,62556
TOP2A	-4,89932	-3,21299	-1,77451	-1,81757
MARCKSL1	-4,83869	0,57367	-0,59453	-0,85012
HMGA1	-4,53402	-4,24157	0,001	-6,36696
TCF20	-4,44869	-1,16877	0,001	-0,59474
TOP2B	-4,1943	-3,40003	-0,25835	-0,81229
TMPO	-4,18515	-0,81585	-0,59019	-0,59964
ZNF318	-4,17471	-2,39338	-0,51129	0,001
RBM12B	-4,13429	0,377104	0,001	-2,7408
NES	-4,10519	0,207752	-1,56799	-1,94762
MGA	-3,81599	-3,63128	0,001	-0,29172
SPTBN1	-3,79524	4,490821	0,554728	-0,66632
SPTBN1	-3,79524	4,490821	-0,5397	-0,66632
NIPBL	-3,50774	0,566023	-0,23593	-0,97853

LIMCH1	-3,41194	0,643176	-0,53909	-1,29342
SON	-3,37599	-4,73238	-1,75734	-0,9758
MYBBP1A	-3,36449	-2,3871	5,794525	-2,62764
SH3BP4	-3,32802	-1,93885	2,607625	0,001
SH3BP4	-3,32802	-1,93885	2,607625	0,001
PRR12	-3,2907	0,568763	0,744208	0,001
PRR12	-3,2907	0,568763	0,744208	0,001
LIMCH1	-3,22808	0,643176	1,938637	-0,74777
RIF1	-3,2007	0,384493	-4,44198	-2,75875
RIF1	-3,2007	0,384493	-4,44198	-2,75875
TRIM28	-3,11536	0,551368	-0,51349	-0,59982
TRIM28	-3,11536	0,551368	-0,51349	-0,69834
PNN	-3,10833	-0,61577	-5,95779	0,001
DKC1	-3,01059	-3,37516	0,402323	-0,50894
NIPBL	-2,90651	0,566023	-0,23593	-0,97853
SRRM1	-2,8718	-0,77408	-2,03909	-3,13466
PRRC2C	-2,84958	-2,38201	0,001	3,37073
PRRC2C	-2,84958	-2,38201	0,001	3,37073
ZYX	-2,84111	-3,80944	0,001	-0,58489
ZNF644	-2,74461	-2,61494	0,001	-3,7629
NPM1	-2,72519	-3,68904	-0,42266	-3,92081
EPB41	-2,71867	2,583334	-1,92712	-1,1682
SSFA2	-2,64137	1,655579	0,001	-0,40164
SSFA2	-2,64137	1,616256	0,001	-0,70103
TCOF1	-2,62506	-0,35255	0,001	-2,25862
MAP1B	-2,6137	-2,82958	-5,84036	-1,1411
RBBP6	-2,48334	-2,30429	-0,42236	0,001
MECP2	-2,4171	-2,10827	-0,74209	-0,70737
ACIN1	-2,1354	0,460214	-0,44548	-4,90715
MFAP1	-2,05266	-0,65132	-0,42034	-0,91808
RBM15	-1,98516	-3,47273	0,001	-0,81334
NOC2L	-1,85652	0,001	-6,12001	-0,38396
RSF1	-1,64971	-1,4808	-4,78482	-0,50249
HMGA1	-1,59258	-1,23415	0,001	1,790286
PRKAR2A	-1,583	-1,6451	0,970877	0,001
PRKAR2A	-1,583	-1,98814	-0,44775	0,001
MYBBP1A	-1,56446	-2,3871	5,794525	-0,99012
PHIP	-1,50415	-1,32363	-0,31139	-0,65624
TOP2A	-1,29663	-1,11468	-1,34403	0,531787
MATR3	-1,26575	0,451829	-0,44907	-1,31095
MATR3	-1,26575	-1,20852	-0,6855	-1,31095
BCLAF1	-1,19555	-0,49741	-4,66994	-1,42205
NOP58	-1,17075	-0,50199	-2,75969	-0,32763
RPLP1	-1,02974	0,22351	-0,48424	-4,55387
RPLP2	-1,02974	0,22351	-0,48424	-4,55387
RBM12B	-0,83526	0,377104	0,001	-2,7408

MAP1A	-0,82814	3,938456	-2,23072	-4,65596
SRSF7	-0,80931	-0,67879	-0,72288	-1,6515
AFF4	-0,77662	1,395327	0,001	-0,92578
AFF4	-0,77662	-1,01733	0,001	-0,92578
THRAP3	-0,76978	-0,70418	-0,40952	-3,47594
CDK11B	-0,76911	3,696332	-0,59742	-0,18623
CDK11A	-0,76911	0,409213	-0,59742	-0,18623
CDK11A	-0,76911	0,409213	-2,50499	-1,02817
CDK11B	-0,76911	0,409213	-2,50499	-1,02817
INTS1	-0,75984	-0,6066	0,001	-0,53924
CTNND1	-0,75455	-0,40795	-0,97749	-3,35231
RBMXL1	-0,72569	-1,25215	0,001	-1,10514
TCF20	-0,72516	-0,76821	0,001	0,23815
SRRT	-0,71841	0,372595	-0,46736	-1,45646
RBM5	-0,71647	-0,43156	-3,81499	0,001
NOP56	-0,67107	0,001	-5,11012	1,494872
PML	-0,66992	-0,76797	0,001	-1,00991
RBMX	-0,65959	-0,7234	0,001	0,182058
RBMXL1	-0,65959	-0,7234	0,001	0,182058
RBMX	-0,65959	-1,25215	0,001	-0,63352
SGOL1	-0,65019	-0,50258	0,001	-0,96107
VIM	-0,6412	-0,87497	0,001	-0,44781
HNRNPM	-0,62275	-0,49438	0,348242	-4,93148
SCAF11	-0,58413	0,445744	-0,66315	-0,65458
SLTM	-0,57812	-0,47961	0,001	-0,57986
NUCKS1	-0,54375	0,359516	-0,66531	-0,16021
FIP1L1	-0,54074	1,349848	0,001	-3,52459
KMT2A	-0,53618	-2,41408	0,367132	-1,06402
RBM15	-0,51454	0,355569	0,001	-0,45147
ATXN2L	-0,49684	0,345888	-3,98939	-0,55479
CDK13	-0,49488	-2,88411	0,001	-3,48186
PRPF4B	-0,48779	0,264339	-1,20274	-4,34807
SRSF6	-0,48549	0,519303	-0,51298	1,958321
SRSF5	-0,48549	-4,3856	3,734304	-0,47528
SRSF4	-0,48549	-4,3856	0,001	-0,49561
SRSF5	-0,48549	-4,3856	3,136909	-0,47528
SRSF6	-0,48549	-4,3856	-0,76869	-0,27816
MTDH	-0,48048	-0,64863	0,001	-0,35059
PPIG	-0,46659	1,941977	-0,67897	-0,19913
SF3B1	-0,45298	0,516631	-0,60423	-0,827
SF3B1	-0,45298	-3,53426	-0,60423	-2,70774
SLC38A1	-0,45218	-0,3417	-0,68199	-0,76715
RGPD3	-0,43785	0,450038	-0,41379	2,422694
RGPD4	-0,43785	0,450038	-0,41379	2,422694
RGPD1	-0,43785	0,450038	-0,41379	2,422694
RGPD2	-0,43785	0,450038	-0,41379	2,422694

RGPD5	-0,43785	0,450038	-0,41379	2,422694
RGPD8	-0,43785	0,450038	-0,41379	2,422694
RANBP2	-0,43785	-0,36417	-0,50538	-1,0934
RGPD4	-0,43785	-0,36417	-0,50538	-1,0934
RGPD3	-0,43785	-0,36417	-0,41379	-1,0934
RGPD1	-0,43785	-0,36417	-0,41379	-1,0934
RGPD2	-0,43785	-0,36417	-0,41379	-1,0934
RGPD5	-0,43785	-0,36417	-0,41379	-1,0934
RGPD8	-0,43785	-0,36417	-0,41379	-1,0934
C17orf85	-0,42504	-1,62992	0,001	-0,30081
ZC3H18	-0,42184	0,610213	0,527725	2,049178
ZC3H18	-0,42184	0,533569	-0,5322	-3,8684
HIST1H1D	-0,41718	-0,43674	0,001	1,283856
HIST1H1D	-0,41718	-0,43674	0,001	1,283856
ZC3H13	-0,41163	-0,54669	0,001	-1,78523
BOD1L1	-0,40478	0,410916	-0,368	-0,37742
BOD1L1	-0,40478	0,410916	-0,368	-0,65237
CDK13	-0,39517	2,957127	0,001	-3,48186
NOP56	-0,39039	0,001	-5,11012	1,494872
SUMO1	-0,38965	0,001	-0,47518	-2,31593
DKC1	-0,38731	0,487816	0,402323	-0,50894
SMARCA5	-0,38656	0,001	-0,9397	-1,05835
SRSF11	-0,36538	1,211461	-0,95367	0,280703
SRSF11	-0,36538	0,696532	-0,95367	-0,84134
SIPA1L2	-0,34447	0,308687	0,001	-0,79483
SIPA1L2	-0,34447	0,308687	0,001	-0,79483
CHAMP1	-0,34446	-2,67553	0,001	-0,16272
RPLP1	-0,34436	0,22351	-0,48424	-4,55387
RPLP2	-0,34436	0,22351	-0,48424	-4,55387
SRSF9	-0,337	-0,55425	-0,74517	-2,55287
TJP1	-0,31735	0,001	-0,34596	-3,85978
BUD13	-0,28842	1,327854	-0,39285	5,388923
BUD13	-0,28842	-1,95575	-0,88423	-2,55289
RANBP2	-0,25215	0,640411	-0,41379	2,422694
SNW1	0,001	0,190334	-0,75848	-0,46598
TRA2A	0,001	0,193564	0,272437	3,22688
HNRNPA1	0,001	0,221145	-6,55731	-0,65794
EIF3F	0,001	0,301905	-0,9912	-0,55386
PBX2	0,001	0,333138	-0,5949	-0,35399
ACLY	0,001	0,361532	-0,49519	-0,94017
SNTB2	0,001	0,50636	-0,51965	-0,72388
EEPD1	0,001	0,400126	-0,85391	-1,25781
AJAP1	0,001	0,409213	-0,59742	-1,02817
HUWE1	0,001	0,416566	-0,46742	-0,26511
SEC62	0,001	0,431928	-0,88047	-0,69103
SCAF1	0,001	0,443221	-0,26333	0,563765

CENPF	0,001	3,341848	-1,36221	-2,60375
WHSC1	0,001	0,475454	1,730133	-0,75704
GOLGA4	0,001	0,482941	-0,42604	-0,65009
NASP	0,001	0,528416	-1,00106	-0,45984
PPFIA1	0,001	0,602275	-0,69593	-0,55011
MLLT1	0,001	0,659063	0,415401	-0,44958
RBM39	0,001	0,768296	-0,29278	5,740386
HNRNPU	0,001	1,122241	2,809338	-1,14585
TRIM24	0,001	1,255535	0,445054	1,011104
ALPP	0,001	1,988506	-0,60546	-0,86523
ALPI	0,001	1,988506	-0,60546	-0,86523
PEAK1	0,001	2,017143	-0,53391	-0,23294
RNPS1	0,001	2,189133	-1,01533	-0,84433
WDR44	0,001	2,777921	-3,47218	-0,5703
SRSF3	0,001	-3,75227	1,539982	-0,75662
SUPT6H	0,001	-2,23764	2,650955	-0,8537
NUP153	0,001	-0,89915	3,031704	5,308404
SCAF1	0,001	-3,44522	-0,48525	-5,98214
CENPF	0,001	0,448447	-1,36221	-2,60375
SNW1	0,001	0,190334	-0,75848	-2,31092
TRA2A	0,001	0,193564	-3,44993	-1,77302
EEPD1	0,001	0,400126	-0,85391	-1,25781
HNRNPU	0,001	1,122241	2,809338	-1,14585
AJAP1	0,001	0,409213	-0,59742	-1,02817
ACLY	0,001	0,361532	-0,49519	-0,94017
ALPP	0,001	1,988506	-0,60546	-0,86523
ALPI	0,001	1,988506	-0,60546	-0,86523
SUPT6H	0,001	-2,23764	2,443687	-0,8537
RNPS1	0,001	2,038117	-1,19979	-0,84433
SRSF3	0,001	-5,00338	1,539982	-0,81307
HNRNPA1	0,001	0,221145	-6,55731	-0,78938
WHSC1	0,001	0,475454	1,730133	-0,75704
SNTB2	0,001	0,383931	-0,51965	-0,72388
SEC62	0,001	0,431928	-0,88047	-0,69103
GOLGA4	0,001	0,482941	-0,42604	-0,65009
WDR44	0,001	2,777921	-3,47218	-0,5703
EIF3F	0,001	0,301905	-0,9912	-0,55386
PPFIA1	0,001	0,602275	-0,69593	-0,55011
NASP	0,001	0,528416	-1,00106	-0,45984
MLLT1	0,001	0,659063	0,415401	-0,44958
PBX2	0,001	0,333138	-0,5949	-0,35399
HUWE1	0,001	0,416566	-0,61647	-0,26511
PEAK1	0,001	2,017143	-0,53391	-0,23294
NUP153	0,001	-0,89915	-1,24292	5,308404
RBM39	0,001	0,768296	-0,37602	5,740386
LMNB1	0,139076	0,242521	3,070992	0,484812

LMNB2	0,139076	0,242521	0,001	-1,00303
EMD	0,230953	0,602684	-0,35053	0,001
EMD	0,230953	0,602684	-0,35053	0,001
CHAMP1	0,242881	5,683702	0,001	2,625764
AEBP2	0,246094	0,520833	-0,21571	0,315734
AEBP2	0,246094	0,520833	-0,21571	0,315734
LMNA	0,252813	0,435485	1,867853	-0,60425
RB1	0,283494	0,577218	-4,64095	-1,81885
SF1	0,284646	0,388975	-0,35466	-3,85053
SF1	0,284646	0,388975	-0,35466	-3,85053
SCRIB	0,288143	0,305503	0,001	-2,59638
SCRIB	0,288143	0,305503	0,001	-2,59638
LIMA1	0,298932	0,464021	-0,48737	-0,44052
SRRT	0,305822	2,891045	-0,46736	-1,45646
FNBP4	0,309923	0,778376	0,001	-0,93197
FNBP4	0,309923	0,778376	0,001	-0,93197
CDK1	0,310713	1,352865	4,456754	0,001
CDK2	0,310713	0,461667	4,456754	0,001
CDK3	0,310713	0,461667	4,456754	0,001
CDK1	0,310713	0,269725	-0,71846	0,001
CDK2	0,310713	0,269725	-0,71846	0,001
CDK3	0,310713	0,269725	-0,71846	0,001
GTF3C4	0,31857	0,467115	0,001	-2,55562
GTF3C4	0,31857	0,467115	0,001	-2,55562
TCOF1	0,323432	0,306494	0,001	-0,39543
EDC3	0,323524	0,58913	-1,50225	0,001
ARID1A	0,324828	0,653651	0,001	-0,63702
ARID1A	0,324828	0,653651	0,001	-0,63702
SCAF11	0,338755	0,445744	-0,62172	-0,65458
MAP4	0,365047	0,001	-3,81415	-4,14607
MIEF1	0,371634	0,547567	-0,54355	0,001
MIEF1	0,371634	0,320996	-0,54355	0,001
CDK12	0,373758	1,15843	-0,29779	-0,29933
CDK12	0,373758	0,603931	-2,95326	-3,48186
LSM14A	0,376769	0,721473	-0,72893	0,001
ATXN2L	0,380507	0,417082	-3,98939	-0,55479
ANLN	0,382578	0,387194	0,001	-0,40425
ANLN	0,382578	0,387194	0,001	-0,40425
RBM14	0,395945	0,59129	0,001	-4,92202
RBM14	0,395945	0,420006	0,001	-4,92202
LAMTOR1	0,400826	0,566316	0,001	-2,72215
LAMTOR1	0,400826	0,566316	0,001	-2,72215
DOCK7	0,409652	1,569761	-0,51354	-0,59668
DOCK7	0,409652	1,569761	-0,51354	-1,0709
GATAD2A	0,411713	0,475627	-1,2561	0,001
IRF2BPL	0,421586	0,698907	0,001	-1,09363

IRF2BPL	0,421586	0,49578	0,001	-1,09363
SRSF1	0,42657	0,321402	0,001	0,3287
CDK7	0,436513	0,551028	-0,33213	-0,88734
CDK7	0,436513	-4,22992	-0,33213	-0,88734
CD2BP2	0,436561	0,408443	-0,60441	0,001
CD2BP2	0,436561	0,408443	-0,60441	0,001
IRF2BP1	0,436859	0,605012	-0,56201	0,001
DDX24	0,455011	0,582376	0,832228	0,001
IRS2	0,465647	0,465171	0,001	-1,34859
IRS2	0,465647	0,465171	0,001	-1,34859
SON	0,46792	0,636773	-0,67031	-0,73192
RBM6	0,478741	0,67577	-0,82827	0,001
RBM6	0,478741	0,67577	-0,82827	0,001
GATAD2A	0,51064	1,58216	-1,2561	0,001
LARP4	0,511262	0,57008	-0,56559	0,001
LARP4	0,511262	0,57008	-0,56559	0,001
MARCKSL1	0,513882	0,781658	0,638214	-0,85012
TOMM22	0,52367	1,090907	-1,08883	0,001
TOMM22	0,52367	1,090907	-1,08883	0,001
MTMR3	0,543033	1,285594	-3,82273	0,001
MTMR3	0,543033	1,285594	-3,82273	0,001
PCYT1A	0,55696	2,649897	-0,5286	-0,44091
PCYT1A	0,55696	0,324832	-0,78792	-0,44091
EIF4G1	0,572642	0,386428	-0,67341	0,001
EIF4G1	0,572642	0,386428	-0,67341	0,001
ZC3H13	0,576222	1,261684	0,001	-0,32608
GSK3B	0,576384	0,555083	0,001	-0,96502
GSK3A	0,576384	0,555083	0,001	-0,96502
GSK3B	0,576384	0,555083	0,001	-0,96502
GSK3A	0,576384	0,555083	0,001	-0,96502
AGFG1	0,583541	0,628723	0,001	-1,04637
AGFG1	0,583541	0,628723	0,001	-1,04637
DNAJC5	0,603501	1,442764	-1,32467	0,001
DNAJC5	0,603501	1,442764	-1,32467	0,001
NPM1	0,607049	3,482898	4,478109	-1,57948
PRPF40A	0,609368	0,368053	-0,86735	-0,70075
PRPF40A	0,609368	0,368053	-1,2922	-0,70075
METTL14	0,60947	0,530241	-0,29918	0,001
METTL14	0,60947	0,530241	-0,29918	0,001
RTN4	0,617367	0,281582	0,001	-0,52673
TP53BP1	0,635668	0,482696	1,967289	1,748468
TP53BP1	0,635668	0,482696	1,967289	-0,83236
AKT1S1	0,653031	0,571016	0,001	-0,8761
AKT1S1	0,653031	0,571016	0,001	-0,8761
SLC39A7	0,667581	0,411122	0,001	-0,42356
SLC39A7	0,667581	0,411122	0,001	-0,42356

RB1	0,706404	0,577218	-4,41771	-1,81885
CFL1	0,706585	0,494004	-0,51272	-0,37206
CFL1	0,706585	0,494004	-0,51272	-0,37206
SRSF9	0,723746	0,451651	-0,74517	0,569741
EDC3	0,740807	0,58913	-1,50225	0,001
RBM10	0,751095	1,154529	-1,14975	0,001
RBM10	0,751095	1,154529	-1,14975	0,001
ZYX	0,7544	0,387401	0,001	-0,58489
DSTN	0,761595	0,620087	0,001	-3,0963
DSTN	0,761595	0,620087	0,001	-3,0963
SRRM1	0,770924	3,70398	0,293521	3,765853
YTHDC1	0,774986	0,974731	-1,05632	-0,62373
YTHDC1	0,774986	0,974731	-1,05632	-0,69
RSL1D1	0,79497	0,235588	-6,1916	-0,80239
CARHSP1	0,80964	0,259975	0,001	-0,51021
LIG3	0,862025	0,590967	-0,53432	-0,41347
LIG3	0,862025	0,590967	-0,53432	-0,41347
EPB41L2	0,871649	1,309	-0,7194	0,001
MAP4	0,875683	0,001	-0,29572	-0,59444
AAK1	0,886848	0,684259	0,001	-0,93287
AAK1	0,886848	0,684259	0,001	-1,08808
WIZ	0,973194	0,921192	-4,60087	-0,37996
WIZ	0,973194	0,921192	-4,60087	-0,37996
HNRNPM	0,973208	0,286126	0,348242	-1,18336
TNKS1BP1	0,982539	4,119469	1,678441	0,001
TNKS1BP1	0,982539	0,261748	-0,53742	0,001
LSM14A	0,99579	1,014923	3,211367	0,001
THRAP3	1,004881	0,525203	0,72361	-0,27111
TMEM109	1,007373	0,605758	0,981699	0,001
CCDC167	1,0155	1,177514	4,153395	0,001
FIP1L1	1,118364	1,349848	0,001	-3,52459
BCLAF1	1,1653	1,086285	-0,2435	-0,26298
MAP2	1,200973	0,001	-0,87634	-0,32654
MAP2	1,200973	0,001	-0,87634	-0,32654
PCF11	1,246636	1,032841	0,541019	0,001
PPIG	1,317253	1,941977	-0,4533	-0,19913
MFF	1,320011	0,646018	0,001	-1,79428
VRK3	1,353073	1,94953	-0,64096	0,001
VRK3	1,353073	1,94953	-0,64096	0,001
EPB41L1	1,471326	2,354739	-0,69064	-6,39105
EPB41L1	1,471326	2,354739	-0,69064	-6,39105
PTMA	1,489132	0,942312	0,001	0,144285
VIM	1,502939	2,171095	0,001	-0,44781
PALLD	1,590287	0,001	-0,56212	-0,94489
PALLD	1,590287	0,001	-0,56212	-0,94489
PRPF4B	1,590652	0,437871	-0,62671	0,316495

MDC1	1,693054	0,89099	-0,37703	-0,73936
NUCKS1	1,701152	0,359516	-0,403	2,235741
EPB41L2	1,840002	2,182586	-0,7194	0,001
ZNF318	1,894281	2,090085	-0,51129	0,001
EPB41	1,958319	2,583334	-1,92712	-1,1682
IRF2BP1	2,263779	2,603798	-0,56201	0,001
CLSPN	2,319791	2,272034	0,001	-0,9364
CLSPN	2,319791	2,272034	0,001	-0,9364
STMN1	2,56871	2,469735	0,001	0,342676
RAB1A	2,79952	3,120824	-0,88265	-0,37477
RAB1A	2,79952	3,120824	-0,88265	-0,37477
MFF	2,966001	3,247051	0,001	-1,79428
FOXK1	3,295987	3,68368	-3,27428	1,206647
SLC38A1	3,324658	3,911891	-0,56567	-0,49464
MECP2	3,36353	-2,10827	-0,74209	-0,70737
RTN4	3,3637	6,971387	0,001	-0,52673
SMARCC2	3,542845	3,938735	-1,45432	-0,30531
SPEN	3,571256	0,505943	-0,46396	-0,58692
LIMA1	3,59955	6,442275	-0,48737	-0,44052
RSL1D1	3,704174	0,235588	-0,55967	-0,80239
KMT2A	3,705776	3,89395	0,367132	0,767792
LMNA	4,221636	3,773628	2,7885	-0,22991
NOLC1	4,535482	0,001	-0,65508	4,47751
NOLC1	4,535482	0,001	-3,50311	-0,44356
PML	4,592904	4,407866	0,001	-1,00991
CARHSP1	4,609348	3,334717	0,001	-0,41702
MAP1B	4,696861	0,876254	-0,54666	3,810483
ACIN1	4,932137	5,112751	-0,44548	-0,55089
SRRM2	5,126127	3,168483	5,193518	7,658363
CTR9	5,350811	5,580898	0,316099	-0,80371
CTR9	5,350811	5,580898	-1,31045	-0,80371
MAP1A	5,857772	6,13886	-0,45286	-0,55501
TMPO	6,623959	6,552733	0,466404	-0,32799
EDC4	7,016837	7,090581	0,825738	0,001
EDC4	7,016837	7,090581	-2,94312	0,001
NES	11,10389	1,039925	0,742666	-1,94762

7.3.2 Total-proteome dataset

The total-proteome dataset was sorted so that at least 3 out of the 4 conditions were significant hits. The hits that were not significant have the value “0,001”.

Name	G7_1h	G7_6h	G144_1h	G144_6h
H3F3A	-4,28622	-6,26872	0,001	-0,6915
H2AFY	-2,91442	-2,87441	-0,21457	-1,41095
TOP2B	-2,4403	-1,76702	-0,40267	-0,85922

HIST2H3A	-1,81373	-2,18818	1,38127	1,878249
HIST2H3A	-1,81373	-2,18818	1,38127	1,878249
TOP2A	-1,66331	-1,59322	-0,18009	-0,84984
HMGN4	-1,61089	-0,67016	0,001	-1,7418
HIST1H3A	-1,59057	-1,87172	0,769836	0,936052
HIST3H3	-1,59057	-1,87172	0,769836	0,936052
HIST1H3A	-1,59057	-1,87172	0,769836	0,936052
HIST3H3	-1,59057	-1,87172	0,769836	0,936052
HIST1H4A	-1,58879	-1,86845	0,001	-0,80311
HMGA1	-1,43332	-1,35593	0,001	-1,07113
HIST2H2BE	-1,37754	-1,71117	0,519	-0,66962
HIST1H2BJ	-1,37754	-1,71117	0,519	-0,66962
HIST1H2BJ	-1,37754	-1,71117	0,519	-0,66962
HIST2H2BE	-1,37754	-1,71117	0,519	-0,66962
H2AFX	-1,31078	-2,10458	1,160304	2,177354
HIST1H2AA	-1,31078	-2,10458	1,160304	2,177354
H2AFX	-1,31078	-2,10458	1,160304	2,177354
HIST1H2AA	-1,31078	-2,10458	1,160304	2,177354
MYH10	-1,26447	-1,31294	-0,25098	0,001
PHIP	-1,11962	-1,81472	0,001	-0,52123
NSA2	-0,98235	-0,853	0,001	-1,6376
C1QBP	-0,93669	-0,97202	0,001	0,232417
C1QBP	-0,93669	-0,97202	0,001	0,232417
H2BFS	-0,92648	-1,11776	0,001	-0,78225
HIST1H2BK	-0,92648	-1,11776	0,001	-0,78225
SON	-0,75986	-0,45693	0,001	-0,4211
RSF1	-0,72923	-0,67204	0,001	-0,25876
CBX5	-0,69927	-0,84719	0,001	-0,35593
MYH9	-0,6896	-0,90077	-0,14883	0,275122
MYH9	-0,6896	-0,90077	-0,14883	0,275122
SOD2	-0,67194	-0,47992	-0,21819	0,758378
SOD2	-0,67194	-0,47992	-0,21819	0,758378
H1FX	-0,65349	-0,19904	0,001	-0,50223
AHCYL1	-0,56326	0,001	-0,90729	-0,90155
AHCYL2	-0,56326	0,001	-0,90729	-0,90155
UTP18	-0,55611	-0,44294	0,001	-0,9085
RPS26	-0,5281	-0,68391	-0,36345	-0,41146
RPL9	-0,52351	-0,62051	-0,32213	-0,3021
KIAA1429	-0,5216	-0,60612	0,001	0,816548
KIAA1429	-0,5216	-0,60612	0,001	0,816548
UTP15	-0,51635	-0,33196	0,001	1,287745
UTP15	-0,51635	-0,33196	0,001	1,287745
BTF3	-0,48462	-0,65879	0,001	0,899259
BTF3	-0,48462	-0,65879	0,001	0,899259
MRPL10	-0,47862	-0,47813	0,001	0,642968
MRPL10	-0,47862	-0,47813	0,001	0,642968

RCN2	-0,4626	-0,42489	-0,44606	0,001
HIST1H1B	-0,45767	-0,31203	0,339255	-0,39331
HIST1H1B	-0,45767	-0,31203	0,339255	-0,39331
RPL37A	-0,42972	0,001	-0,70051	-0,73711
EIF3M	-0,41967	0,001	-0,41504	0,355385
EIF3M	-0,41967	0,001	-0,41504	0,355385
CDIPT	-0,41668	-0,62157	0,001	-0,49222
RPS9	-0,4118	-0,11048	-0,36077	-0,26676
DLD	-0,41115	-0,38911	0,001	0,187092
DLD	-0,41115	-0,38911	0,001	0,187092
RPL18A	-0,40811	-0,24163	-0,40213	-0,6364
RPS2	-0,39695	0,001	-0,43241	-0,21606
EIF4A1	-0,36416	-0,35807	-0,32931	-0,37278
SRP72	-0,3608	-0,38567	0,001	0,925221
SRP72	-0,3608	-0,38567	0,001	0,925221
RPS4X	-0,35651	-0,19735	-0,4588	-0,55545
NOP58	-0,35109	-0,28088	0,001	-0,25501
NPM1	-0,34135	-0,30242	0,548857	0,229242
NPM1	-0,34135	-0,30242	0,548857	0,229242
RPL7L1	-0,33957	-0,34609	0,001	-1,75591
SCAF4	-0,33878	-0,55117	0,001	-0,61477
RPL23	-0,33183	-0,31061	-0,18574	-0,50198
HNRNPDL	-0,31847	-0,25964	0,534363	-0,30833
HNRNPDL	-0,31847	-0,25964	0,534363	-0,30833
MYL6	-0,31751	-0,48023	0,001	-0,27047
RPS15	-0,31524	-0,27104	0,001	-0,65245
GAR1	-0,31219	-0,18699	0,402918	0,001
GAR1	-0,31219	-0,18699	0,402918	0,001
GTPBP4	-0,30793	0,001	-0,27634	-0,8261
KAT7	-0,30208	-0,18053	0,001	-0,28345
AHCTF1	-0,30016	-0,11561	0,346231	0,001
AHCTF1	-0,30016	-0,11561	0,346231	0,001
NOC2L	-0,28981	-0,21774	-0,16632	0,001
NUP107	-0,28741	-0,28753	0,001	0,180982
NUP107	-0,28741	-0,28753	0,001	0,180982
RPL15	-0,2823	-0,27206	-0,46488	-0,73795
MRPS35	-0,28103	-0,36135	0,001	0,691077
MRPS35	-0,28103	-0,36135	0,001	0,691077
DDX3X	-0,27173	-0,23396	-0,19097	-0,23621
DDX3Y	-0,27173	-0,23396	-0,19097	-0,23621
MT-CO2	-0,26638	-0,15748	0,223929	0,001
MT-CO2	-0,26638	-0,15748	0,223929	0,001
CAMK2D	-0,25931	0,001	0,24103	0,201214
CAMK2D	-0,25931	0,001	0,24103	0,201214
SRSF1	-0,25721	-0,15745	0,001	-0,11925
NUP160	-0,25686	-0,12675	0,001	0,285094

NUP160	-0,25686	-0,12675	0,001	0,285094
HIST1H1C	-0,25672	-0,18846	0,440781	-0,55513
HIST1H1C	-0,25672	-0,18846	0,440781	-0,55513
PES1	-0,25562	-0,45243	0,001	-0,81275
ILF3	-0,24788	-0,17954	0,001	-0,49732
CEBPZ	-0,24736	-0,17435	0,48022	0,414747
CEBPZ	-0,24736	-0,17435	0,48022	0,414747
MRPS30	-0,23924	-0,18565	0,001	0,32406
MRPS30	-0,23924	-0,18565	0,001	0,32406
NOP56	-0,23886	-0,08451	0,001	-0,22476
NDUFA10	-0,23744	-0,27884	0,001	1,856864
NDUFA10	-0,23744	-0,27884	0,001	1,856864
RPS14	-0,23564	0,001	-0,27736	-0,37214
PDS5B	-0,23552	-0,16217	0,001	0,343018
PDS5B	-0,23552	-0,16217	0,001	0,343018
HDLBP	-0,22813	-0,20206	-0,23548	-0,39105
RPS15A	-0,22088	-0,16634	-0,42196	-0,29011
DDX5	-0,21593	-0,13363	0,001	-0,33368
HNRNPC	-0,21425	-0,12527	0,001	-0,1911
RPS18	-0,21304	0,001	-0,23348	-0,13608
EIF3B	-0,21242	-0,2134	-0,30777	-0,09633
HEATR1	-0,21235	-0,27645	-0,33959	-0,43085
SMC1A	-0,207	0,001	-0,09811	-0,15348
TNC	-0,20696	0,001	-0,21215	-0,1239
PDS5A	-0,20603	-0,13232	0,001	-0,19461
SNRNP200	-0,20486	-0,1991	0,001	0,054392
SNRNP200	-0,20486	-0,1991	0,001	0,054392
NDUFS2	-0,20019	0,001	-0,25776	-0,38891
C7orf50	-0,1917	0,001	0,222341	0,241055
C7orf50	-0,1917	0,001	0,222341	0,241055
ATP2A2	-0,19063	0,001	-0,14291	-0,13162
SMARCA5	-0,18738	-0,20629	0,129731	0,113978
SMARCA5	-0,18738	-0,20629	0,129731	0,113978
PRPF8	-0,18501	-0,1591	-0,30064	-0,38563
NUP188	-0,18489	0,132987	-0,15379	0,001
NUP188	-0,18489	0,132987	-0,15379	0,001
HNRNPR	-0,18364	0,001	0,138426	-0,33558
HNRNPR	-0,18364	0,001	0,138426	-0,33558
RPL12	-0,18273	-0,17164	-0,11705	-0,16854
TPR	-0,17946	0,001	0,091246	-0,03954
TPR	-0,17946	0,001	0,091246	-0,03954
CDC5L	-0,17752	-0,04889	0,171741	-0,28084
CDC5L	-0,17752	-0,04889	0,171741	-0,28084
ILF2	-0,16934	-0,098	-0,14264	-0,4806
DDX39B	-0,16779	-0,29343	0,146472	-0,50691
DDX39B	-0,16779	-0,29343	0,146472	-0,50691

SLC25A4	-0,16762	-0,21549	-0,26561	0,001
RPL7A	-0,16475	0,001	-0,3062	-0,4791
DDX1	-0,16133	-0,25721	-0,177	0,296467
DDX1	-0,16133	-0,25721	-0,177	0,296467
CALU	-0,16133	0,001	-0,16984	-0,10239
HNRNPUL2	-0,15689	0,001	0,186728	-0,18253
HNRNPUL2	-0,15689	0,001	0,186728	-0,18253
MTDH	-0,15651	0,001	-0,17435	-0,28167
NUP205	-0,1522	-0,15836	-0,24719	0,001
RSL1D1	-0,14465	-0,2594	0,165454	-1,40012
RSL1D1	-0,14465	-0,2594	0,165454	-1,40012
PRKDC	-0,14251	-0,31656	-0,41034	-0,64223
NCL	-0,1392	-0,4133	0,157637	-0,4258
NCL	-0,1392	-0,4133	0,157637	-0,4258
EIF4A3	-0,1213	-0,41925	-0,26986	-1,11683
EMD	-0,11931	0,187476	0,001	-0,51668
EMD	-0,11931	0,187476	0,001	-0,51668
HNRNPU	-0,11697	-0,09675	0,241494	-0,51008
HNRNPU	-0,11697	-0,09675	0,241494	-0,51008
DIDO1	-0,10602	-0,34912	0,001	-0,37128
SRRT	-0,09467	0,184786	-0,19551	-0,13711
SRRT	-0,09467	0,184786	-0,19551	-0,13711
HNRNPL	-0,08379	0,001	0,196765	-0,34399
HNRNPL	-0,08379	0,001	0,196765	-0,34399
SF3B1	-0,0739	0,001	-0,06858	-0,26082
HCFC1	-0,03429	0,172163	0,001	-0,26745
HCFC1	-0,03429	0,172163	0,001	-0,26745
HIST1H2AC	0,001	-0,77888	2,089957	0,278015
HIST3H2A	0,001	-0,77888	2,089957	0,278015
HIST1H2AB	0,001	-0,77888	2,089957	0,278015
UPF1	0,001	-0,73222	-0,31965	-0,7665
RBM8A	0,001	-0,62378	-0,5534	-0,97694
DDX54	0,001	-0,5898	0,44035	-0,28292
APEX1	0,001	-0,5426	-0,22314	0,169442
HNRNPLL	0,001	-0,40206	-0,44085	-0,56184
SURF4	0,001	-0,39763	-0,40897	-0,33901
CIRBP	0,001	-0,39008	0,189462	-0,44685
STRAP	0,001	-0,36166	-0,39989	-0,44638
NIFK	0,001	-0,35783	0,119837	-0,87393
RPL14	0,001	-0,33244	-0,33599	-0,47557
SNW1	0,001	-0,31081	-0,24418	-1,02581
DAD1	0,001	-0,30805	-0,48331	-0,23354
DDX39A	0,001	-0,29308	0,225269	-0,58827
INTS1	0,001	-0,27831	0,382259	0,366619
XRCC6	0,001	-0,24305	-0,13156	-0,1042
ARF4	0,001	-0,23822	-0,82061	-0,43254

COX7A2	0,001	-0,22106	2,930656	3,068439
COPB2	0,001	-0,22011	-0,28712	-0,24716
RPS3	0,001	-0,21749	-0,42484	-0,2621
PSMC6	0,001	-0,20398	-0,09016	-0,08483
RPS11	0,001	-0,18959	-0,42402	-0,61812
SET	0,001	-0,17048	-0,56414	-0,08271
SETSIP	0,001	-0,17048	-0,56414	-0,08271
TOMM40	0,001	-0,16624	0,240746	0,254405
RPL6	0,001	-0,16157	-0,30044	-0,46793
NIPSNAP1	0,001	-0,13969	0,751761	0,498177
EIF4G1	0,001	-0,12465	-0,39383	-0,24167
EIF3E	0,001	-0,12455	-0,3008	-0,46039
SAFB	0,001	-0,10966	0,378728	-0,17616
SPTAN1	0,001	-0,10762	-0,16264	0,113149
VARS	0,001	-0,10626	-0,51721	-0,13864
CLTC	0,001	-0,10364	-0,16957	0,149751
HADHA	0,001	-0,10233	0,169663	0,269295
STT3A	0,001	-0,09867	-0,44103	-0,29534
CCT4	0,001	-0,0846	-0,26478	-0,07944
DARS	0,001	-0,08337	-0,45692	-0,23306
EEA1	0,001	0,406608	-0,78067	-0,43183
RPL21	0,001	0,164456	-0,54147	-0,90523
OSBP	0,001	0,294346	-0,51154	-0,41509
USMG5	0,001	0,370996	-0,48146	-0,20663
LGALS1	0,001	0,289758	-0,46216	-0,24361
GNG12	0,001	0,355462	-0,39624	-0,45021
DSTN	0,001	0,458986	-0,37943	-0,18578
RCN1	0,001	0,112899	-0,342	-0,13897
TGOLN2	0,001	0,354299	-0,32625	-0,26771
TMED7	0,001	0,171054	-0,30693	-0,86777
UBE2N	0,001	0,594477	-0,30005	-0,29423
UBE2NL	0,001	0,594477	-0,30005	-0,29423
SMNDC1	0,001	0,143989	-0,29002	-0,52634
TWF1	0,001	0,341545	-0,28706	-0,26302
MSN	0,001	0,119806	-0,26126	-0,11805
ATXN2L	0,001	0,437197	-0,26113	-0,30767
PUF60	0,001	0,244853	-0,2601	-0,7616
ATP5L	0,001	0,423672	-0,24744	-0,32316
PPA1	0,001	0,455271	-0,23671	0,198229
CALR	0,001	0,132329	-0,22532	-0,20501
LBR	0,001	0,163656	-0,22394	-0,20515
FABP7	0,001	0,662625	-0,21153	-0,24911
EWSR1	0,001	0,234444	-0,18385	-0,76627
IGF2R	0,001	0,253325	-0,18115	-0,27828
SNRPA1	0,001	0,11655	-0,16567	-0,38367
MARCH5	0,001	0,173508	-0,16231	-0,21701

SF3A2	0,001	0,24192	-0,13451	-0,44626
GANAB	0,001	0,140395	-0,13254	-0,07989
LSS	0,001	0,14034	-0,04966	-0,10135
MYEF2	0,001	0,347951	0,335932	-0,52351
HNRNPA1	0,001	0,193984	0,242006	-0,34993
HNRNPA1L2	0,001	0,193984	0,242006	-0,34993
ADNP	0,001	0,264296	0,168303	-0,32632
HNRNPH1	0,001	0,093953	0,120652	-0,2805
NUP153	0,001	0,137044	0,105487	-0,27238
XRN2	0,001	0,104984	0,286383	-0,237
RBM14	0,001	0,25953	0,133589	-0,21218
ADAR	0,001	0,147576	0,23029	-0,19134
SUMF2	0,001	0,205835	0,291143	-0,18473
DDX23	0,001	0,151586	0,100204	-0,15924
RBM4	0,001	0,308905	0,168589	-0,15151
SART1	0,001	0,082831	0,176394	-0,10163
COX7A2	0,001	-0,22106	2,930656	3,068439
PSMB3	0,001	0,234456	0,937518	0,990948
PTMS	0,001	0,591748	0,848155	0,807238
NIPSNAP1	0,001	-0,13969	0,751761	0,498177
HSPD1	0,001	0,063268	0,422125	0,483885
INTS1	0,001	-0,27831	0,382259	0,366619
GRSF1	0,001	0,436184	0,22923	0,306048
HIST1H2AB	0,001	-0,77888	2,089957	0,278015
HIST1H2AC	0,001	-0,77888	2,089957	0,278015
HIST3H2A	0,001	-0,77888	2,089957	0,278015
SHMT2	0,001	0,070925	0,250306	0,274453
HADHA	0,001	-0,10233	0,169663	0,269295
TOMM40	0,001	-0,16624	0,240746	0,254405
TMPO	0,001	0,163073	0,402851	0,235319
LMNB1	0,001	0,121197	0,265624	0,20299
OAT	0,001	0,369732	0,166571	0,199247
PPA1	0,001	0,455271	-0,23671	0,198229
APEX1	0,001	-0,5426	-0,22314	0,169442
CLTC	0,001	-0,10364	-0,16957	0,149751
P4HB	0,001	0,07651	0,106582	0,138154
CKAP4	0,001	0,092887	0,181359	0,121255
SPTAN1	0,001	-0,10762	-0,16264	0,113149
GANAB	0,001	0,140395	-0,13254	-0,07989
LSS	0,001	0,14034	-0,04966	-0,10135
SART1	0,001	0,082831	0,176394	-0,10163
MSN	0,001	0,119806	-0,26126	-0,11805
RCN1	0,001	0,112899	-0,342	-0,13897
RBM4	0,001	0,308905	0,168589	-0,15151
DDX23	0,001	0,151586	0,100204	-0,15924
SAFB	0,001	-0,10966	0,378728	-0,17616

SUMF2	0,001	0,205835	0,291143	-0,18473
DSTN	0,001	0,458986	-0,37943	-0,18578
ADAR	0,001	0,147576	0,23029	-0,19134
CALR	0,001	0,132329	-0,22532	-0,20501
LBR	0,001	0,163656	-0,22394	-0,20515
USMG5	0,001	0,370996	-0,48146	-0,20663
RBM14	0,001	0,25953	0,133589	-0,21218
MARCH5	0,001	0,173508	-0,16231	-0,21701
XRN2	0,001	0,104984	0,286383	-0,237
LGALS1	0,001	0,289758	-0,46216	-0,24361
FABP7	0,001	0,662625	-0,21153	-0,24911
TWF1	0,001	0,341545	-0,28706	-0,26302
TGOLN2	0,001	0,354299	-0,32625	-0,26771
NUP153	0,001	0,137044	0,105487	-0,27238
IGF2R	0,001	0,253325	-0,18115	-0,27828
HNRNPH1	0,001	0,093953	0,120652	-0,2805
DDX54	0,001	-0,5898	0,44035	-0,28292
UBE2N	0,001	0,594477	-0,30005	-0,29423
UBE2NL	0,001	0,594477	-0,30005	-0,29423
ATXN2L	0,001	0,437197	-0,26113	-0,30767
ATP5L	0,001	0,423672	-0,24744	-0,32316
ADNP	0,001	0,264296	0,168303	-0,32632
HNRNPA1	0,001	0,193984	0,242006	-0,34993
HNRNPA1L2	0,001	0,193984	0,242006	-0,34993
SNRPA1	0,001	0,11655	-0,16567	-0,38367
OSBP	0,001	0,294346	-0,51154	-0,41509
EEA1	0,001	0,406608	-0,78067	-0,43183
SF3A2	0,001	0,24192	-0,13451	-0,44626
CIRBP	0,001	-0,39008	0,189462	-0,44685
GNG12	0,001	0,355462	-0,39624	-0,45021
MYEF2	0,001	0,347951	0,335932	-0,52351
SMNDC1	0,001	0,143989	-0,29002	-0,52634
DDX39A	0,001	-0,29308	0,225269	-0,58827
PUF60	0,001	0,244853	-0,2601	-0,7616
EWSR1	0,001	0,234444	-0,18385	-0,76627
TMED7	0,001	0,171054	-0,30693	-0,86777
NIFK	0,001	-0,35783	0,119837	-0,87393
RPL21	0,001	0,164456	-0,54147	-0,90523
NES	0,048398	0,157279	-0,28323	0,096128
NES	0,048398	0,157279	-0,28323	0,096128
ALDH9A1	0,056426	0,287074	0,001	-0,29475
ALDH9A1	0,056426	0,287074	0,001	-0,29475
TFRC	0,070405	0,164129	-0,17021	0,001
TFRC	0,070405	0,164129	-0,17021	0,001
EPHX1	0,089582	0,09152	-0,56474	0,001
EPHX1	0,089582	0,09152	-0,56474	0,001

FLNA	0,090574	0,069481	-0,18557	0,12253
FLNA	0,090574	0,069481	-0,18557	0,12253
CDC73	0,091023	0,001	0,412439	0,665754
TUBB8	0,096015	-0,26912	0,784761	0,73988
TUBB8	0,096015	-0,26912	0,784761	0,73988
FKBP9	0,097961	0,182971	0,001	1,20532
IDH3G	0,103883	0,186845	0,001	0,787363
HNRNPA2B1	0,106032	0,181489	0,196313	-0,34299
HNRNPA2B1	0,106032	0,181489	0,196313	-0,34299
PDIA6	0,109141	0,125991	0,001	0,515802
ETFA	0,111229	0,001	0,146334	0,318863
GOT2	0,113838	0,316776	0,001	-0,24527
GOT2	0,113838	0,316776	0,001	-0,24527
SF3A1	0,119717	0,233688	0,001	-0,29337
SF3A1	0,119717	0,233688	0,001	-0,29337
VCP	0,120209	0,20783	0,144187	0,160446
IPO5	0,12372	0,001	-0,28049	0,118955
IPO5	0,12372	0,001	-0,28049	0,118955
CORO2B	0,131169	0,001	-0,31311	-0,68197
CORO2B	0,131169	0,001	-0,31311	-0,68197
VIM	0,144418	0,238949	-0,1312	0,173215
VIM	0,144418	0,238949	-0,1312	0,173215
AK2	0,144654	0,271758	0,365854	0,466377
UQCRC1	0,145275	0,183889	0,001	0,189823
ATP5F1	0,145471	0,277947	-0,34271	-0,37439
ATP5F1	0,145471	0,277947	-0,34271	-0,37439
PHB	0,147831	0,173181	0,001	0,104148
EZR	0,147834	0,164832	0,001	0,240244
PSMD2	0,148179	0,134341	0,001	0,167251
SLC25A3	0,160789	0,254867	-0,07495	-0,13822
SLC25A3	0,160789	0,254867	-0,07495	-0,13822
KHSRP	0,165207	-0,06738	0,001	-1,07757
KHSRP	0,165207	-0,06738	0,001	-1,07757
CTSD	0,167525	0,160005	0,149085	0,190861
SF1	0,168013	0,144288	0,088011	-0,38489
SF1	0,168013	0,144288	0,088011	-0,38489
HSPE1	0,168015	0,149628	0,305316	0,001
SF3B2	0,170647	0,260149	0,001	-0,169
SF3B2	0,170647	0,260149	0,001	-0,169
PTBP1	0,172317	-0,10394	0,001	-0,92083
PTBP1	0,172317	-0,10394	0,001	-0,92083
ISOC2	0,17278	0,001	0,556296	1,094234
TIMM13	0,173592	0,338776	0,001	0,190478
CS	0,175739	0,138908	0,106585	0,105609
HSP90AB1	0,175872	0,130578	-0,21455	0,001
HSP90AB1	0,175872	0,130578	-0,21455	0,001

PSMD11	0,178312	0,185951	0,001	0,138095
PRDX5	0,185765	0,193644	-0,16667	0,34352
PRDX5	0,185765	0,193644	-0,16667	0,34352
RAB11B	0,189621	0,20906	-0,2636	-0,10023
RAB11B	0,189621	0,20906	-0,2636	-0,10023
SEC22B	0,197374	0,001	0,232548	0,225968
TMED9	0,207628	0,114268	0,453964	0,20658
GPX1	0,210377	0,212941	0,001	0,179198
HSPA8	0,216457	0,20463	0,001	0,150001
MAP4	0,216953	0,001	-0,28511	-0,25253
MAP4	0,216953	0,001	-0,28511	-0,25253
KIF5B	0,226545	0,197467	-0,12189	-0,19407
KIF5B	0,226545	0,197467	-0,12189	-0,19407
SDF4	0,228694	0,315421	0,001	0,701406
DYNC1H1	0,228964	-0,19167	-0,34086	-0,04281
DYNC1H1	0,228964	-0,19167	-0,34086	-0,04281
MLEC	0,22974	0,176851	0,001	0,275721
CYCS	0,229888	0,265998	0,854959	1,506748
SEPT2	0,232362	-0,17138	-0,16072	0,323616
SEPT2	0,232362	-0,17138	-0,16072	0,323616
ATP6V1A	0,233729	0,267877	0,001	0,521988
COX5B	0,234907	0,454506	0,001	-0,41854
COX5B	0,234907	0,454506	0,001	-0,41854
SNRPB2	0,23657	0,197252	0,001	-0,50106
SNRPB2	0,23657	0,197252	0,001	-0,50106
ERO1L	0,237197	0,298801	0,001	0,196877
LAP3	0,23941	0,001	0,402472	0,932049
IGFBP2	0,243667	0,393154	0,001	0,169044
AARS	0,244869	0,001	-0,29014	-0,17587
AARS	0,244869	0,001	-0,29014	-0,17587
SNRNP70	0,249034	0,476674	0,001	-0,55252
SNRNP70	0,249034	0,476674	0,001	-0,55252
CCT3	0,253227	0,108519	-0,14114	0,001
CCT3	0,253227	0,108519	-0,14114	0,001
HNRNPH3	0,257913	0,001	0,249418	-0,32176
HNRNPH3	0,257913	0,001	0,249418	-0,32176
TPI1	0,259637	0,251764	0,098488	-0,1597
TPI1	0,259637	0,251764	0,098488	-0,1597
FASN	0,267714	-0,15558	0,001	0,280994
FASN	0,267714	-0,15558	0,001	0,280994
TUBB2B	0,273978	-0,22608	0,001	0,269873
TUBB2B	0,273978	-0,22608	0,001	0,269873
ANXA1	0,295296	0,263074	0,001	0,395049
PYGB	0,297226	-0,1521	-0,38866	0,349876
PYGB	0,297226	-0,1521	-0,38866	0,349876
TXN2	0,29903	0,369825	0,4117	0,730688

UBAP2L	0,299299	0,186656	0,001	-0,25319
UBAP2L	0,299299	0,186656	0,001	-0,25319
PPP2R1A	0,301022	0,001	-0,16779	0,368609
PPP2R1A	0,301022	0,001	-0,16779	0,368609
GRPEL1	0,303474	0,275875	0,154903	0,001
YWHAH	0,304599	0,001	-0,48423	-0,10253
YWHAH	0,304599	0,001	-0,48423	-0,10253
HIST1H2AG	0,311853	0,001	-1,9424	-1,62741
HIST1H2AJ	0,311853	0,001	-1,9424	-1,62741
H2AFJ	0,311853	0,001	-1,9424	-1,62741
HIST1H2AH	0,311853	0,001	-1,9424	-1,62741
HIST1H2AD	0,311853	0,001	-1,9424	-1,62741
H2AFJ	0,311853	0,001	-1,9424	-1,62741
HIST1H2AD	0,311853	0,001	-1,9424	-1,62741
HIST1H2AG	0,311853	0,001	-1,9424	-1,62741
HIST1H2AH	0,311853	0,001	-1,9424	-1,62741
HIST1H2AJ	0,311853	0,001	-1,9424	-1,62741
ATP5H	0,314671	0,194146	0,332423	0,282359
TKT	0,316314	0,001	0,388315	0,166675
STIP1	0,325429	0,170309	-0,19513	-0,20045
STIP1	0,325429	0,170309	-0,19513	-0,20045
CAND1	0,326789	0,001	-0,42246	0,209851
CAND1	0,326789	0,001	-0,42246	0,209851
YWHAB	0,326852	0,321512	-0,41245	0,001
YWHAB	0,326852	0,321512	-0,41245	0,001
ADD1	0,331256	0,289427	-0,18717	-0,43487
ADD1	0,331256	0,289427	-0,18717	-0,43487
HSPA4	0,333508	0,001	-0,16952	0,099476
HSPA4	0,333508	0,001	-0,16952	0,099476
TUBB4B	0,343452	-0,25477	0,224648	0,207259
TUBB4B	0,343452	-0,25477	0,224648	0,207259
CCT5	0,349181	0,001	-0,19194	-0,09708
CCT5	0,349181	0,001	-0,19194	-0,09708
YWHAE	0,350167	0,001	-0,42732	-0,23634
YWHAE	0,350167	0,001	-0,42732	-0,23634
ATP5I	0,353575	0,549884	-0,29752	-0,44151
ATP5I	0,353575	0,549884	-0,29752	-0,44151
CLIC4	0,356225	0,30943	-0,20252	0,001
CLIC4	0,356225	0,30943	-0,20252	0,001
SLIRP	0,362116	0,356478	0,001	0,315384
FSCN1	0,367861	0,327319	0,001	-0,12811
FSCN1	0,367861	0,327319	0,001	-0,12811
PSME3	0,374967	0,266062	0,001	0,214102
NASP	0,375707	0,295919	-0,16227	0,241995
NASP	0,375707	0,295919	-0,16227	0,241995
NFU1	0,380448	0,438415	-1,40642	0,001

NFU1	0,380448	0,438415	-1,40642	0,001
SCP2	0,387379	0,499786	0,086067	0,001
TUBB3	0,388128	0,001	0,254777	0,42028
TCEB1	0,388811	0,383989	0,001	-0,34332
TCEB1	0,388811	0,383989	0,001	-0,34332
EEF2	0,390493	-0,09683	-0,15114	0,001
EEF2	0,390493	-0,09683	-0,15114	0,001
DBNL	0,397013	0,485428	0,001	-0,32993
DBNL	0,397013	0,485428	0,001	-0,32993
CCT8	0,397144	0,23192	-0,09922	0,001
CCT8	0,397144	0,23192	-0,09922	0,001
LDHA	0,399593	0,138095	-0,33848	0,001
LDHA	0,399593	0,138095	-0,33848	0,001
PNP	0,399647	0,001	-0,50307	-0,43789
PNP	0,399647	0,001	-0,50307	-0,43789
PKM	0,405949	0,059533	-0,13865	0,001
PKM	0,405949	0,059533	-0,13865	0,001
YWHAZ	0,413928	0,159409	0,001	0,279703
TUBA1A	0,415711	-0,1712	0,001	0,124191
TUBA3E	0,415711	-0,1712	0,001	0,124191
TUBA1A	0,415711	-0,1712	0,001	0,124191
TUBA3E	0,415711	-0,1712	0,001	0,124191
RCC2	0,429663	0,312884	-0,26376	-0,29667
RCC2	0,429663	0,312884	-0,26376	-0,29667
FKBP4	0,44225	0,370206	0,001	0,047836
CBR1	0,442729	0,208548	0,001	0,341896
PAFAH1B1	0,446012	0,001	-0,40679	-0,4324
PAFAH1B1	0,446012	0,001	-0,40679	-0,4324
UBA1	0,446814	0,140785	0,001	0,252855
ENAH	0,462933	0,370076	-0,27208	0,001
ENAH	0,462933	0,370076	-0,27208	0,001
SLC35A4	0,480029	0,447866	-0,4068	0,001
SLC35A4	0,480029	0,447866	-0,4068	0,001
ANP32B	0,489905	0,474442	-0,3731	-0,28933
ANP32B	0,489905	0,474442	-0,3731	-0,28933
UBE2M	0,506961	0,386802	-0,36422	-0,14716
UBE2M	0,506961	0,386802	-0,36422	-0,14716
LDHB	0,507196	0,230441	-0,16168	0,001
LDHB	0,507196	0,230441	-0,16168	0,001
AHCY	0,51756	0,261017	0,001	-0,18593
AHCY	0,51756	0,261017	0,001	-0,18593
CFL1	0,520304	0,141563	0,001	0,213253
YWHAQ	0,525249	0,351108	-0,37259	0,001
YWHAQ	0,525249	0,351108	-0,37259	0,001
PRDX2	0,53541	0,229077	-0,32472	0,001
PRDX2	0,53541	0,229077	-0,32472	0,001

GDI2	0,541491	0,001	-0,13069	0,557282
GDI2	0,541491	0,001	-0,13069	0,557282
ENO1	0,548169	0,124468	0,123219	0,001
GPI	0,551584	0,211938	-0,19748	0,001
GPI	0,551584	0,211938	-0,19748	0,001
GDI1	0,551723	0,001	-0,27781	0,341806
GDI1	0,551723	0,001	-0,27781	0,341806
TCEB2	0,553101	0,238335	0,001	0,490531
AKR1B1	0,556223	0,249667	-0,21038	0,001
AKR1B1	0,556223	0,249667	-0,21038	0,001
UBE2I	0,562949	0,326185	0,001	0,357602
NME2	0,569965	0,211099	-0,19711	0,001
NME2P1	0,569965	0,211099	-0,19711	0,001
NME2	0,569965	0,211099	-0,19711	0,001
NME2P1	0,569965	0,211099	-0,19711	0,001
IDH1	0,570232	0,301633	-0,2692	0,001
IDH1	0,570232	0,301633	-0,2692	0,001
PAFAH1B3	0,578228	0,408455	0,001	0,245646
PRDX1	0,583487	0,338504	-0,17772	-0,14954
PRDX1	0,583487	0,338504	-0,17772	-0,14954
PEBP1	0,585111	0,321902	0,369601	0,432242
CLIC1	0,592646	0,287633	-0,33592	-0,13466
CLIC1	0,592646	0,287633	-0,33592	-0,13466
UCHL1	0,603385	0,371593	0,001	-0,17327
UCHL1	0,603385	0,371593	0,001	-0,17327
PLIN3	0,651004	0,566994	0,001	-0,31957
PLIN3	0,651004	0,566994	0,001	-0,31957
PGK1	0,660967	0,351503	0,001	0,121809
CKB	0,677928	0,001	0,220808	0,318249
ACAT2	0,702854	0,256629	0,162394	0,497276
MDH1	0,706476	0,520345	0,001	-0,22424
MDH1	0,706476	0,520345	0,001	-0,22424
GSTP1	0,741046	0,366896	0,001	0,122462
PPIA	0,752166	0,182381	0,301954	0,521877
PFN1	0,757238	0,374272	-0,1858	-0,1571
PFN1	0,757238	0,374272	-0,1858	-0,1571
GOT1	0,786635	0,001	-0,14071	0,150799
GOT1	0,786635	0,001	-0,14071	0,150799
TLE1	0,792253	1,272827	0,001	1,149919
TLE2	0,792253	1,272827	0,001	1,149919
TLE3	0,792253	1,272827	0,001	1,149919
SEC61B	0,854479	0,965691	-0,17929	-0,37968
SEC61B	0,854479	0,965691	-0,17929	-0,37968
TAGLN2	0,878413	0,309225	-0,28889	0,001
TAGLN2	0,878413	0,309225	-0,28889	0,001
SOD1	0,894906	0,473567	0,001	0,740367

UBE2L3	0,915166	0,405561	0,001	0,621047
SSBP1	0,942393	0,914774	0,001	0,846053
TMSB4X	0,954001	0,755349	0,001	-0,45662
TMSB4X	0,954001	0,755349	0,001	-0,45662
ARHGDIA	0,973007	0,473764	0,001	0,180822
STMN1	2,665945	2,147843	0,001	0,266703

Norges miljø- og biovitenskapelige universitet
Noregs miljø- og biovitskapelege universitet
Norwegian University of Life Sciences

Postboks 5003
NO-1432 Ås
Norway